








**Two specific publications/research papers of the applicant relevant to the research work mentioned above (see below)**

- Kalarikkal M, Saikia R, Oliveira L, Bhorkar Y, Lonare A, Varshney P, Dhamale P, Majumdar A, **Joseph J\***. Nup358 restricts ER-mitochondria connectivity by modulating mTORC2/Akt/GSK3 $\beta$  signalling. **EMBO Rep.** 2024 Jul 18. doi: 10.1038/s44319-024-00204-8 (*Selected as cover page article for the October 2024 Issue*).
- Sahoo MR, Gaikwad S, Khuperkar D, Ashok M, Helen M, Yadav SK, Singh A, Magre I, Deshmukh P, Dhanvijay S, Sahoo PK, Ramtirtha Y, Madhusudhan MS, Gayathri P, Seshadri V, **Joseph J\***. Nup358 binds to AGO proteins through its SUMO-interacting motifs and promotes the association of target mRNA with miRISC. **EMBO Rep.** 2017 Feb;18(2):241-263. doi: 10.15252/embr.201642386.

# Nup358 restricts ER-mitochondria connectivity by modulating mTORC2/Akt/GSK3 $\beta$ signalling

Misha Kalarikkal, Rimpi Saikia , Lizanne Oliveira , Yashashree Bhorkar, Akshay Lonare , Pallavi Varshney, Prathamesh Dhamale , Amitabha Majumdar  & Jomon Joseph  

## Abstract

ER-mitochondria contact sites (ERMCSs) regulate processes, including calcium homeostasis, energy metabolism and autophagy. Previously, it was shown that during growth factor signalling, mTORC2/Akt gets recruited to and stabilizes ERMCSs. Independent studies showed that GSK3 $\beta$ , a well-known Akt substrate, reduces ER-mitochondria connectivity by disrupting the VAPB-PTPIP51 tethering complex. However, the mechanisms that regulate ERMCSs are incompletely understood. Here we find that annulate lamellae (AL), relatively unexplored subdomains of ER enriched with a subset of nucleoporins, are present at ERMCSs. Depletion of Nup358, an AL-resident nucleoporin, results in enhanced mTORC2/Akt activation, GSK3 $\beta$  inhibition and increased ERMCSs. Depletion of Rictor, a mTORC2-specific subunit, or exogenous expression of GSK3 $\beta$ , was sufficient to reverse the ERMCS-phenotype in Nup358-deficient cells. We show that growth factor-mediated activation of mTORC2 requires the VAPB-PTPIP51 complex, whereas, Nup358's association with this tether restricts mTORC2/Akt signalling and ER-mitochondria connectivity. Expression of a Nup358 fragment that is sufficient for interaction with the VAPB-PTPIP51 complex suppresses mTORC2/Akt activation and disrupts ERMCSs. Collectively, our study uncovers a novel role for Nup358 in controlling ERMCSs by modulating the mTORC2/Akt/GSK3 $\beta$  axis.

**Keywords** Annulate Lamellae; ER-mitochondria Contact Sites; mTORC2; Nucleoporins; GSK3 $\beta$

**Subject Categories** Membranes & Trafficking; Organelles; Signal Transduction

<https://doi.org/10.1038/s44319-024-00204-8>

Received 30 August 2023; Revised 24 June 2024;

Accepted 27 June 2024

## Introduction

Contrary to the general perception that organelles in the cell exist and function independently, recent developments highlight that multiple organelles make physical and dynamic contacts with each other to coordinate the many functions they perform (Henne, 2016; Wu et al, 2018; Prinz et al, 2020; Scorrano et al, 2019). Endoplasmic

reticulum (ER), an organelle characterized by its membranous network that extends throughout the cytoplasm, interacts with other organelles through specific contact sites (López-Crisosto et al, 2015; Petkovic et al, 2021; Phillips and Voeltz, 2016; Cohen et al, 2018). ER-mitochondria contact sites (ERMCSs), also known as mitochondria-associated ER membrane (MAM), are maintained through physical interactions between proteins present on both the organelles (Marchi et al, 2014; Raturi and Simmen, 2013; Wu et al, 2018; Rowland and Voeltz, 2012; Filadi et al, 2017). One of the well-characterized tethers is a complex between an ER-resident vesicle-associated membrane protein-associated protein B (VAPB) and a mitochondrial outer membrane protein, protein tyrosine phosphatase-interacting protein 51 (PTPIP51) (Stoica et al, 2014; De vos et al, 2012; Gomez-Suaga et al, 2017; Stoica et al, 2016; Obara et al, 2024). The others include Mfn2-Mfn1/2 (De Brito and Scorrano, 2008), IP3R-GRP75-VDAC (Szabadkai et al, 2006) and BAP31-Fis1 (Iwasawa et al, 2011).

ERMCSs regulate inter-organelle Ca<sup>2+</sup> transfer, lipid transfer, energy metabolism, inflammation, apoptosis, autophagy and several other ER/mitochondria-dependent functions (Perrone et al, 2020; Barazzuol et al, 2021; Vance, 2020; Csordás et al, 2018; Madreiter-Sokolowski et al, 2019; Giordano, 2018). The ER-resident Ca<sup>2+</sup> channel IP3R is enriched at the ERMCSs where it mediates Ca<sup>2+</sup> transfer from the ER to the mitochondria to regulate energy metabolism and apoptosis (Grimm, 2012; Csordás et al, 2018). Although many critical cellular functions are dependent on ERMCSs, the molecular interplay regulating the dynamic interaction between ER and mitochondria remains unclear. Nevertheless, it has been shown that growth factor-stimulated mTORC2 pathway stabilizes ERMCSs through Akt-mediated phosphorylation of ERMCS proteins such as IP3R3 and PACS2 (Betz et al, 2013). Independent reports also show that GSK3 $\beta$  destabilizes ERMCSs by disrupting the VAPB-PTPIP51 tethering complex (Stoica et al, 2016, 2014; Kors et al, 2022). Growth factor signalling activates mTORC2, which phosphorylates Akt at S473 and completely activates Akt, which has been shown to phosphorylate GSK3 $\beta$  at S9 (Manning and Toker, 2017). However, whether growth factor signalling dependent ERMCS stability involves mTORC2/Akt-mediated inhibition of GSK3 $\beta$  is not known.

The ER is involved in a multitude of physiological functions, which are performed by specialized subdomains of the organelle (Cohen et al, 2018). Annulate lamellae (AL), an underexplored subdomain of the ER, majorly characterized in germ cells, are stacked membranes containing pore-like assemblies that

structurally resemble the nuclear pore complexes (NPCs) present on the nuclear envelope (NE) (Kessel, 1992). Although AL are reported in somatic cells, their structural details are unclear. Many functions for AL have been proposed based on electron microscopic observations, which include roles in infection, cancers, gene expression, mRNA regulation and development (Kessel, 1992). AL are remodelled extensively during embryonic development, infection by intracellular pathogens, including SARS-CoV-2 and in cancers (Kessel, 1992; Eymieux et al, 2021). Recently, the involvement of AL in the functional assembly of NPCs has been reported (Hampoezel et al, 2016). AL possess only a subset of nucleoporins as compared to the NPCs (Sahoo et al, 2017; Cordes et al, 1996), thus implying a compositional, structural and functional difference between AL pore complexes and NPCs. A role for the AL-resident nucleoporin Nup358 in microRNA-mediated translational suppression of mRNAs has been documented (Sahoo et al, 2017).

Consistent with the range of processes the ERMCSs regulate, dysfunctional ER-mitochondria crosstalk is implicated in many disorders including diabetes (Rieusset, 2018; Tubbs et al, 2014), cancers (Doghman-Bouguerra and Lalli, 2019; Simoes et al, 2020; Peruzzo et al, 2020) and neurodegeneration (Paillusson et al, 2016; Petkovic et al, 2021). Specifically, ERMCSs and their functions are compromised in neurodegenerative disorders such as amyotrophic lateral sclerosis (ALS)/frontotemporal dementia (FTD), Alzheimer's (AD), Parkinson's (PD) and Huntington's diseases (HD) (Petkovic et al, 2021; Paillusson et al, 2016; Markovinic et al, 2022). VAPB, an ERMCS tethering protein, is mutated in amyotrophic lateral sclerosis (ALS) (Nishimura et al, 2004). The pathogenic mutation in VAPB, P65S, is shown to stabilise the VAPB-PTPIP51 tethering complex, thus affecting the abundance and functions of ERMCSs (De vos et al, 2012). Impaired ERMCSs are also implicated in the more common forms of ALS/FTD (Fallini et al, 2020). Ectopic expression of the wild-type or ALS/FTD-associated mutant versions of FUS and TDP-43 is shown to decrease ERMCSs through GSK3 $\beta$ -mediated disruption of VAPB-PTPIP51 interaction (Stoica et al, 2014, 2016).

Recently, multiple reports have linked impaired nucleocytoplasmic transport (NCT) to neurodegenerative diseases (Ding and Sepelchmanesh, 2021; Fahrenkrog and Harel, 2018). This may be due to the perturbation of the NPCs, mislocalization and/or degradation of nucleoporins and other components of the NCT (Kim and Taylor, 2017; Spead et al, 2022). However, whether there exists any relationship between the NCT pathway/components and the ERMCS tethering complexes or their functions is unclear.

Since ER makes functional contacts with mitochondria through specialized subdomains at the ERMCSs, and AL represent another subdomain of the ER in the cytoplasm, we explored if these two subdomains associate with each other. We found that Nup358-positive AL are often present at the contact sites between ER and mitochondria. Moreover, Nup358 interacts with the ERMCS tethering complex VAPB-PTPIP51, and loss of Nup358 leads to enhanced ER-mitochondria connectivity through increased mTORC2/Akt pathway activation and GSK3 $\beta$  inhibition. Together, our studies reveal a role for Nup358 in modulating growth factor-mediated remodelling of ERMCSs through a mechanism involving the suppression of mTORC2/Akt pathway and activation of GSK3 $\beta$ .

## Results

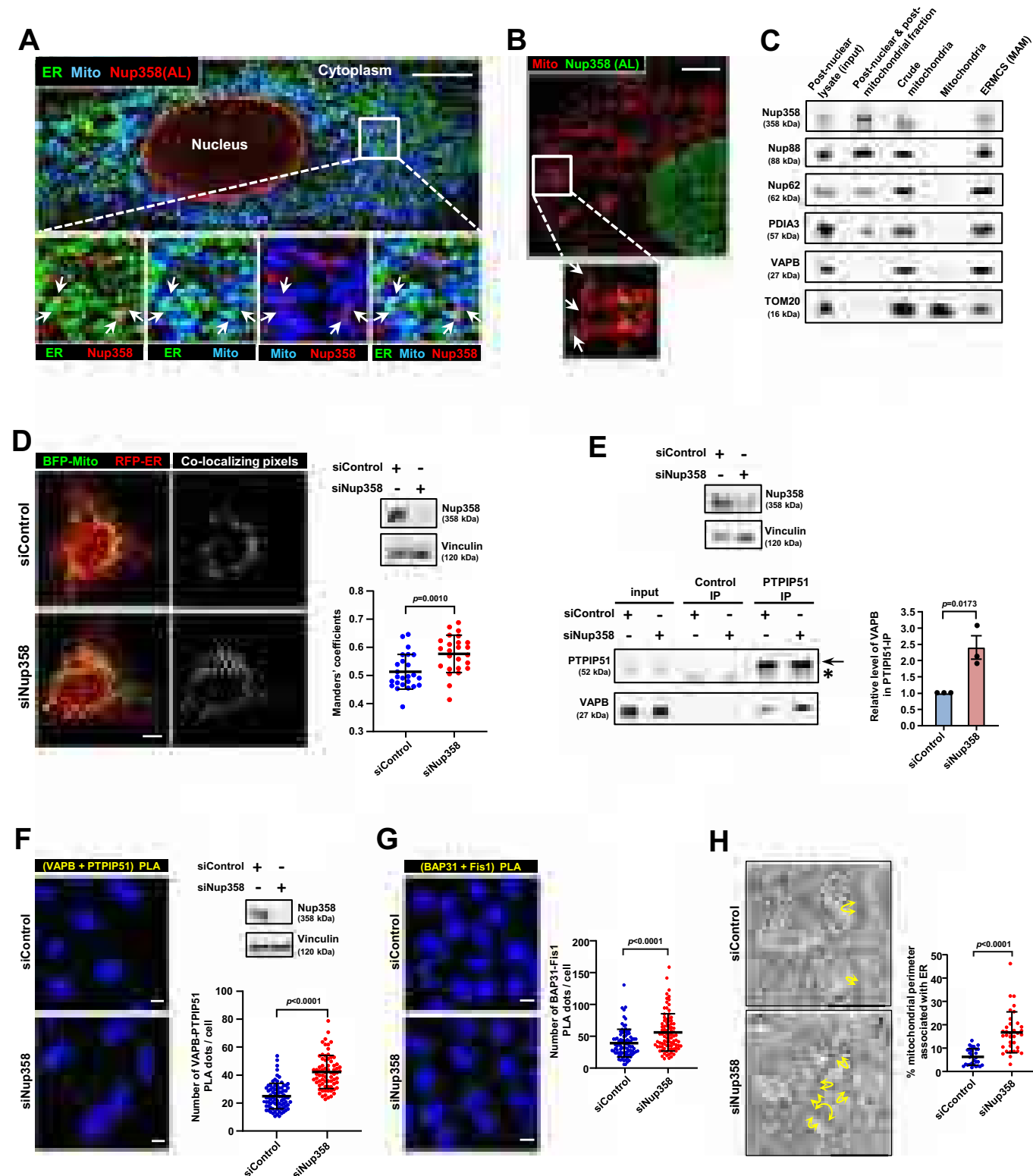
### Annulate lamellae are present at ER-mitochondria contact sites

As AL are subdomains of ER, and the ER makes extensive contacts with multiple organelles, including mitochondria, we tested the hypothesis that AL are present at the contacts between ER and mitochondria. Microscopic images of cells co-stained for Nup358 as an AL marker (Sahoo et al, 2017), PDIA3 as an ER marker and MitoTracker for mitochondria revealed that AL ( $40 \pm 6\%$ ; 18 cells) are often present at ERMCSs (Fig. 1A). Consistent with this, super-resolution images obtained by stimulated emission depletion microscopy (STED) of AL (Nup358) and mitochondria (Tom20) showed that many of the AL structures were present adjacent to mitochondria (Fig. 1B). Fractionation of organelles from HeLa cells confirmed that a pool of Nup358, along with other known AL-associated nucleoporins (Nup62 and Nup88) (Sahoo et al, 2017), was present in the mitochondria-associated membrane (MAM) fraction, which represents ERMCSs (Montesinos and Area-Gomez, 2020) (Fig. 1C). In addition, disruption of ERMCSs by depletion of the tethering proteins VAPB/PTPIP51, Mitofusin 2 (Mfn2) or IP3R3, which are essential for ERMCS integrity, led to disappearance of AL, as determined by the absence of cytoplasmic puncta of Nup358 and other AL-associated nucleoporins (Fig. EV1). However, the localization of these nucleoporins to the nuclear membrane remained unaffected under the above condition. Collectively, the results show that AL reside at ERMCSs and the assembly and/or stability of AL depends on ERMCSs.

### Nup358 depletion increases the connectivity between ER and mitochondria

We tested if the AL component Nup358 controls the contacts between the ER and the mitochondria by assessing the ERMCS integrity in Nup358-depleted cells in multiple ways. Knockdown of Nup358 led to increased colocalization between ER and mitochondria in fluorescence microscopy (Fig. 1D). Moreover, siRNA-mediated depletion of Nup358 led to increased interaction between components of the ERMCS tethering complex, VAPB (ER) and PTPIP51 (mitochondria), as monitored by co-immunoprecipitation assays (Fig. 1E). Furthermore, proximity ligation assay (PLA) for two of the ERMCS tethering complexes, VAPB-PTPIP51 and BAP31-Fis1, also indicated that there was increased interaction between the ER and mitochondria (Fig. 1F,G; Appendix Fig. S1). In addition, the relative increase in ERMCSs in Nup358-deficient cells, as compared to control cells, was also evident from the transmission electron microscopy (TEM) studies (Fig. 1H). Collectively, these results suggest that Nup358 depletion led to increased ER-mitochondria connectivity.

Previous studies have shown a role for Nup358 in the miRNA pathway (Shen et al, 2021; Sahoo et al, 2017). However, disruption of the miRNA pathway via depletion of GW182 (Pfaff and Meister, 2013) did not affect ERMCSs (Fig. EV2A), showing that Nup358 modulates ER-mitochondria contacts independent of its function in the miRNA pathway. Moreover, contrary to Nup358 depletion, depletion of Nup214, another AL-resident nucleoporin, led to a decrease in ERMCSs (Fig. EV2B), indicating that different nucleoporins at the AL might have different roles in the regulation of ER-mitochondria contacts. We also found that the absence of Nup358 did not affect AL integrity (Appendix Fig. S2). Depletion of



Nup358 by siRNA or CRISPR-mediated knockout (KO, Appendix Fig. S3) did not alter mitochondrial mass or DNA (Appendix Fig. S4), suggesting that the enhanced ER-mitochondria connectivity found in Nup358 depleted cells was not a consequence of increased mitochondrial content.

### Increased ER-mitochondria connectivity in Nup358-deficient cells depends on mTORC2

Growth factor signalling results in the recruitment of mTORC2 to ERMCSs, which in turn increases the ER-mitochondria contacts

**Figure 1. AL-resident Nup358 localizes to and restricts ERMCSs.**

(A) Nup358-positive AL are present at ERMCSs. Confocal microscopic image of a U2OS cell displaying the relative localization of indicated proteins; Nup358 for AL (red), PDIA3 for ER (green) and MitoTracker for mitochondria (blue). Arrows show Nup358-positive AL associated with mitochondria. Scale bar, 10  $\mu$ m. The proportion of Nup358-positive AL associated with mitochondria was  $42.8 \pm 6.6\%$  ( $n = 20$  cells). (B) Association of Nup358-positive AL with mitochondria. Stimulated emission depletion (STED) super-resolution microscopy of a Huh7 cell immunostained with the AL marker (Nup358, green) and mitochondria marker (TOM20, red). Arrows indicate Nup358-positive AL associated with mitochondria. Scale, bar 5  $\mu$ m. (C) Nup358, along with other AL-resident nucleoporins like Nup88 and Nup62, is present in the ERMCS fraction. HeLa cells were processed to obtain ERMCS (MAM) fractions, which along with other fractions were analysed for the presence of specific proteins by western blotting. PDIA3, ER marker; TOM20, mitochondrial marker; VAPB, ERMCS marker. (D) Increased ER-mitochondria contacts in Nup358-deficient cells. U2OS cells were initially transfected with control (siControl) or Nup358 (siNup358)-specific siRNA and later co-transfected with RFP-ER (red) and BFP-Mito (pseudo-coloured in green) constructs for labelling ER and mitochondria, respectively. Left: The co-localizing pixels are shown in grey. Scale bar, 10  $\mu$ m. Right top: The extent of Nup358 depletion was evaluated by western blotting with Nup358-specific antibody. Vinculin was used as a loading control. Right bottom: Analysis of individual Manders' overlap coefficient values of RFP-ER with BFP-Mito from siControl and siNup358-treated HeLa cells ( $n = 25$  cells from three independent experiments). Data are mean  $\pm$  SD, Student's  $t$  test.  $P$  value is indicated. (E) Extent of VAPB interacting with PTPIP51 as analysed by co-immunoprecipitation (co-IP) assay. Top: Extent of Nup358 depletion was assessed by western blotting. Bottom left: IP of endogenous PTPIP51 from HeLa cells treated with siControl or siNup358 was performed and the extent of VAPB co-immunoprecipitated was assessed by western blotting. The arrow indicates PTPIP51 bands and asterisk indicates IgG heavy chain cross-reaction. Bottom right: Quantitation of the amount of VAPB associated with PTPIP51 ( $n = 3$  independent experiments). Data are mean  $\pm$  SEM, unpaired Student's  $t$  test.  $P$  value is indicated. (F) Enhanced in situ interaction between VAPB and PTPIP51 in the absence of Nup358. In situ proximity ligation assay (PLA) was performed for assessing the interaction between VAPB and PTPIP51 using specific antibodies. Left: Representative images showing PLA puncta (red) in HeLa cells treated with siControl or siNup358. DNA was stained with Hoechst 33342 (blue). Scale bar, 10  $\mu$ m. Right top: Extent of Nup358 depletion as analysed by western blotting, along with vinculin as loading control. Right bottom: Quantitation of the number of PLA puncta per cell from siControl and siNup358 HeLa cells ( $n = 82$  cells for siControl and 73 cells for siNup358 from three independent experiments). Data are mean  $\pm$  SD, Student's  $t$  test.  $P$  value is indicated. (G) Increased interaction between BAP31 and Fis1 in Nup358-deficient cells. The cells were treated and processed as described in (F). Left: PLA was performed for monitoring the in situ interaction between BAP31 and Fis1, components of another ER-mitochondria tethering complex. Right: Quantitation of the number of PLA puncta per cell from siControl and siNup358 HeLa cells ( $n = 90$  cells for siControl and siNup358 from three independent experiments). Data are mean  $\pm$  SD, Student's  $t$  test.  $P$  value is indicated. (H) Increased contacts between ER and mitochondria in Nup358-deficient cells as assessed by transmission electron microscopy (TEM). Left: TEM images displaying ER-mitochondria contacts in the presence (siControl) and absence of Nup358 (siNup358). Contact sites are highlighted with yellow arrows. Scale bar, 1  $\mu$ m. Right: Quantitative data depicting percentage (%) of mitochondrial surface (perimeter) showing  $\leq 30$  nm proximity with the ER membrane ( $n = 30$  mitochondria for siControl and 35 mitochondria for siNup358-treated conditions). Data are mean  $\pm$  SD, Student's  $t$  test.  $P$  value is indicated. Source data are available online for this figure.

via Akt-mediated phosphorylation of proteins such as PACS2, hexokinase and IP3R (Betz et al, 2013). Therefore, we examined if the increased ER-mitochondria connectivity that we observed in Nup358-deficient cells depends on mTORC2/Akt. Interestingly, siRNA-mediated depletion of Nup358 from HeLa cells led to the activation of mTORC2, as determined by the phosphorylation of its downstream substrate Akt at S473 (Fig. 2A). Activation of mTORC2 was also confirmed in Nup358 KO HeLa cells (Fig. 2B). Exogenous expression of siRNA-resistant human Nup358 in Nup358-deficient cells rescued the increased activation of mTORC2/Akt (Fig. EV3). Interestingly, depletion of Nup358 in *Drosophila* also activated mTORC2/Akt pathway, pointing to a conserved role for Nup358 in regulating this pathway (Fig. EV4). Co-depletion of Rictor, a key subunit of mTORC2, reversed the hyper-phosphorylation of Akt resulting from growth factor (insulin and EGF) signalling in Nup358-depleted HeLa cells (Fig. 2C; Appendix Fig. S5). Knockdown of Nup358 also enhanced phosphorylation of Akt at T308 and activated mTORC1, as indicated by the phosphorylation the mTORC1 substrate S6 at S235/S236, which were almost completely reversed by co-depletion of Rictor (Fig. 2D). This suggests that the hyperactivation of mTORC1 in Nup358-deficient cells primarily depends on mTORC2 (Szwed et al, 2021).

As both mTORC1 and mTORC2 pathways were activated in the absence of Nup358, we tested if the consequent increase in ER-mitochondria contacts in Nup358-deficient cells depended on the mTORC1 and/or mTORC2 pathway. Depletion of Rictor (mTORC2-specific subunit), but not Raptor (mTORC1-specific subunit), reversed the increase in ERMCSs observed in Nup358 knocked down cells (Fig. 2E,F). These results suggest that Nup358 restricts ERMCSs by specifically suppressing mTORC2/Akt activation.

### VAPB-PTPIP51 complex is important for mTORC2/Akt activation upon growth factor stimulation and Nup358 depletion

Previously, it was shown that mTORC2 complex and Akt are recruited to the ERMCSs in response to growth factor signalling (Betz et al, 2013). We confirmed that insulin increased the interaction between VAPB and PTPIP51, as assessed by PLA (Fig. 3A). This increased ER-mitochondria connectivity was mediated by mTORC2, as VAPB-PTPIP51 interactions decreased in the presence of insulin when two of the mTORC2-specific subunits, Rictor and Sin1, were individually depleted (Fig. 3A).

It was already known that ERMCSs are required for proper insulin signalling (Tubbs et al, 2014). To check if specific components at the ERMCSs are involved in the recruitment and/or activation of mTORC2/Akt, different proteins that localize to and regulate ERMCSs such as VAPB/PTPIP51, PACS2, IP3R3 and Mfn2 were depleted in HeLa cells. Interestingly, loss of VAPB and PTPIP51, but not others, significantly attenuated insulin-stimulated mTORC2/Akt activation (Fig. 3B). Under these conditions, the levels of other ERMCS tether proteins remained unchanged (Appendix Fig. S6). Also, the depletion of VAPB and PTPIP51 did not significantly affect the levels of mTORC2 components (Appendix Fig. S7). These results suggested that the VAPB-PTPIP51 complex plays a specific role in growth factor-stimulated activation and/or stabilization of activated mTORC2/Akt.

Based on our observation that the ER-mitochondria tethering complex VAPB-PTPIP51 is involved in growth factor-induced mTORC2/Akt activation, we tested if the enhanced mTORC2 activity in the absence of Nup358 was mediated by VAPB-PTPIP51. Interestingly, depletion of VAPB or PTPIP51

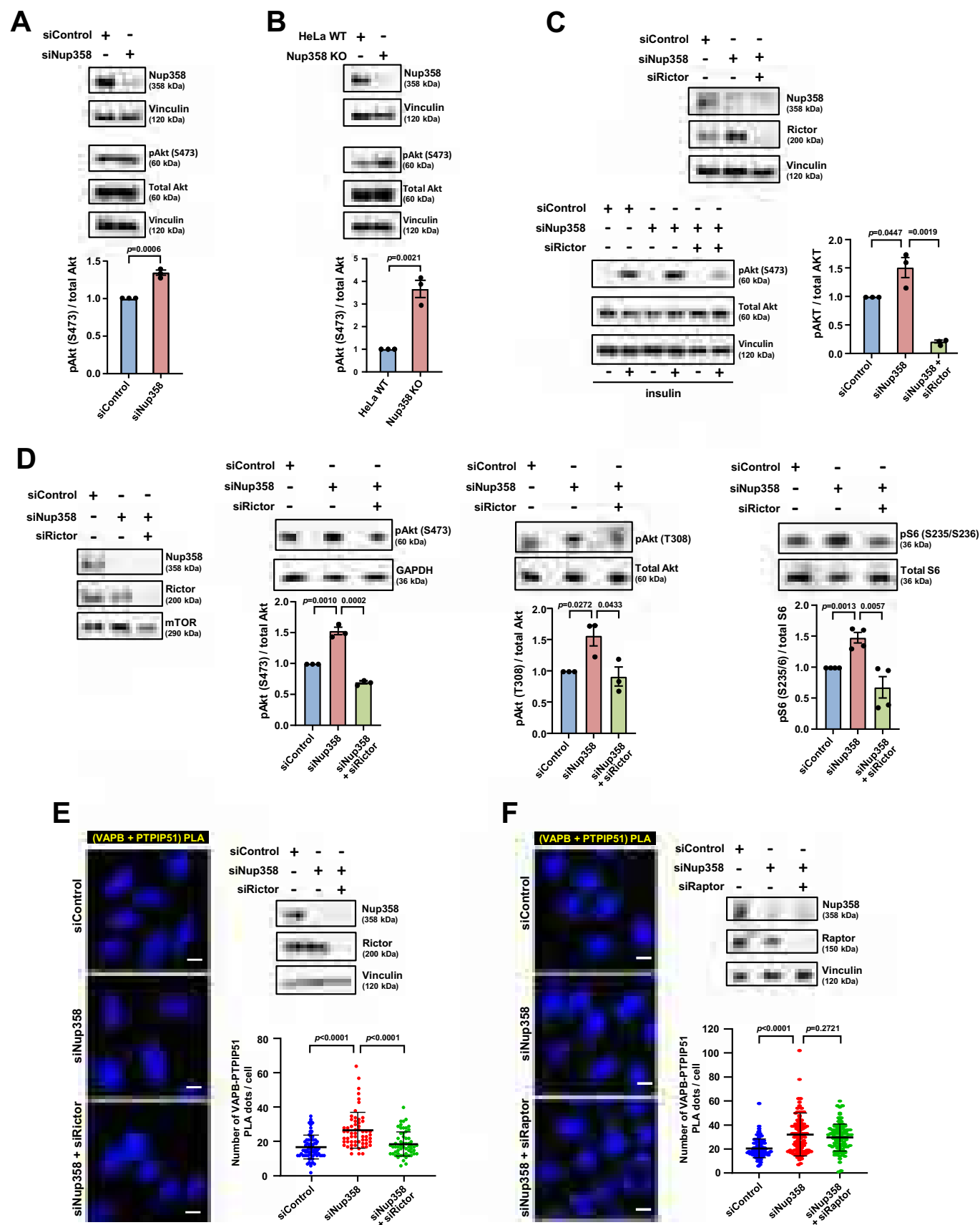




**Figure 2. mTORC2, but not mTORC1, activation is required for enhanced ER-mitochondria contacts in Nup358-downregulated cells.**

(A) Nup358 depletion leads to elevated mTORC2/Akt activation. HeLa cells were treated with Control (siControl) and Nup358 (siNup358) specific siRNA. Top: The cells were then analysed for the extent of mTORC2/Akt activation by western blotting using indicated antibodies. Vinculin was used as a loading control. Bottom: Quantitative representation of the relative levels of pAkt (S473) as compared to total Akt under the above-mentioned experimental conditions ( $n = 3$  independent experiments). Data are mean  $\pm$  SEM, unpaired Student's  $t$  test.  $P$  value is indicated. (B) Increased activation of mTORC2/Akt signalling occurs in Nup358 knockout (KO) HeLa cells as compared to wild-type (WT) cells. Top: Cells were lysed and subjected to western blotting with indicated antibodies. Bottom: Quantitative data depicting the relative level of pAkt (S473) as compared to total Akt under indicated conditions ( $n = 3$  independent experiments). Data are mean  $\pm$  SEM, unpaired Student's  $t$  test.  $P$  value is indicated. (C) Nup358 restricts mTORC2-mediated phosphorylation of Akt at S473 upon growth factor signalling. HeLa cells, transfected with indicated siRNAs, were serum starved for 3 h. The cells were then treated with (+) or without (–) insulin (1 nM for 20 min) and analysed for mTORC2/Akt activation by western blotting. Top: The extent of depletion of indicated proteins analysed by western blotting, with vinculin used as a loading control. Bottom left: The extent of Akt phosphorylation at S473 under indicated conditions was determined. Vinculin was used as a loading control. Bottom right: Quantitative representation of the relative levels of pAkt (S473) as compared to total Akt ( $n = 3$  independent experiments). Data are mean  $\pm$  SEM, unpaired Student's  $t$  test.  $P$  values are indicated. (D) Nup358 depletion leads to mTORC1 activation, which was rescued by co-depletion of Rictor. HeLa cells, treated with indicated specific siRNAs, were analysed for the extent of protein depletion using western blotting, with mTOR being used as a loading control (left). Right top panels: mTORC2 activation was assessed by examining the phosphorylation of Akt at S473. mTORC1 activation was assessed by monitoring the phosphorylation of Akt at T308 and the mTORC1 target S6 at S235 and S236 using western blotting. Lower panels: Quantitation of the relative levels of phosphorylation of specific proteins normalised to GAPDH (for pAkt-S473) or respective total proteins as indicated ( $n = 3$  or 4 independent experiments). Data are mean  $\pm$  SEM, unpaired Student's  $t$  test.  $P$  values are indicated. (E) Co-depletion of Rictor reverses the increase in ER-mitochondria connectivity in Nup358-depleted cells. HeLa cells were treated with specific siRNAs to deplete indicated proteins and analysed for the extent of ERMCSs present using in situ PLA (yellow) with VAPB and PTPIP51 antibodies (left). DNA was stained with Hoechst 33342 (blue). Scale bar, 10  $\mu$ m. The extent of protein depletion (right top) and quantitation of PLA dots per cell (right bottom) are shown ( $n = 72$  cells for siControl; 59 cells for siNup358; 58 cells for siNup358 + siRictor from three independent experiments). Data are mean  $\pm$  SD, Student's  $t$  test.  $P$  values are indicated. (F) The experiment was conducted as described in (E), except that instead of Rictor, as indicated, Raptor-specific siRNA was used. Left: Representative microscopic images displaying the PLA dots (yellow). DNA was stained with Hoechst 33342 (blue). Scale bar, 10  $\mu$ m. The extent of protein depletion (right top) and quantitation of PLA dots per cell (right bottom) are shown ( $n = 90$  cells for siControl; 107 cells for siNup358; 98 cells for siNup358 + siRaptor from three independent experiments). Data are mean  $\pm$  SD, Student's  $t$  test.  $P$  values are indicated. Source data are available online for this figure.

rescued the hyperactivation of mTORC2/Akt signalling in Nup358 knockdown cells (Fig. 3C), indicating that Nup358 restricts mTORC2/Akt activity in a VAPB–PTPIP51-dependent manner. This also suggests that assembly of the VAPB–PTPIP51 complex might be essential for mTORC2/Akt activation and/or stabilization of the activated mTORC2/Akt.

### Binding of Nup358 or mTORC2 to VAPB–PTPIP51 complex may determine the extent of ER-mitochondria connectivity

To test if the VAPB–PTPIP51 tethering complex physically interacts with the mTORC2 complex for regulation of the latter, a co-immunoprecipitation assay was performed. Myc-VAPB and HA-PTPIP51 co-immunoprecipitated with FLAG-mTOR (Fig. 4A). Moreover, specific endogenous interaction of mTOR and the mTORC2-specific subunit Rictor with VAPB was confirmed by PLA (Fig. 4A), whereas no interaction between VAPB and the mTORC1-specific subunit Raptor was detected (Fig. EV5). Collectively, the data reveal a specific physical interaction of mTORC2 complex with VAPB, and possibly with the VAPB–PTPIP51 complex.

So far, our data indicate that the ERMCS tethering complex VAPB–PTPIP51 is important for growth factor-induced mTORC2/Akt activation and, thereby, possibly increases the connectivity between ER and mitochondria. The results also suggest that Nup358 restricts ERMCSs by suppressing mTORC2/Akt activation (Fig. 2E). Interestingly, Nup358 also interacts with VAPB and PTPIP51, as determined by co-IP and PLA (Fig. 4B). Given that the associations of Nup358 and mTORC2 with the VAPB–PTPIP51 complex had opposing effects, we hypothesized that perhaps Nup358, when present at the ERMCSs, prevents the association of mTORC2 with the VAPB–PTPIP51 complex, thereby reducing mTORC2/Akt activity and ER-mitochondria connectivity. In other words, Nup358 may inhibit the interaction between mTORC2

complex and VAPB–PTPIP51, in the absence of growth factor signalling. On the contrary, the Nup358-mediated inhibition of mTORC2 association with VAPB–PTPIP51 complex should be relieved in the presence of growth factor signalling, thereby enhancing mTORC2 activity and ER-mitochondria connectivity. To test this possibility, the kinetics of complex formation between Nup358, mTOR, Rictor and Sin1 with VAPB was monitored by PLA in the presence and absence of insulin. Consistent with the hypothesis, as compared to the untreated control condition, insulin treatment resulted in decreased VAPB–Nup358 interaction, but increased VAPB–mTOR, VAPB–Rictor and VAPB–Sin1 association (Fig. 4C). These results indicated a counteracting role for Nup358 and mTORC2 in regulating the extent of ER-mitochondria connectivity during growth factor signalling, possibly mediated by their mutually exclusive interaction with the VAPB–PTPIP51 tethering complex at ERMCSs.

In an attempt to understand how insulin mediates the decreased Nup358–VAPB interaction, we explored a role for PI3 kinase—a well-known mediator of insulin/growth factor signalling (Saxton and Sabatini, 2017). Towards this, cells were treated with insulin in the presence or absence of wortmannin, a PI3 kinase-specific inhibitor, and the interaction between Nup358 and VAPB was assessed using PLA. Insulin decreased Nup358–VAPB interaction as compared to that in untreated control; however, wortmannin did not have any effect on insulin's ability to decrease the interaction (Fig. 4D). These results suggest that Nup358–VAPB interaction may be modulated by growth factor signalling in a PI3 kinase-independent manner.

### Ectopic expression of GSK3 $\beta$ rescues increased ER-mitochondria connectivity caused due to Nup358 depletion

Growth factor signalling has been shown to inhibit GSK3 $\beta$  (Cohen and Frame, 2001). GSK3 $\beta$  independently has been reported

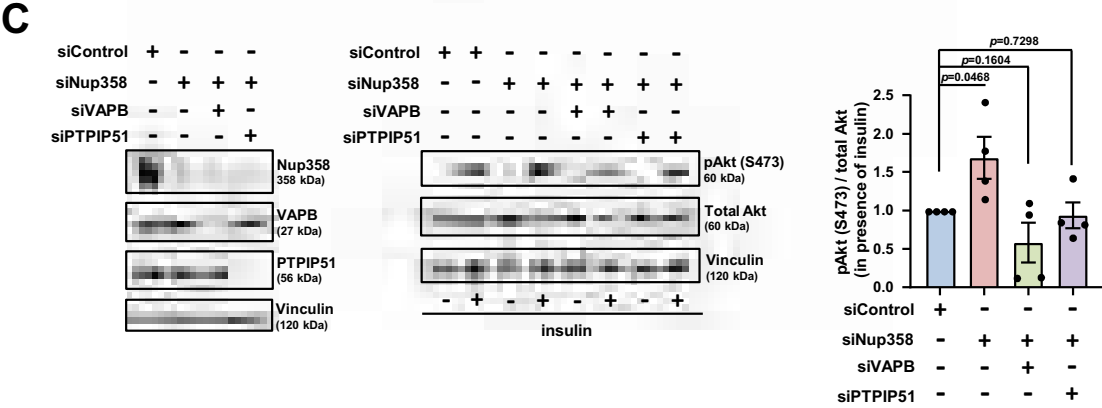
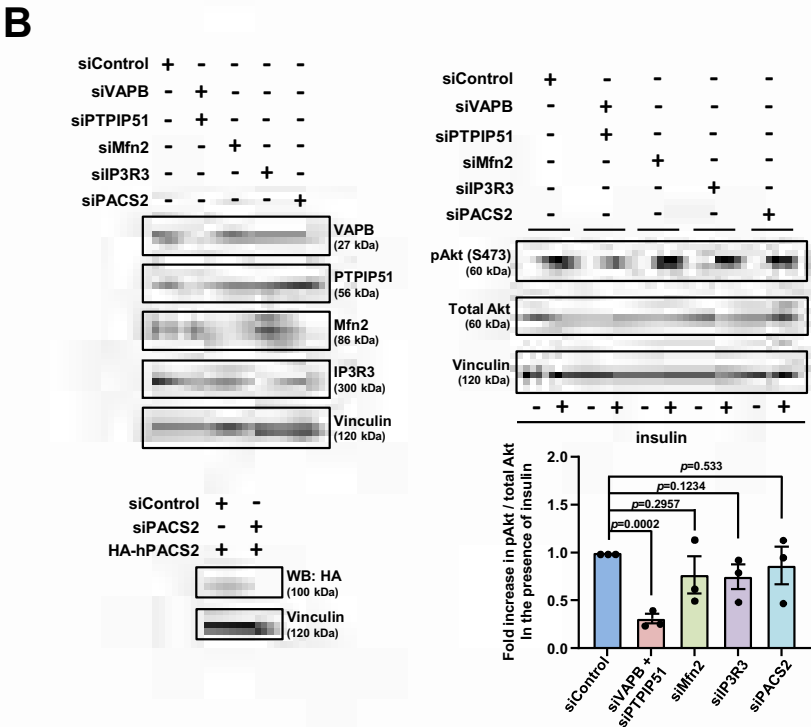
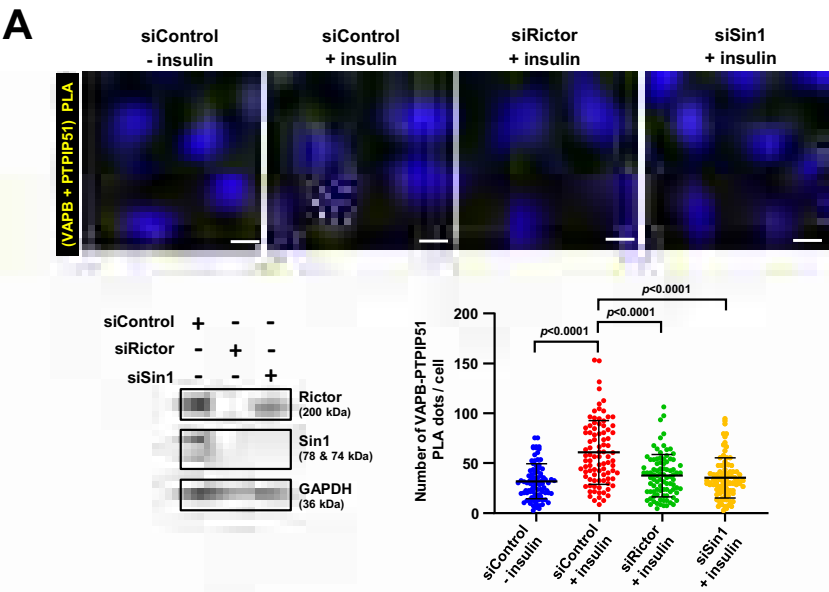




**Figure 3. VAPB–PTPIP51 tethering complex contributes to increased mTORC2 activation mediated by insulin signalling and caused by Nup358 depletion.**

(A) Insulin-dependent increase in VAPB–PTPIP51 interaction is dependent on mTORC2. HeLa cells were transfected with control (siControl), Rictor (siRictor) or Sin1 (siSin1). Cells were later serum starved for 12 h and treated with (+) or without (–) 2 nM insulin for 20 min. Top: Cells were fixed and processed for PLA using VAPB and PTPIP51-specific antibodies (yellow dots). DNA was stained with Hoechst 33342 (blue). Scale bar, 10  $\mu$ m. Bottom left: Depletion of Rictor and Sin1 was monitored by western blotting using specific antibodies GAPDH was used as loading control. Note that Rictor depletion led to co-depletion of Sin1 as reported earlier (Yang et al, 2006). Bottom right: Quantitation of PLA dots per cell are shown ( $n = 90$  cells for siControl, siRictor or siSin1 condition from three independent experiments). Data are mean  $\pm$  SD, Student's  $t$  test.  $P$  values are indicated. (B) Depletion of VAPB/PTPIP51 interferes with growth factor-stimulated activation of mTORC2/Akt signalling. HeLa cells were depleted of different proteins using specific siRNAs as mentioned. Left top: The extent of depletion was verified by western blotting using specific antibodies. Left bottom: The ability of PACS2 siRNA to deplete the human PACS2 was confirmed by co-transfecting HeLa cells with control (siControl) or PACS2 (siPACS2) siRNA along with HA-human PACS2 construct. The expression of HA-PACS2 was monitored by western blotting (WB) with a HA-specific antibody. Vinculin was used as a loading control. Right top: HeLa cells depleted of indicated proteins were serum starved for 3 h, and later treated with (+) or without (–) insulin (1 nM) for 20 min. The cells were then analysed for the specific proteins by western blotting. Right bottom: Quantitative analysis of the relative phosphorylation of Akt at S473 under the described conditions ( $n = 3$  independent experiments). Data are mean  $\pm$  SEM, unpaired Student's  $t$  test.  $P$  values are indicated. (C) Hyperactivation of mTORC2/Akt signalling upon Nup358 loss depends on the VAPB–PTPIP51 tethering complex. HeLa cells were depleted of indicated proteins and serum starved for 3 h. The cells were then treated with (+) or without (–) insulin (1 nM) for 20 min. Cells were analysed for insulin-induced mTORC2/Akt activation. Left: Western analysis to monitor the extent of protein depletion by siRNAs. Middle: Western blot showing the extent of phosphorylation of Akt at Ser473, along with total Akt levels, in the described conditions. Vinculin was used as a loading control. Right: Quantitative data depicting the change in a relative amount of pAkt (S473) under the indicated conditions ( $n = 4$  independent experiments). Data are mean  $\pm$  SEM, unpaired Student's  $t$  test.  $P$  values are indicated. Source data are available online for this figure.

to reduce ERMCSs via disruption of the interaction between VAPB and PTPIP51 (Stoica et al, 2016, 2014). We found that Nup358 depletion led to inhibition of GSK3 $\beta$ , evident by the increase in phosphorylation of GSK3 $\beta$  at S9 as compared to control cells, which could be reversed by co-depletion of Rictor (Fig. 5A). Further we assessed if this inhibition of GSK3 $\beta$  activity is responsible for increased connectivity between ER and mitochondria. Nup358 depletion from GFP-control expressing cells showed increased ERMCSs compared to control siRNA-treated cells. Interestingly, GSK3 $\beta$ -GFP expression reversed the increase in the ER–mitochondria connectivity that was observed in GFP-control expressing Nup358-deficient cells (Fig. 5B). Moreover, co-immunoprecipitation and proximity ligation assays revealed that Nup358 specifically interacts with GSK3 $\beta$  (Fig. 5C). Collectively, these results support the conclusion that in Nup358-deficient cells increased ER–mitochondria connectivity primarily results from decreased GSK3 $\beta$  activity.

### Insulin-dependent remodelling of ERMCSs is abrogated in Nup358-deficient cells

Based on the results so far, it appears that Nup358, possibly along with GSK3 $\beta$ , attenuates the growth factor-dependent increase in ER–mitochondrial connectivity. This requires Nup358-dependent restriction of the mTORC2 activity, maybe at the ERMCS, which could lead to increased GSK3 $\beta$  activity, thereby decreasing ERMCSs. This predicts that in the absence of Nup358, insulin-dependent stabilization of ERMCSs could be significantly more than that in the control cells. To test this, insulin-dependent remodelling of ERMCSs was monitored in control and Nup358 siRNA-treated cells. In control siRNA-transfected cells, insulin treatment led to a significant increase in the ERMCSs (Fig. 5D). In Nup358-depleted cells, even in the absence of insulin, ERMCSs were increased as compared to siControl cells without insulin treatment (Fig. 5D). Interestingly, insulin did not further enhance the contacts between ER and mitochondria in Nup358-depleted cells, as compared to insulin-untreated Nup358-deficient cells (Fig. 5D). These results showed that absence of Nup358 leads to increase in the ERMCSs in an insulin-independent manner, indicating that growth factor signalling mediated removal of Nup358 possibly from the contact sites is sufficient to achieve increased ERMCSs.

### A region of Nup358 encompassing 1949–2786 amino acid residues is sufficient to interact with VAPB/PTPIP51, restrict mTORC2 activity and reduce ERMCSs

Nup358 is a large nucleoporin with multiple domains (Fig. 6A). Different fragments of Nup358 were assessed for their ability to interact with VAPB/PTPIP51. Co-immunoprecipitation assays showed that a fragment of Nup358—Nup358-MC1 (1949–2786 aa)—possessing two Ran-binding domains (RBD2 and RBD3), a kinesin/dynein-binding domain (KBD/DBD) and internal repeats (IR), was sufficient to interact with VAPB and PTPIP51 (Fig. 6A,B). In vitro interaction studies using purified recombinant proteins indicated that PTPIP51 directly interacts with Nup358-MC2 (2012–2771 aa) (Fig. 6C). Moreover, ectopic expression of Nup358-MC1 resulted in attenuation of mTORC2-dependent Akt phosphorylation as compared to GFP-control expressing cells (Fig. 6D). In addition, expression of Nup358-MC1 was sufficient to rescue the increased mTORC2/Akt activation caused due to Nup358 depletion (Fig. 6E). Nup358-MC1 expression also decreased the abundance of ERMCSs in cells as assessed by VAPB–PTPIP51 PLA (Fig. 6F). Collectively, these results suggest that Nup358-MC1 is sufficient to interact with VAPB–PTPIP51 and restrict mTORC2/Akt-dependent enhancement of ERMCSs.

Based on our study, we propose the following working model (Fig. 7). When growth factors are absent, interaction of Nup358 with VAPB–PTPIP51 complex restricts mTORC2/Akt access to the ERMCS tether, thus activating GSK3 $\beta$ , leading to destabilization of the ER–mitochondria contacts. Upon activation of growth factor signalling, through an unknown mechanism, Nup358 may be removed from the ERMCS, allowing mTORC2/Akt to get recruited to the preformed VAPB–PTPIP51 complex, and further stabilize the ERMCS though a mechanism involving inhibitory phosphorylation of GSK3 $\beta$ . In other words, fine tuning of ERMCSs is achieved by a reciprocal binding of Nup358 or mTORC2 complex to the VAPB–PTPIP51 tethering complex and regulating GSK3 $\beta$ -dependent destabilization of the VAPB–PTPIP51 tethering complex.

## Discussion

Our studies provide new insights into the potential functions of the underexplored organelle AL. We find that Nup358-positive AL are

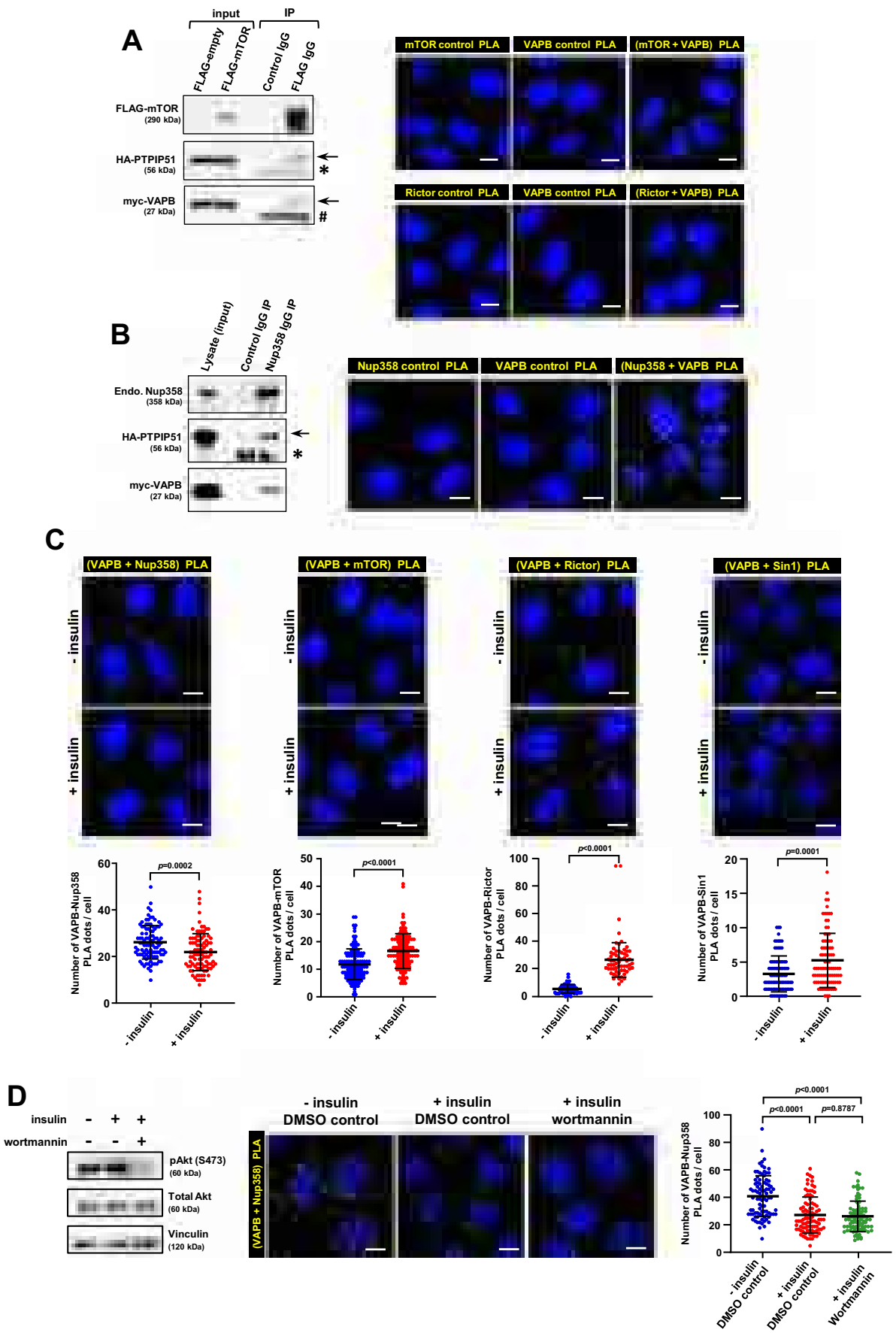


**Figure 4. Growth factor signalling modulates reciprocal binding of mTORC2 and Nup358 to VAPB-PTPIP51 complex.**

(A) mTORC2 interacts with VAPB and PTPIP51. Left: HEK293T cells expressing FLAG-control (Empty vector) or FLAG-mTOR along with HA-PTPIP51 and myc-VAPB were subjected to immunoprecipitation (IP) using FLAG-specific antibodies. Presence of HA-PTPIP51 and myc-VAPB in the IP samples was examined by western analysis. Arrow indicates HA-PTPIP51 or myc-VAPB as shown; \* indicates IgG heavy chain and # indicates IgG light chain cross-reaction. Right: In situ interaction of VAPB with mTOR and Rictor. Interaction between endogenous VAPB with mTOR (top) and the mTORC2-specific subunit Rictor (bottom) was confirmed by in situ PLA in HeLa cells. An increase in the number of PLA dots (yellow) was observed with mTOR or Rictor in combination with VAPB antibodies, as compared to single-antibody controls (mTOR, Rictor or VAPB alone). DNA was stained with Hoechst 33342 (blue). Scale bar, 10  $\mu$ m. (B) Nup358 interacts with PTPIP51 and VAPB. Left: HEK293T cells expressing HA-PTPIP51 and myc-VAPB were subjected to endogenous Nup358 IP (Nup358 IgG IP) using specific antibodies. Presence of HA-PTPIP51 and myc-VAPB was examined by western analysis of the IP samples. Rabbit IgG (Control IgG IP) was used as control. Arrow indicates HA-PTPIP51 and \* indicates IgG heavy chain cross-reaction. Right: Interaction between endogenous Nup358 and VAPB was confirmed by in situ PLA using specific antibodies in HeLa cells. Nup358 or VAPB antibody alone was used as control. DNA was stained with Hoechst 33342 (blue). Scale bar, 10  $\mu$ m. (C) Reciprocal binding of Nup358 and mTORC2 to VAPB is modulated by growth factor signalling. HeLa cells were serum starved for 3 h (12 h for VAPB-Sin1 PLA experiment). Cells were later treated with (+) or without (–) insulin (1–2 nM) for 20 min. Representative images showing the extent of the interaction between Nup358 and VAPB (top first), mTOR and VAPB (top second), Rictor and VAPB (top third) or Sin1 and VAPB (top fourth) as assessed by PLA (yellow dots). DNA was stained with Hoechst 33342 (blue). Scale bar, 10  $\mu$ m. Bottom panels: Quantitative data depicting the number of PLA dots per cell under the indicated scenario. Number of Nup358–VAPB PLA dots per cell ( $n = 98$  cells for insulin-untreated and  $n = 97$  for insulin-treated condition from three independent experiments), number of mTOR–VAPB PLA dots per cell ( $n = 131$  cells for insulin-untreated and 125 cells for the insulin-treated condition from three independent experiments), number of Rictor–VAPB PLA dots per cell is shown ( $n = 67$  cells for insulin-untreated and 61 cells for insulin-treated condition from three independent experiments) and Sin1–VAPB PLA dots per cell ( $n = 90$  cells, from three independent experiments) is shown. Data are mean  $\pm$  SD, Student's *t* test. *P* values are indicated. (D) PI3 kinase activity is not required for insulin-dependent decrease in the interaction between Nup358 and VAPB. As indicated, HeLa cells were serum starved for 12 h, post which they were treated without (–) or with (+) the PI3 kinase inhibitor wortmannin (2.5  $\mu$ M). The cells were then left untreated (–) or treated with 2 nM insulin for 20 min. Left: Cells were lysed and analysed for different proteins as shown. Middle: Cells were subjected to PLA for monitoring the in situ interaction between Nup358 and VAPB (yellow dots). Scale bar, 10  $\mu$ m. Right: Quantitation of PLA dots per cell for different conditions is shown ( $n = 90$  cells for each indicated condition from three independent experiments). Data are mean  $\pm$  SD, Student's *t* test. *P* values are indicated. Source data are available online for this figure.

often present at the contact sites between ER and mitochondria, which are known to play a pivotal role in cellular homeostasis by regulating critical processes such as inter-organelle transfer of  $\text{Ca}^{2+}$  and lipids, mitochondrial energetics, cellular metabolism, apoptosis and autophagy. Depletion of Nup358 increased the contacts between ER and mitochondria via enhanced activation of mTORC2/Akt and inhibition of the Akt substrate GSK3 $\beta$ . Thus, the findings of our study highlight the importance of the AL-resident nucleoporin Nup358 in modulating the ER–mitochondria connectivity.

How does Nup358, which interacts with both VAPB and PTPIP51, eventually disrupt the VAPB–PTPIP51 interaction to decrease the ER–mitochondria connectivity? One possibility is that Nup358 somehow increases the accessibility and/or activity of GSK3 $\beta$ , which is known to disrupt VAPB–PTPIP51 interactions (Stoica et al, 2014, 2016). The other possibility is that Nup358 may make independent complexes with VAPB and PTPIP51 to achieve the disruption of ERMCSs. Understanding the molecular details requires further investigation.

While investigating the role of Nup358-positive AL in cellular functions, we also uncovered a mechanism by which ERMCS components regulate mTORC2/Akt activation in response to growth factor signalling. Earlier studies have shown that growth factors can stimulate the recruitment of mTORC2/Akt to ERMCSs, leading to Akt-mediated phosphorylation of proteins at the contacts, thereby regulating the dynamics and functions of ERMCSs (Betz et al, 2013). The mTORC2/Akt complex has been shown to be present at multiple intracellular locations, but the site and mechanism of its activation upon growth factor signalling remain undetermined (Ebner et al, 2017; Fu and Hall, 2020). Our studies indicate that the ERMCS tethering complex VAPB–PTPIP51 is important for the activation of the mTORC2/Akt pathway, possibly via its recruitment to the ERMCSs. This is consistent with an earlier report that illustrated the significance of the ERMCS integrity for insulin signalling (Tubbs et al, 2014; Tubbs and Rieusset, 2017). However, we cannot rule out the

possibility that mTORC2 activation could occur elsewhere (for example, at the plasma membrane or endosomes (Fu and Hall, 2020; Knudsen et al, 2020; Szwed et al, 2021)), and the VAPB–PTPIP51 complex may be required to stabilize the activated mTORC2/Akt at the ERMCSs. Nevertheless, our study highlights the importance of VAPB–PTPIP51 tethering complex in regulating the growth factor-dependent activity of mTORC2.

Our results suggest a molecular interplay between Nup358 and mTORC2/Akt at the ERMCSs for regulating ERMCS dynamics. A mutually exclusive binding of Nup358 and mTORC2 complex to the ERMCS tethering complex VAPB–PTPIP51 appears to regulate the ERMCSs, and, perhaps their functions, in response to growth factors. Localization of Nup358 to the ERMCSs, as indicated by the interaction between Nup358 and VAPB, was dependent on insulin signalling. Interestingly, this was independent of the PI3 kinase activity. Currently, the mechanistic details of how Nup358–VAPB interaction is reduced upon insulin signalling remain unresolved.

It is well-established that growth factor signalling can activate Akt, which in turn can inactivate GSK3 $\beta$  through inhibitory phosphorylation of the S9 residue (Cohen and Frame, 2001; Frame and Cohen, 2001). Earlier, it has been shown that GSK3 $\beta$  destabilizes the ERMCSs by disrupting the VAPB–PTPIP51 interaction (Stoica et al, 2016; Paillusson et al, 2016; Stoica et al, 2014). Independently, growth factor signalling, through the mTORC2/Akt activity, is shown to stabilize ERMCSs (Betz et al, 2013). Our results suggest that one of the main mechanisms by which the growth factor-induced stabilization of ERMCSs is achieved is through mTORC2/Akt-mediated suppression of GSK3 $\beta$ .

How is Nup358 function at the ERMCSs regulated? Interestingly, in Nup358-depleted cells, ER–mitochondria connectivity is significantly increased even in the absence of insulin signalling. Moreover, insulin failed to enhance the ERMCSs further in Nup358-deficient cells. This indicates that one of the mechanisms by which growth factors may stabilize ERMCSs is through the removal of Nup358 from the contacts. This allows mTORC2/Akt

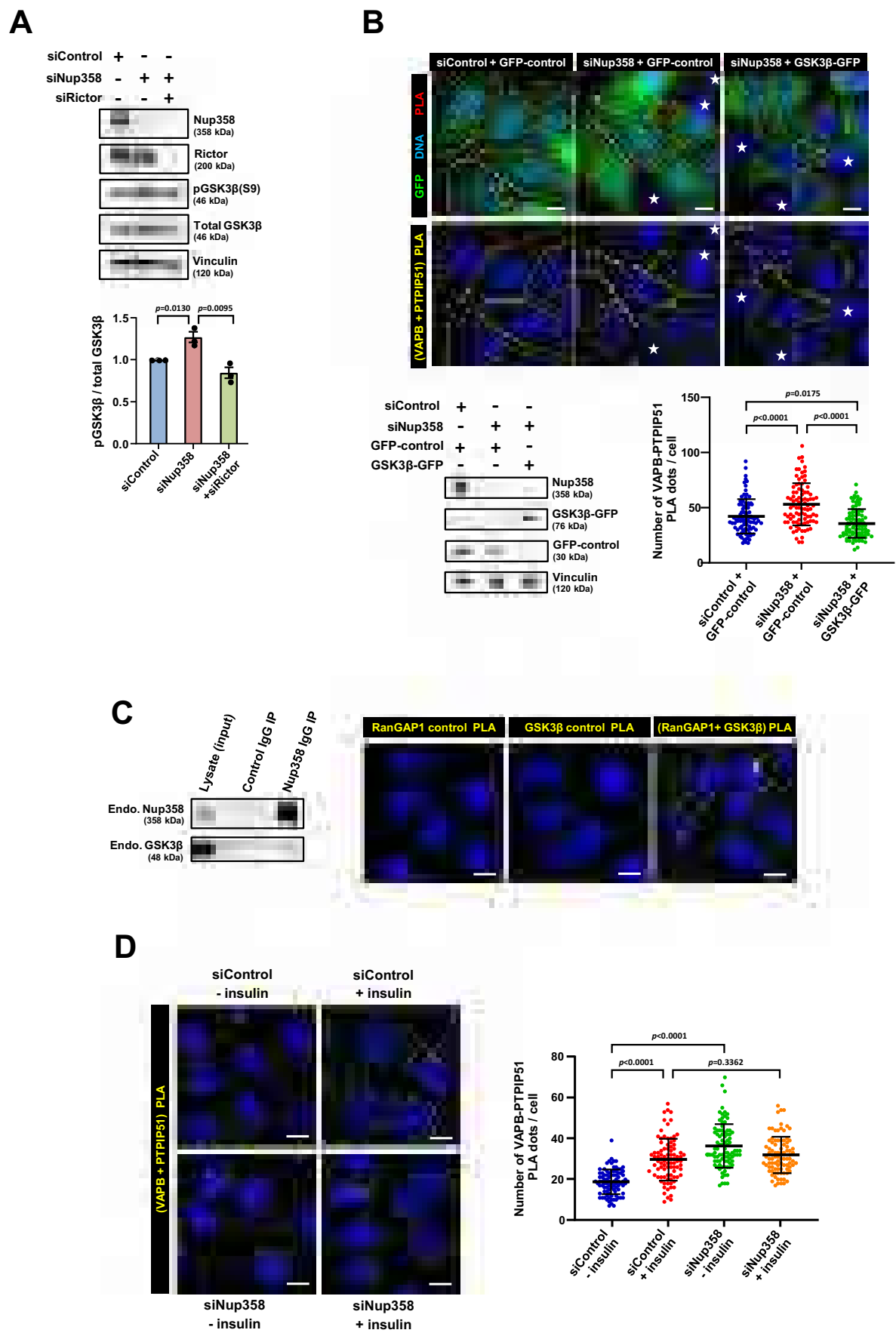


**Figure 5. Inhibition of GSK3 $\beta$  is required for increase in ER-mitochondria contacts upon Nup358 depletion.**

(A) Nup358 depletion leads to increased inhibitory phosphorylation of GSK3 $\beta$  (S9), which could be reversed by co-depletion of the mTORC2-specific subunit Rictor. Cells were transfected with siControl, siNup358 or siNup358 along with siRictor. Top: Cells were lysed and checked for the depletion and the relative levels of phospho-GSK3 $\beta$  (S9) as compared to total GSK3 $\beta$  and Vinculin (loading control) by western blotting. Bottom: Quantitative data depicting the change in a relative amount of pGSK3 $\beta$  (S9) under the indicated conditions ( $n = 3$  independent experiments). Data are mean  $\pm$  SEM, unpaired Student's  $t$  test.  $P$  values are indicated. (B) Ectopic expression of GSK3 $\beta$  reverses the enhanced ER-mitochondria connectivity found in Nup358-depleted cells. Stable tetracycline-inducible HeLa cell lines expressing GFP-control or GSK3 $\beta$ -GFP were transfected with either control (siControl) or Nup358-specific (siNup358) siRNAs as depicted. The medium was then replaced with 10% FBS-containing medium with doxycycline to induce GFP or GSK3 $\beta$ -GFP for 24 h. Top: PLA was performed for examining the interaction between VAPB and PTPIP51 (yellow dots). DNA was stained with Hoechst 33342 (blue). Scale bar, 10  $\mu$ m. \*Indicates low or no GFP-expressing cells. Cell boundaries are demarcated with dotted lines. Bottom left: Nup358 depletion and GFP-control or GSK3 $\beta$ -GFP expression was monitored by western blotting. Bottom right: Quantitation of PLA dots per cell (GFP-positive) for different indicated conditions is shown ( $n = 90$  cells for each indicated condition from three independent experiments). Data are mean  $\pm$  SD, Student's  $t$  test.  $P$  values are indicated. (C) Nup358 interacts with GSK3 $\beta$ . Left: Endogenous (Endo.) Nup358 was immunoprecipitated (IP) from HEK293T cells using specific antibodies (Nup358 IgG IP) and Rabbit IgG was used as a negative control. The IP samples were analysed for the presence of indicated proteins by western blotting. Right: Interaction between endogenous RanGAP1 and GSK3 $\beta$  was examined by in situ PLA using specific antibodies in HeLa cells. Here, RanGAP1 was used as a surrogate for Nup358, as RanGAP1 is known as a strong binding partner that colocalizes with Nup358 at the nuclear envelope and AL (Joseph et al, 2004; Sahoo et al, 2017). RanGAP1 or GSK3 $\beta$  antibody alone was used as control. PLA dots are indicated in yellow colour. DNA was stained with Hoechst 33342 (blue). Scale bar, 10  $\mu$ m. (D) Nup358-deficient cells show increased ER-mitochondria contacts even in the absence of insulin. HeLa cells transfected with siControl or siNup358 for 60 h were serum starved for 12 h, post which they were treated with (+) or without (–) 2 nM insulin for 20 min. Left: Cells were processed for PLA to monitor the interaction between VAPB and PTPIP51 (yellow dots). Right: Quantitation of PLA dots per cell is shown [ $n = 90$  cells for siControl (– insulin), siControl (+ insulin), siNup358 (– insulin) or siNup358 (+ insulin) from three independent experiments]. Data are mean  $\pm$  SD, Student's  $t$  test.  $P$  values are indicated. Source data are available online for this figure.

recruitment to the ERMCS and inhibition of GSK3 $\beta$  by Akt-mediated S9 phosphorylation. Our study also shows that GSK3 $\beta$  functions downstream to Nup358, as ectopic expression of GSK3 $\beta$  was sufficient to negate the increased ERMCSs in Nup358-depleted cells. Nup358 interacts with GSK3 $\beta$  and may be required for its recruitment to and/or activation at the ERMCSs. Nup358 depletion may result in almost complete inactivation of GSK3 $\beta$  and consequently a maximum increase in the ERMCSs, and therefore, insulin may not further stabilize ER-mitochondria connectivity in the absence of Nup358. Understanding the mechanistic details of how the molecular interplay between VAPB-PTPIP51 complex, mTORC2/Akt, Nup358 and GSK3 $\beta$  are functionally linked with ERMCS remodelling requires future investigation.

In light of the new findings, it is unclear why AL components such as Nup358 are involved in regulating cellular signalling and cytoplasmic processes. It is possible that there exists a crosstalk between nucleocytoplasmic transport (NCT) and cytoplasmic signalling at the ERMCSs. Based on the ultra-structural studies, an interconnection between the nuclear envelope and AL has been proposed (Kessel, 1992). Moreover, the budding of nucleoporin-containing structures and fusion of them with pre-existing AL in the cytoplasm have been observed (Sahoo et al, 2017). The possible interplay between NCT and AL is particularly interesting in light of the implications of dysregulated NCT in the pathogenesis of neurodegenerative diseases (Ding and Sepehrmanesh, 2021). The newly identified role of AL-resident nucleoporins in controlling events other than NCT might be relevant in understanding the pathophysiology of neurodegenerative diseases.

From this study, it is evident that Nup358 and GSK3 $\beta$  function together to destabilize the ERMCSs. Impaired ER-mitochondria connection and its functions are implicated in a wide range of neurodegenerative diseases (Markovinic et al, 2022). Moreover, increased GSK3 $\beta$  activity appears to be a common feature of most of these diseases (Wang et al, 2023). GSK3 $\beta$  has been shown to be activated upon expression of ALS/FTD-linked genes TDP-43 and FUS, leading to decreased ER-mitochondria connectivity and a concomitant decrease in the levels of mitochondrial Ca<sup>2+</sup> (Stoica et al, 2014, 2016), potentially altering the mitochondrial bioenergetics. Interestingly, mice lacking Nup358 expression in Thyl<sup>+</sup>-

motor neurons develop ALS-like symptoms (Cho et al, 2017). The finding that Nup358 regulates the ERMCSs through GSK3 $\beta$  opens up avenues to look into the possible mechanisms of how nucleoporin dysregulations impinge on multiple neurodegenerative diseases.

Nup358 mutations are linked with acute necrotizing encephalopathy 1 (ANE-1), a disease condition triggered by viral infection, and characterized by lesions in specific regions within the brain of affected individuals (Neilson et al, 2009; Neilson, 2010). The pathophysiology includes cytokine storm, exemplified by increased levels of pro-inflammatory cytokines such as INF- $\alpha$  and IL-6 in the serum and cerebrospinal fluid of the patients (Levine et al, 2020). Impairment in the miRNA-mediated translation regulation by Nup358 might contribute to the development of ANE-1 (Deshmukh et al, 2021; Shen et al, 2021). However, dysregulation of the functions identified from our studies for the AL-associated Nup358 may provide an additional/alternative mechanism for the pathogenesis of ANE-1.

In summary, our results suggest that AL structures are often present at the ERMCSs, and one of the AL-resident nucleoporins, Nup358, can restrict ERMCSs via mTORC2/Akt inhibition and GSK3 $\beta$  activation. Our findings also highlight a role for the ERMCS tethering complex—VAPB-PTPIP51—in the recruitment and activation of mTORC2/Akt in response to growth factors. Alternatively, mTORC2/Akt that is activated elsewhere in response to growth factor signalling may be recruited to and stabilized at the VAPB-PTPIP51 complex. Irrespective of the site of activation, it appears that the association of an active mTORC2 complex with the ERMCS tether VAPB-PTPIP51 further increases the contacts between ER and mitochondria possibly via phosphorylation of contact site proteins (Betz et al, 2013) and/or inhibiting GSK3 $\beta$ -mediated disruption of VAPB-PTPIP51 tethering complex (Stoica et al, 2016, 2014; Paillusson et al, 2016). Our study thus reveals a hitherto unidentified role for the AL-associated nucleoporin Nup358, in the regulation of growth factor-mediated ERMCS remodelling as described above. Further studies may shed light on the potential implication of this finding in understanding the mechanisms involved in neurodegenerative diseases and ANE-1.



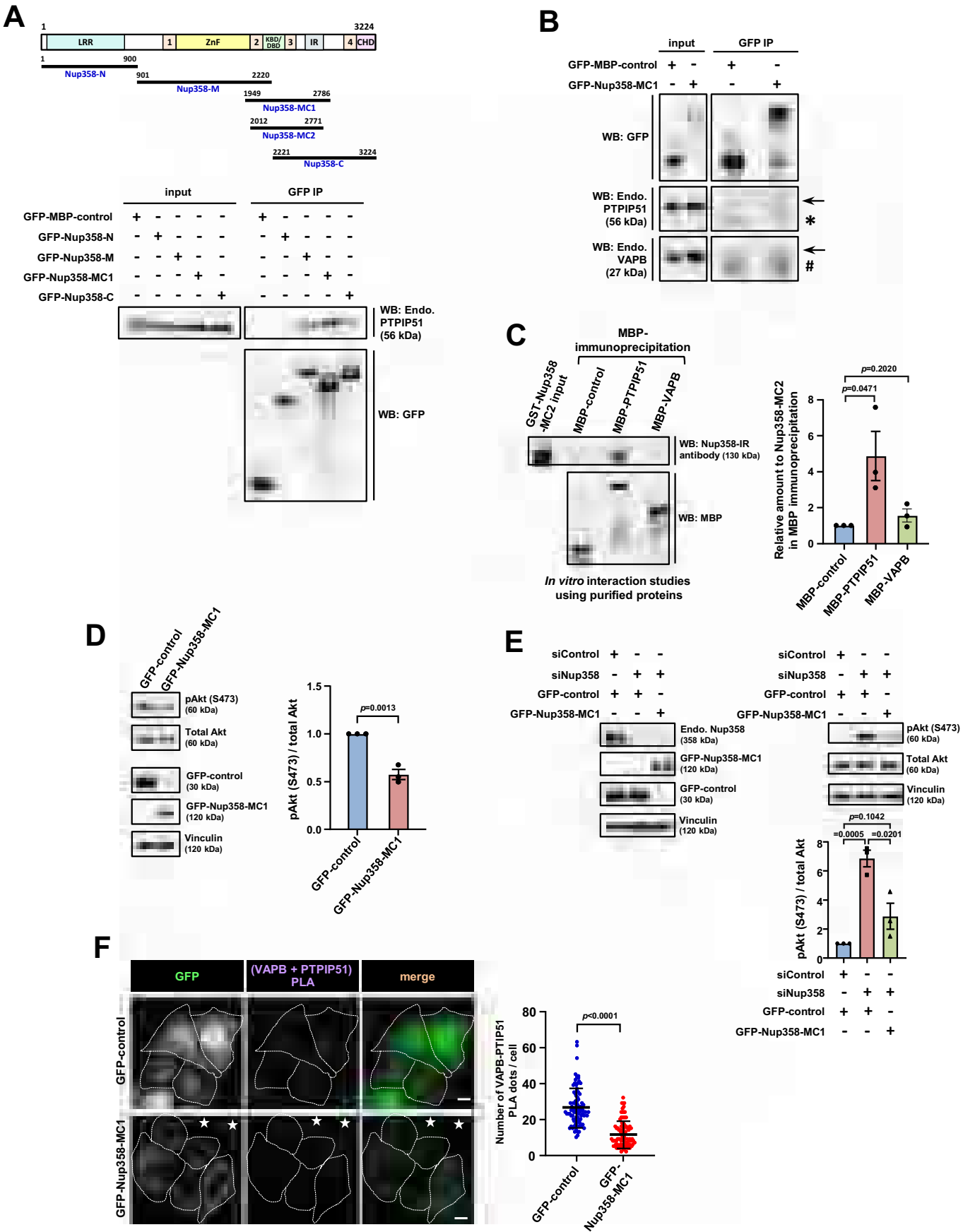




**Figure 6. A region of Nup358 encompassing 1949 to 2786 amino acid residues is sufficient to restrict mTORC2 activity and ERMCSs.**

(A) A fragment of Nup358 encompassing RBD2, KBD/DBD, RBD3 and IR (Nup358-MC1; 1949–2786 amino acid residues) is sufficient to interact with PTPIP51. Domain architecture and fragments of Nup358 used in this study. LRR leucine-rich region, 1,2,3,4 RanGTP-binding domains (RBDs), ZnF zinc-finger domains, KBD/DBD kinesin-binding domain/dynein-binding domain, IR internal repeats, CHD cyclophilin-homology domain. Amino acid residues are numbered. Bottom: HEK293T cells expressing GFP-MBP-control or GFP-tagged version of different Nup358 fragments as indicated were subjected to IP using GFP-specific antibodies. The IP samples were probed for the presence of endogenous PTPIP51 by western blotting. (B) Nup358-MC1 is sufficient to interact with both VAPB and PTPIP51. HEK293T cells expressing GFP-MBP-control or GFP-Nup358-MC1 were subjected to IP using GFP-specific antibodies. The IP samples were probed for the presence of endogenous PTPIP51 and VAPB by western blotting. Arrow indicates the bands corresponding to PTPIP51 and VAPB. \* and # indicate bands corresponding to antibody heavy and light chains, respectively. (C) Nup358-MC2 directly interacts with PTPIP51. Purified GST-tagged Nup358-MC2 (2012 to 2771 amino acid residues) was incubated with MBP-control, MBP-PTPIP51 or MBP-VAPB. The MBP proteins were immunoprecipitated with specific antibodies. Left: The IP samples were analysed for the presence of Nup358-MC2 by western blotting (WB) Nup358-MC2 was detected using an antibody raised against the IR region (Joseph et al, 2004). Right: Quantitative analysis showing the relative levels of Nup358-MC2 detected in the indicated MBP IP samples ( $n = 3$  independent experiments). Data are mean  $\pm$  SEM, Student's  $t$  test.  $P$  values are indicated. (D) Nup358-MC1 is sufficient to restrict mTORC2/Akt signalling. Left: HeLa cells stably expressing inducible GFP-control or GFP-Nup358-MC1 were induced with doxycycline, lysed and subjected to western blotting using indicated antibodies. Right: Quantitative representation depicting the relative levels of pAkt normalized to total Akt ( $n = 3$  independent experiments). Data are mean  $\pm$  SEM, Student's  $t$  test.  $P$  values are indicated. (E) Nup358-MC1 expression is sufficient to rescue increased activation of mTORC2/Akt signalling in Nup358-deficient cells. siControl or siNup358 were initially transfected into HeLa cells expressing inducible GFP-control or GFP-Nup358-MC1 as indicated. GFP-control or GFP-Nup358-MC1 was later induced by doxycycline, lysed and subjected to western blotting using indicated antibodies. The extent of Nup358 depletion and expression of GFP-proteins (left) and the relative levels of pAkt (right top) were monitored by western blotting using indicated antibodies. Right bottom: Quantitative representation depicting the relative levels of pAkt normalized to total Akt ( $n = 3$  independent experiments). Data are mean  $\pm$  SEM, Student's  $t$  test.  $P$  value is indicated. (F) Nup358-MC1 expression is sufficient to restrict ERMCSs. HeLa cells stably expressing inducible GFP-control or GFP-Nup358-MC1 were induced with doxycycline, fixed and subjected to PLA. Left: Representative images showing the extent of the interaction between VAPB and PTPIP51 as assessed by PLA (purple dots). Cell boundaries are demarcated with dotted lines. \*Indicates low or no GFP-expressing cells. Scale bar, 10  $\mu$ m. Right: Quantitative data depicting the number of PLA dots per cell GFP-positive cell under the indicated scenario. Number of Nup358-VAPB PLA dots per cell ( $n = 90$  for both GFP-control and GFP-Nup358-MC1 from three independent experiments). Data are mean  $\pm$  SD, Student's  $t$  test.  $P$  values are indicated. Source data are available online for this figure.

## Methods

### Mammalian cell culture and treatments

HeLa S3, HEK293T, U2OS and Huh7 cells were cultured in DMEM (10569010, Gibco/Invitrogen) with 10% FBS (16000044, Gibco/Invitrogen) and 10  $\mu$ g/ml ciprofloxacin (Fresenius Kabi, India). The cell lines were routinely tested for mycoplasma contamination. Lipofectamine RNAimax (13778150, Invitrogen) was used for siRNA transfections, while polyethyleneimine, linear (PEI, MW-25,000; Polysciences Inc.) or Lipofectamine 2000 (11668019, Invitrogen) was used for transfection of plasmid constructs.

### Chemicals

The following reagents were used in the study: insulin (I6634 and I0516, Sigma), EGF (E9644, Sigma), Mifepristone-RU486 (M8046, Sigma), Wortmannin (W1628, Sigma), MitoTracker Green FM (M7514, Invitrogen), Puromycin (Invitrogen #A11138-03) and Polybrene (Sigma #107689).

### Antibodies

The following antibodies were used in this study. Anti-Nup358 (Joseph et al, 2004), (western blot (WB), 1:3000; immunofluorescence (IF); proximity ligation assay (PLA), 1:600). Anti-mTOR (2983; WB, 1:4,000; PLA, 1:400), -Rictor (2140; PLA, 1:100), Sin1 (12860; WB, 1:3000; PLA, 1:100), Mitofusin 2 (9482S; WB, 1:4000), -pAkt-S473 (9271; WB, 1:3000), -pAkt-T308 (9275; WB, 1:3000), -Akt (9272; WB, 1:3000), pGSK3 $\beta$  (5558; WB, 1:2000), pS6K (9205; WB, 1:3000), S6K (9202; WB, 1:3000), pS6 (2211; WB, 1:4000), S6 (2317; WB, 1:4000) and G $\beta$ L/mLST8 (3274; WB, 1:3000) were purchased from Cell Signalling Technology. Anti-Nup88 (6111896; WB, 1:3000), -Nup62 (610497; WB, 1:4000), -Tom20 (612278; IF, 1:200) and -GSK3 $\beta$  (610202; WB, 1:3000) were purchased from BD

biosciences. Anti-PDIA3 (AMAB90988; WB, 1:3000; IF, 1:500) was from Sigma and anti-RanGAP1 (33-0800; IF, 1:300; PLA, 1:500) was from Invitrogen. Anti-VAPB (66191-1-1 g; WB, 1:4,000; PLA, 1:900), -PTPIP51 (20641-1-AP; WB, 1:3000; PLA, 1:900), - $\alpha$ -tubulin (66031-1-Ig, WB, 1:5000), -GSK3 $\beta$  (22104-1-AP; WB, 1:2000; PLA, 1:1000), -BAP31 (11200-1-AP; PLA, 1:4000), -Fis1 (66635-1-Ig; PLA, 1:3000) and -Sin1 (15463-1-AP; WB, 1:3000) were purchased from Proteintech. Anti-Rictor (ab104838; WB, 1:2000), Nup214 (ab70497; IF, 1:100) were purchased from Abcam. Anti-myc (sc-401; WB, 1000), -Tom20 (sc17764; WB, 1:3000) and GAPDH (sc-166574; WB, 1:5000) were from Santa Cruz Biotechnology Inc. Other antibodies used in the studies were Anti-FLAG (F3165; WB, 1:5000) and -vinculin (V9131; WB, 1:10,000) from Sigma, anti-VAPB (VMA00454; PLA, 1:600) from Bio-Rad, Anti-IP3R3 (07-1213; PLA, 1:500) from Millipore, anti-HA (MMS-101R; WB, 1:5000) from Covance Research Products (BioLegend), anti-TNRC6A/GW182 (A302-329A; WB, 1:500) from Bethyl Laboratories and anti-MBP antibody from New England BioLabs (E8032S; WB, 1:3500). Anti-dNup358 (WB, 1:3000) and -PTPIP51 (PLA, 1:250) were produced in-house as detailed below.

### DNA constructs

pCI-neo-HA-PTPIP51 and pCI-neo-myc-VAPB were gifts from Christopher Miller (King's College London, UK). pCRISPR-CG01 (HCP216100-CG01-1-10) was purchased from GeneCopoeia and pcDNA3-Flag-mTOR wt (ID-26603) was procured from Addgene. Mito-BFP and RFP-KDEL (ER) were provided by Jennifer Lippincott-Schwartz (Janelia Research Campus, USA), pLVX-TetOne-Puro Vector (21915, Addgene), psPax2 (12260, Addgene), pMD2.G (12259, Addgene), Tet-pLKO-puro (Addgene #21915) and pcDNA3-hPACS2-3HA was from Gary Thomas (University of Pittsburgh, USA).

pEGFP-Nup358 (full length), pEGFP-siRES-Nup358, pEGFP-Nup358-N, pEGFP-Nup358-M and pEGFP-Nup358-C were described

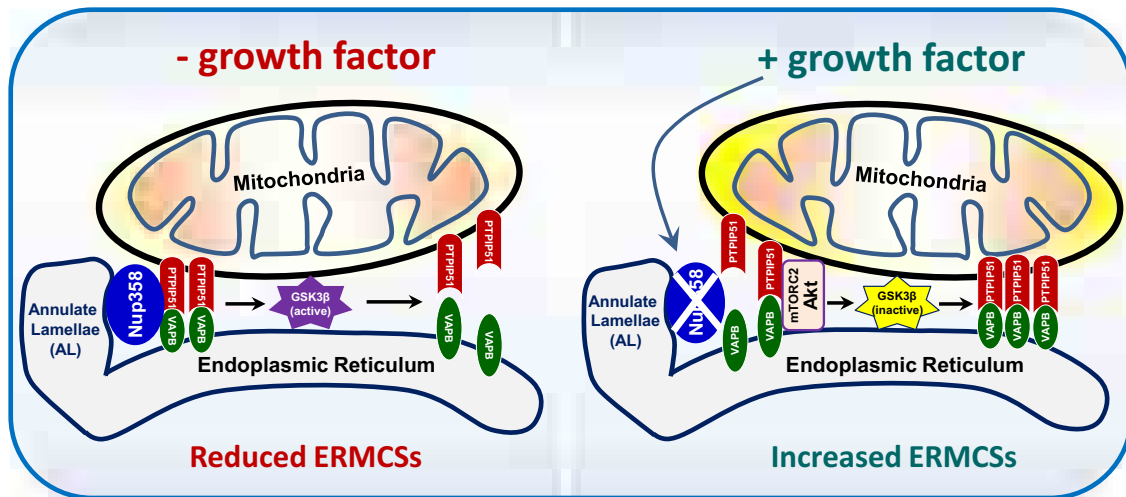


**Figure 7. Model for the role of Nup358 in ERMCS remodelling during growth factor signalling.**

Left: In the absence of growth factor signalling, presence of Nup358 at the ERMCSs due to its interaction with VAPB and PTPIP51 prevents the recruitment and activation of mTORC2 at the ERMCSs, leading to inhibition of Akt, activation of GSK3 $\beta$  and thereby decreased ER-mitochondria connectivity. Right: In the presence of growth factors, through an unknown (but PI3 kinase-independent) mechanism, interaction of Nup358 with VAPB/PTPIP51 is reduced. This allows the recruitment of mTORC2/Akt complex to the ERMCSs through interaction with preformed VAPB-PTPIP51 tether. This results in activation of mTORC2 and its downstream target Activated Akt which in turn phosphorylates and inhibits GSK3 $\beta$ . This prevents GSK3 $\beta$ -mediated disruption of VAPB-PTPIP51 interaction which subsequently increases ER-mitochondrial contacts. Thus, a reciprocal binding of Nup358 and mTORC2 with VAPB-PTPIP51 complex, ultimately determines the extent of ER-mitochondria connectivity by modulating the activity of GSK3 $\beta$ .

earlier (Joseph and Dasso, 2008; Sahoo et al, 2017). pEGFP-Nup358-MC1 (GFP-Nup358-MC1, amino acids 1949–2786) was generated from pEGFP-Nup358 full length by deleting sequences corresponding to both N-terminal and C-terminal regions using appropriate restriction digestion and self-ligation. The lentiviral construct expressing GFP-Nup358-MC1 was generated by subcloning the region encoding GFP-Nup358-MC1 from pEGFP-Nup358-MC1 into pLVX-TetOne-Puro.

Nup358-MC2 (1012–2771 aa) encoding region was PCR-amplified and cloned into BamHI/ XhoI sites of pGEX-6P1 vector (GE Healthcare). MBP-PTPIP51 (36–470 aa) was obtained by cloning the corresponding region of PTPIP51 into pMAL-c2 (New England BioLabs) at the appropriate sites to generate PTPIP51 containing MBP tag at N terminus and 6XHis tag at C terminus. MBP-VAPB (1–218 aa) was generated by PCR amplifying the corresponding region and cloning it into XmnI/XbaI sites of pMAL-c2 vector (GE Healthcare).

GSK3 $\beta$  was initially PCR-amplified from pcDNA3-hGSK3 $\beta$ -V5-WT (a kind gift from Thilo Hagen, National University of Singapore) and cloned into pEGFP-N1 vector (Clontech). For generation of pLVX-TetOne-GSK3 $\beta$ -GFP, GSK3 $\beta$  and GFP was subcloned from pEGFP-N1-GSK3 $\beta$  and pEGFP-C2, respectively, into pLVX-TetOne-Puro vector (21915, Addgene) using appropriate restriction digestions. The construct expresses GSK3 $\beta$  with GFP fused at its C terminus (GSK3 $\beta$ -GFP).

Constructs harbouring inducible shRNA control (shControl) and shRNA against Nup358 (shNup358) were generated by cloning the following target sequences into the Tet-pLKO-puro (Addgene #21915). shControl (5'-GTGGACTCTTGAAAGTACTAT-3') and shNup358 (5'-GGTGAAGATGGATGGAATA-3') were cloned into the Tet-pLKO-puro vector (Addgene #21915) at the AgeI/EcoRI sites.

## siRNAs

The following sequences were used for siRNAs. siNup358 (5'-GGTGAAGATGGATGGAATA-3') (Sahoo et al, 2017), siControl 5'-TCTCCGAACGTGTCACGT-3') (Sahoo et al, 2017), siVAPB (5'-GCTCTGGCTCTGGTGGTT-3'), siPTPIP51 (5'-CCTTAGACCTTGCTGAGAT-3'), siMfn2 (5'-GTGATGTGGCCCAACTCTA-3'), siRictor (5'-GCAGCCTTGAAGTGTAA-3') and ON-TARGET plus Human MAPKAP1/Sin1 (79109) siRNA SMARTpool (L-014315-00-0005) were purchased from Dharmacon. siRNAs against GW182 isoforms, siTNRC6A/GW182 (4390824, ID s26154) and siTNRC6B (4392420, IDs 23060), were obtained from ThermoFisher Scientific (Ambion). All siRNA transfections (40 nM, 72 h) were performed using Lipofectamine RNAiMAX (13778150, Invitrogen) as per the manufacturer's instruction.

## Co-immunoprecipitation (co-IP) and western blot (WB) analysis

In general, cell lysates for immunoblot analysis were prepared in 1% NP-40 buffer [20 mM Tris-HCl (pH 8), 137 mM NaCl, 10% glycerol, 2 mM EDTA, supplemented with 7.5 mM NaF, 0.75 mM sodium orthovanadate, 1 mM PMSF, protease inhibitor cocktail of leupeptin (50  $\mu$ g/ml), aprotinin (5  $\mu$ g/ml), and pepstatin (2  $\mu$ g/ml)]. After thorough retro pipetting, the cell lysates were centrifuged at 12,900 $\times$ g for 10 min to pellet the cell debris. Clear supernatant was collected and protein concentration was estimated using Bradford (Bio-Rad) assay. Samples were subjected to SDS-PAGE and transferred to PVDF membrane (Millipore) for western analysis.

For extracting phosphoproteins, cell lysis was performed in Phospho-lysis buffer [50 mM Tris-HCl (pH 7.5), 1 mM EDTA, 1%

Triton X-100, 10% glycerol] or RIPA buffer [50 mM Tris-HCl (pH 7.4), 150 mM NaCl, 1% NP-40, 0.1% SDS, 0.5% sodium deoxycholate], supplemented with 1 mM DTT, 50 mM NaF, 5 mM sodium pyrophosphate, 1 mM PMSF and protease inhibitor cocktail (Roche).

For immunoprecipitation of endogenous PTPIP51, Nup358 or ectopically expressed GFP-tagged proteins, the cell extracts were made in 1% NP-40 cell lysis buffer as previously described. The whole cell extracts were incubated with Protein A sepharose beads (101041, Invitrogen) coated with anti-PTPIP51, anti-Nup358 or anti-GFP antibody for 2 h at 4°C. The precipitates were washed once with 1% NP-40 cell lysis buffer, followed by two washes with tris-buffered saline (TBS). The IP samples were subjected to SDS-PAGE and analysed by WB.

For IP of mTOR, cells were lysed in 0.5% CHAPS buffer containing 120 mM NaCl, 40 mM HEPES (pH 7.5), 0.2 mM EDTA, 10% glycerol, and FLAG-mTOR was immunoprecipitated with anti-FLAG beads (EZview™ Red ANTI-FLAG® M2 Affinity Gel, Sigma, F3165). The immunoprecipitates were washed three times with 0.5% CHAPS buffer before proceeding with WB.

### Subcellular fractionation—ERMCS isolation

ERMCS (MAM) fractionation was performed from HeLaS3 cells based on the standardized MAM isolation protocol (Williamson et al, 2015; Wieckowski et al, 2009). Cells from six T-175 confluent flasks were trypsinized and centrifuged at 600 *g* for 5 min. All the further steps were performed at 4°C using fractionation buffers supplemented with a protease inhibitor cocktail. The cell pellet was resuspended in IB-1 buffer [225 mM mannitol, 75 mM sucrose, 0.1 mM EGTA and 30 mM Tris-HCl (pH 7.4)] and homogenized by passing through syringes of different nozzle sizes (21Ga, 23Ga and 24Ga), 10 times each. Post nuclear fraction (PNF) was collected from the homogenate by centrifugation at 600× *g* for 5 min. Later, crude mitochondria was pelleted from the PNF by centrifuging at 7000× *g* for 10 min and the supernatant containing soluble proteins and ER/microsomes was collected as cytoplasmic fraction. To avoid the microsomal contamination, the crude mitochondrial pellet was resuspended in IB-2 buffer [225 mM mannitol, 75 mM sucrose, and 30 mM Tris-HCl (pH 7.4)] and centrifuged at 7000× *g* for 10 min. This step was repeated once again, centrifuging at 10,000× *g*, this turn. The final pellets were washed and reconstituted in MRB buffer [250 mM mannitol, 5 mM HEPES (pH 7.4), and 0.5 mM EGTA] and gently layered on top of the percoll medium [225 mM mannitol, 25 mM HEPES (pH 7.4), 1 mM EGTA, and 30% percoll]. After 30 min of centrifugation at 95,000× *g*, the ERMCS (MAM) fraction, a whitish diffused band at the middle of tube, was carefully collected with a Pasteur pipette. The remaining lower layer, containing mitochondrial suspension, was diluted in MRB solution, and mitochondria were extracted by centrifugation at 6300× *g* for 20 min. Similarly, the ERMCS fraction was resuspended in MRB buffer and centrifuged at 100,000× *g* for 60 min to obtain the ERMCS pellet. All final fractions were dissolved in RIPA buffer [50 mM Tris-HCl (pH 7.4), 150 mM NaCl, 1% NP-40, 0.1% SDS and 0.5% sodium deoxycholate] and analysed by western blotting.

### Immunofluorescence (IF) and proximity ligation assay (PLA)

Cells seeded on coverslips were fixed using methanol (−20°C) for 5 min. After washing with phosphate-buffered saline (PBS), cells

were incubated in primary antibodies diluted in 2% normal horse serum (NHS, Vector Laboratories) for 60 min. After a PBS wash, Alexa Fluor labelled secondary antibodies (Molecular probes, ThermoFisher Scientific) diluted in 2% NHS were added and incubated for 30 min. For staining of the nucleus, Hoechst 33342 dye (Sigma) was added to the secondary antibody solution. After three washes with PBS, the coverslips were mounted with Vectashield medium (Vector Laboratories). Images were acquired using Olympus FV3000 confocal laser scanning microscope with the ×60 (1.42 NA) or ×100 (1.45 NA) objective. The images were processed with cellSens (ver.2.3) constrained iterative deconvolution for better resolution of ER and mitochondrial network.

Proximity Ligation assay (PLA) was used to identify in situ protein interactions. Briefly, cells grown on coverslips were fixed with methanol (−20°C) for 5 min and probed with the respective primary antibodies. PLA was performed using Duolink reagents (Sigma; DUO92002; DUO92004) as described in Duolink® PLA Fluorescence Protocol (Sigma). The PLA signals developed by Duolink® In Situ Detection Reagents Red (DUO92101) or Duolink® In Situ Detection Reagents Green (DUO92014) were detected and acquired by Olympus FV 3000 microscope and quantitated using NIH ImageJ or CellProfiler (Irvine et al, 2004). Phase-contrast images were used to demarcate the cell boundaries.

### Stimulated emission depletion microscopy (STED)

Huh7 cells grown on high-precision microscope cover glasses (Marienfeld, Germany) were fixed with 4% paraformaldehyde (20 min), followed by permeabilization with 0.1% Triton X-100 (10 min). The cells were then incubated with primary antibodies diluted in 2% NHS. After washing the coverslips thrice with PBS, secondary antibodies (Alexa Fluor 568 and Alexa Fluor 657) prepared in 2% NHS were added, washed thrice with PBS and the coverslips were mounted in Prolong Gold (Invitrogen). Images were acquired using Leica TCS SP8 STED 3× with the ×100, 1.4 NA objective.

### Quantitation of ER and mitochondria colocalization

RFP-ER and Mito-BFP plasmids were co-expressed to visualize the contacts between ER and mitochondria in live cells. Images were analysed for co-localisation between ER and mitochondria using ImageJ JACoP software. Manders' coefficient was calculated from the fraction of mitochondria overlapping with the ER. To visualize the overlapping pixels, represented as ERMCSs, ImageJ Co-localisation Finder was used.

### Transmission electron microscopy

For ultrastructure analysis, the monolayer culture cells were washed with 1× PBS and fixed with 3% glutaraldehyde for 2 h at 4°C and post fixed in 1% aqueous osmium tetroxide for 1 h at 4°C, followed by en block staining in 2% aqueous uranyl acetate. The cells were then subsequently dehydrated in increasing grade of alcohol for 15 min each. The cells were further infiltrated with an increasing series of hydroxypropyl methacrylate (HPMA) followed by Epon resin infiltration for 15 min each and polymerised in Epon resin.

The Epon sheet was then cut into small pieces and re-embedded on the pre-polymerized block. Ultrathin sections of 70 nm were cut and contrasted with lead citrate and images were acquired using JEM 1400 Plus Transmission Electron Microscope (JEOL, Japan) at 120 kV.

For quantitation of ERMCS from the electron micrographs, regions of mitochondria at a distance of  $\leq 30$  nm from the ER were identified using ImageJ (Lam et al, 2021). The percentage of mitochondrial perimeter associated with ER was then determined using ImageJ.

### Generation of Nup358 knockout (KO) cell lines

HeLa Nup358 KO cells were generated using CRISPR-Cas9 technology. HeLa cells were co-transfected with Nup358 CRISPR-Cas9 (pCRISPR-CG01, GeneCopoeia) and pTSiN-puro-Cre constructs. Transfected cells were selected for puromycin resistance. Single-cell clones were obtained, which were verified for Nup358 KO by IF and immunoblotting. The sgRNA target region within the *Nup358* gene was PCR-amplified and sequenced to confirm that the genomic manipulation occurred (Fig. EV4).

### Generation of inducible HEK293T and HeLa lines expressing control and Nup358-specific shRNA

Stable inducible shRNA HEK293T cell lines for shControl and shNup358 were generated using lentivirus transduction. To generate lentivirus, HEK293T cells were co-transfected with psPAX2 (Addgene #12260) and pMD2.G (Addgene #12259) along with the shRNA-specific Tet-pLKO-puro construct, using Lipofectamine 2000 (Invitrogen). The cells were replenished with fresh medium the following day, and the conditioned medium containing lentivirus was collected after 48 h. HEK293T and HeLa cells were transduced with the lentivirus-containing medium diluted 1:1 with DMEM and a final concentration of 8  $\mu$ g/ml Polybrene. Forty-eight hours post transduction, the stable cell pool, resistant to puromycin (2.5  $\mu$ g/ml), was selected.

### Generation of inducible HeLa lines expressing GFP-control, GFP-Nup358-MC1 and GSK3 $\beta$ -GFP

The pLVX-TetOne-Puro Vector (21915, Addgene) containing a doxycycline-inducible CMV promoter and puromycin resistance gene was utilized to generate stable GFP-control, GFP-Nup358-MC1 or GSK3 $\beta$ -GFP-expressing HeLa S3 cells. For this, HEK293T cells were seeded at a density of 700,000 cells in a 35-mm cell culture plate. After cell adhesion, individual transfections were conducted using 1.9  $\mu$ g of pLVX-GFP, pLVX-GFP-Nup358-MC1 or pLVX-GSK3 $\beta$ -GFP plasmid, along with 2.14  $\mu$ g of PsPax2 and 0.56  $\mu$ g of pMD2.G plasmids, using Lipofectamine 2000. Twenty-four hours post transfection, the medium was replaced with fresh medium, and the viral soup was collected after 24 h. The collected viral soup was filtered through a 0.45- $\mu$ m filter and mixed with 10% FBS-containing DMEM in a 1:1 ratio. This mixture was added to HeLa S3 cells, which were seeded a day before, along with 8  $\mu$ g/ml of polybrene. The medium containing the viral soup and polybrene was replaced again in the next 24 h and subsequently in the subsequent 24 h. After the final transduction, the medium was replaced with 10% FBS-containing DMEM supplemented with

puromycin. The cells were then subjected to puromycin selection for a week to obtain stable cell lines expressing the desired proteins. Confirmation of the stable cell line expressing the desired proteins was done through doxycycline induction and western blotting.

### Treatments

In general, prior to western analysis, cells were replenished with fresh medium containing 10% FBS for 24 h. In case when growth factor (insulin and EGF) signalling was assessed under siRNA-treated conditions, cells were initially transfected with siRNA for 69 h and the old medium was replaced with serum-free DMEM for 3 h (for western analysis) or 12 h (for PLA). In the case of rescue experiments using stable inducible HEK293T shControl and shNup358 cells, pEGFP-MBP-control or pEGFP-Nup358-siRES was transfected for 24 h following which the cells were kept in fresh DMEM containing 1% FBS for 24 h before processing for WB. For WB and PLA analyses of inducible GFP-control or GFP-Nup358-MC1 HeLa cells, the cells were seeded in and cultured for 36 h in DMEM containing 10% FBS and doxycycline (1  $\mu$ g/ml). For PI3 kinase inhibition experiments, cells were cultured in DMEM containing 10% FBS for 36 h post which the medium was replaced with serum-free DMEM for 9 h. The cells were then treated with 2.5  $\mu$ M wortmannin for 3 h post which the medium was replaced with serum-free medium with/without 2 nM insulin.

### Antibody production

Antibody against human PTP1B was raised in rabbits. Bacterially expressed and purified His-tagged PTP1B fragment corresponding to amino acids 244–470 was used as the antigen. Specific antibodies were affinity purified using the antigen and used in this study. Antibodies for *Drosophila* Nup358 were generated in mice against a region corresponding to amino acids 2319–2555 (variant B), expressed and purified from bacteria.

### Purification of recombinant proteins

Nup358-MC2 protein was expressed in *E. coli* BL21 CodonPlus RIL (DE3) cells and the culture was induced with 0.3 mM isopropyl-D-thiogalactoside at 18 °C overnight. The cells were lysed in 50 mM Tris-HCl (pH 8.0), 150 mM NaCl, 0.1% NP-40, 1 mM dithiothreitol, 1 mM EDTA, 1 mM phenylmethylsulfonyl fluoride and 20 mg/ml concentrated lysozyme (2.5  $\mu$ l/ml). Sonication with 70% amplitude, 2 s pulse on –15 s pulse off for 1 min was used to lyse the cells. After centrifugation at 12,900 $\times$ g, 4 °C for 30 min, the supernatant was added to Glutathione Agarose Beads (Bio Bharati Life Sciences). The protein was eluted with 50 mM Tris-HCl (pH 8.0), 30 mM reduced glutathione and 1 mM PMSF.

PTP1B (36–470 aa) was expressed in *E. coli* BL21 Star (DE3) cells and induced with 0.5 mM isopropyl-D-thiogalactoside at 18 °C for ~5 h. Cells were resuspended in lysis buffer containing 50 mM Tris-HCl (pH 8.0), 300 mM NaCl, 0.1% NP-40, 5% glycerol, 1 mM dithiothreitol, 1 mM phenylmethylsulfonyl fluoride and 20 mg/ml concentrated lysozyme (2.5  $\mu$ l/ml) and sonicated at 70% amplitude, 2 s pulse on –15 s pulse off for 1 min. The supernatant was first added to Ni-NTA resin (Invitrogen), and the protein was eluted



using 250 mM imidazole in the lysis buffer. The eluted protein was further bound to Amylose resin (New England BioLabs), followed by washing. The final elution of the protein was done using 15 mM maltose in the lysis buffer.

VAPB (1–218 aa) was expressed *E. coli* BL21 CodonPlus RIL (DE3) cells and induced with 0.5 mM isopropyl-D-thiogalactoside at 27 °C for ~6 h. Cells were lysed in 50 mM Tris-HCl (pH 8.0), 300 mM NaCl, 0.1% NP-40, 5% glycerol, 1 mM dithiothreitol, 1 mM phenylmethylsulfonyl fluoride and 20 mg/ml concentrated lysozyme (2.5 µl/ml) and sonicated at 70% amplitude, 2 s pulse on –15 s pulse off for 1 min. The supernatant was added to the Amylose resin (New England BioLabs), and the protein elution was done using 15 mM maltose in lysis buffer.

All recombinant proteins were dialysed in 1× TBS, 5% glycerol and 1 mM PMSF.

### In vitro protein-protein interaction assay

Magnetic Protein G Dynabeads (10004D, ThermoFisher Scientific) were bound with 2 µg of monoclonal anti-MBP antibody (E8032S, New England BioLabs). Meanwhile, 2 µM of MBP (Control), MBP-PTPIP51 or MBP-VAPB was incubated with 1.5 µM of GST-Nup358-MC2 in the assay buffer (in a reaction volume of 100 µl) containing 25 mM Tris-HCl (pH 7.4), 150 mM NaCl, 5% glycerol, 0.01% v/v Tween20 for 2 h at 4 °C with gentle retro pipetting. Later, the MBP-tagged recombinant proteins were immunoprecipitated and the beads were washed with the assay buffer, and the IP samples were subjected to western blotting.

### MitoTracker Green FM staining

HeLa cells transfected with siControl or siNup358 were trypsinized and washed with PBS. One million cells were resuspended in 0.5 ml of PBS and 50 nM MitoTracker Green FM (M7514, Invitrogen) was added, followed by gentle pipetting for mixing. The Cells were then incubated at 37 °C in CO<sub>2</sub> incubator for 15 min. Cells were washed again with PBS to remove any unbound dye. Unstained cells were used as control. FACS analysis was performed using BD FACSCanto™ II System.

### Drosophila strains and rearing

Flies were maintained on standard Cornmeal Agar at 25 °C and 65% relative humidity in a 12 h light: dark cycle. Gal4/UAS system was used to induce the expression of our gene of interest. Fly strains used in our experiments were Cg-Gal4 (BDSC: 7011), Elav-Gal4 (BDSC: 458), Elav-Gene Switch (BDSC: 43642), UAS-Nup358 RNAi (BDSC: 34967), UAS-Luc Val10 RNAi (BDSC: 35788).

### Drosophila gene switch expression

F1 progeny from the cross of Elav-Gene Switch with either UAS-Nup358 RNAi or UAS-Luc Val10 RNAi were collected upon eclosion. The progeny were starved overnight in vials containing moist paper and fed 500 µM mifepristone (RU486) dissolved in 80% ethanol for 72 h post starvation. Later, the fly heads ( $n = 5$ ) were chopped and lysed in S2 buffer [100 mM NaCl,

50 mM Tris-HCl (pH 7.5), 0.1% NP-40 with protease inhibitors] and processed for western blotting.

### Statistics and reproducibility

All statistical analyses were done in GraphPad Prism version 8, calculated from independently repeated experiments as indicated in the respective Figure Legends. For western blot analysis, values were considered from at least three independent experiments ( $n = 3$ ) and a two-sided unpaired Student's *t* test was performed. The values were graphically expressed as mean ± SEM and *P* values were as indicated in legends. All immunostaining data was also analysed by a two-sided unpaired Student's *t* test. The mean ± SD was schematically represented and the level of significance is as stated in the Figure Legends. In all plots, *P* values are as indicated;  $P \leq 0.05$  are considered significant and  $P > 0.5$ , not significant.

### Data availability

This study includes no data deposited in external repositories.

The source data of this paper are collected in the following database record: [biostudies:S-SCDT-10\\_1038-S44319-024-00204-8](https://www.ebi.ac.uk/biostudies/studies/S-SCDT-10_1038-S44319-024-00204-8).

Expanded view data, supplementary information, appendices are available for this paper at <https://doi.org/10.1038/s44319-024-00204-8>.

### Peer review information

A peer review file is available at <https://doi.org/10.1038/s44319-024-00204-8>

### References

- Barazzuol L, Giamogante F, Cali T (2021) Mitochondria associated membranes (MAMs): architecture and physiopathological role. *Cell Calcium* 94:102343
- Betz C, Stracka D, Prescianotto-Baschong C, Frieden M, Demareux N, Hall MN (2013) MTOR complex 2-Akt signaling at mitochondria-associated endoplasmic reticulum membranes (MAM) regulates mitochondrial physiology. *Proc Natl Acad Sci USA* 110:12526–12534
- Cho KI, Yoon D, Qiu S, Danziger Z, Grill WM, Wetsel WC, Ferreira PA (2017) Loss of Ranbp2 in motoneurons causes disruption of nucleocytoplasmic and chemokine signaling, proteostasis of hnRNPH3 and Mmp28, and development of amyotrophic lateral sclerosis-like syndromes. *Dis Model Mech* 10:559–579
- Cohen P, Frame S (2001) The renaissance of GSK3. *Nat Rev Mol Cell Biol* 2:769–776
- Cohen S, Valm AM, Lippincott-Schwartz J (2018) Interacting organelles. *Curr Opin Cell Biol* 53:84–91
- Cordes VC, Reidenbach S, Franke WW (1996) Cytoplasmic annulate lamellae in cultured cells: composition, distribution, and mitotic behavior. *Cell Tissue Res* 284:177–191
- Csordás G, Weaver D, Hajnóczky G (2018) Endoplasmic reticulum-mitochondrial contactology: structure and signaling functions. *Trends Cell Biol* 28:523–540
- De Brito OM, Scorrano L (2008) Mitofusin 2 tethers endoplasmic reticulum to mitochondria. *Nature* 456:605–610

- De vos KJ, Mórotz GM, Stoica R, Tudor EL, Lau KF, Ackerley S, Warley A, Shaw CE, Miller CCJ (2012) VAPB interacts with the mitochondrial protein PTP1P51 to regulate calcium homeostasis. *Hum Mol Genet* 21:1299–1311
- Deshmukh P, Singh A, Khuperkar D, Joseph J (2021) Acute necrotizing encephalopathy-linked mutations in Nup358 impair interaction of Nup358 with TNRC6/GW182 and miRNA function. *Biochem Biophys Res Commun* 559:230–237
- Ding B, Sepehrimanesh M (2021) Nucleocytoplasmic transport: regulatory mechanisms and the implications in neurodegeneration. *Int J Mol Sci* 22:4165
- Doghman-Bouguerra M, Lalli E (2019) ER-mitochondria interactions: both strength and weakness within cancer cells. *Biochim Biophys Acta - Mol Cell Res* 1866:650–662
- Ebner M, Sinkovics B, Szczygieł M, Ribeiro DW, Yudushkin I (2017) Localization of mTORC2 activity inside cells. *J Cell Biol* 216:343–353
- Eymieux S, Blanchard E, Uzbekov R, Hourieux C, Roingeard P (2021) Annulate lamellae and intracellular pathogens. *Cell Microbiol* 23:e13328
- Fahrenkrog B, Harel A (2018) Perturbations in traffic: aberrant nucleocytoplasmic transport at the heart of neurodegeneration. *Cells* 7:232
- Fallini C, Khalil B, Smith CL, Rossoll W (2020) Traffic jam at the nuclear pore: all roads lead to nucleocytoplasmic transport defects in ALS/FTD. *Neurobiol Dis* 140:104835
- Filadi R, Theurey P, Pizzo P (2017) The endoplasmic reticulum-mitochondria coupling in health and disease: molecules, functions and significance. *Cell Calcium* 62:1–15
- Frame S, Cohen P (2001) GSK3 takes centre stage more than 20 years after its discovery. *Biochem J* 359:1–16
- Fu W, Hall MN (2020) Regulation of MTORC2 signaling. *Genes* 11:1–19
- Giordano F (2018) Non-vesicular lipid trafficking at the endoplasmic reticulum-mitochondria interface. *Biochem Soc Trans* 46:437–452
- Gomez-Suaga P, Paillusson S, Stoica R, Noble W, Hanger DP, Miller CCJ (2017) The ER-mitochondria tethering complex VAPB-PTPIP51 regulates autophagy. *Curr Biol* 27:371–385
- Grimm S (2012) The ER-mitochondria interface: the social network of cell death. *Biochim Biophys Acta Mol Cell Res* 1823:327–334
- Hampoez B, Mackmull M-TT, Machado P, Ronchi P, Bui KH, Schieber N, Santarella-Mellwig R, Necakov A, Andrés-Pons A, Philippe JM et al (2016) Pre-assembled nuclear pores insert into the nuclear envelope during early development. *Cell* 166:664–678
- Henne WM (2016) Organelle remodeling at membrane contact sites. *J Struct Biol* 196:15–19
- Irvine K, Stirling R, Hume D, Kennedy D (2004) Rasputin, more promiscuous than ever: a review of G3BP. *Int J Dev Biol* 48:1065–1077
- Iwasawa R, Mahul-Mellier AL, Datler C, Pazarentzos E, Grimm S (2011) Fis1 and Bap31 bridge the mitochondria-ER interface to establish a platform for apoptosis induction. *EMBO J* 30:556–568
- Joseph J, Dasso M (2008) The nucleoporin Nup358 associates with and regulates interphase microtubules. *FEBS Lett* 582:190–196
- Joseph J, Liu ST, Jablonski SA, Yen TJ, Dasso M (2004) The RanGAP1-RanBP2 complex is essential for microtubule-kinetochore interactions in vivo. *Curr Biol* 14:611–617
- Kessel RG (1992) Annulate lamellae: a last frontier in cellular organelles. *Int Rev Cytol* 133:43–120
- Kim HJ, Taylor JP (2017) Lost in transportation: nucleocytoplasmic transport defects in ALS and other neurodegenerative diseases. *Neuron* 96:285–297
- Knudsen JR, Fritzen AM, James DE, Jensen TE, Kleinert M, Richter EA (2020) Growth factor-dependent and -independent activation of mTORC2. *Trends Endocrinol Metab* 31:13–24
- Kors S, Hacker C, Bolton C, Maier R, Reimann L, Kitchener EJA, Warscheid B, Costello JL, Schrader M (2022) Regulating peroxisome-ER contacts via the ACBD5-VAPB tether by FFAT motif phosphorylation and GSK3 $\beta$ . *J Cell Biol* 221:e202003143
- Lam J, Katti P, Biete M, Mungai M, Ashshareef S, Neikirk K, Lopez EG, Vue Z, Christensen TA, Beasley HK et al (2021) A universal approach to analyzing transmission electron microscopy with ImageJ. *Cells* 10:2177
- Levine JM, Ahsan N, Ho E, Santoro JD (2020) Genetic acute necrotizing encephalopathy associated with RANBP2: clinical and therapeutic implications in pediatrics. *Mult Scler Relat Disord* 43:102194
- López-Crisosto C, Bravo-Sagua R, Rodríguez-Peña M, Mera C, Castro PF, Quest AFG, Rothermel BA, Cifuentes M, Lavandero S (2015) ER-to-mitochondria miscommunication and metabolic diseases. *Biochim Biophys Acta Mol Basis Dis* 1852:2096–2105
- Madreiter-Sokolowski CT, Ramadani-Muja J, Ziomek G, Burgstaller S, Bischof H, Koshenov Z, Gottschalk B, Malli R, Graier WF (2019) Tracking intra- and inter-organelle signaling of mitochondria. *FEBS J* 286:4378–4401
- Manning BD, Toker A (2017) AKT/PKB signaling: navigating the network. *Cell* 169:381–405
- Marchi S, Patergnani S, Pinton P (2014) The endoplasmic reticulum-mitochondria connection: one touch, multiple functions. *Biochim Biophys Acta - Bioenerg* 1837:461–469
- Markovinov A, Greig J, Mariá S, Martín-Guerrero M, Salam S, Paillusson S (2022) Endoplasmic reticulum-mitochondria signaling in neurons and neurodegenerative diseases. *J Cell Sci* 135:jcs248534
- Montesinos J, Area-Gomez E (2020) Isolation of mitochondria-associated ER membranes. In: Pon LA, Schon EA (eds) *Methods in cell biology*. Academic Press Inc., pp 33–44
- Neilson DE (2010) The interplay of infection and genetics in acute necrotizing encephalopathy. *Curr Opin Pediatr* 22:751–757
- Neilson DE, Adams MD, Orr CMD, Schelling DK, Eiben RM, Kerr DS, Anderson J, Bassuk AG, Bye AM, Childs AM et al (2009) Infection-triggered familial or recurrent cases of acute necrotizing encephalopathy caused by mutations in a component of the nuclear pore, RANBP2. *Am J Hum Genet* 84:44–51
- Nishimura AL, Mitne-Neto M, Silva HCA, Richieri-Costa A, Middleton S, Cascio D, Kok F, Oliveira JRM, Gillingwater T, Webb J et al (2004) A mutation in the vesicle-trafficking protein VAPB causes late-onset spinal muscular atrophy and amyotrophic lateral sclerosis. *Am J Hum Genet* 75:822–831
- Obara CJ, Nixon-Abell J, Moore AS, Riccio F, Hoffman DP, Shtengel G, Xu CS, Schaefer K, Pasolli HA, Masson JB et al (2024) Motion of VAPB molecules reveals ER-mitochondria contact site subdomains. *Nature* 626:169–176
- Paillusson S, Stoica R, Gomez-Suaga P, Lau DHW, Mueller S, Miller T, Miller CCJ (2016) There's something wrong with my MAM; the ER-mitochondria axis and neurodegenerative diseases. *Trends Neurosci* 39:146–157
- Perrone M, Carocci N, Genovese I, Missiroli S, Modesti L, Pedriali G, Vezzani B, Vitto VAM, Antenori M, Lebedzinska-Arciszewska M et al (2020) The role of mitochondria-associated membranes in cellular homeostasis and diseases. In: Kepp O, Galluzi L (eds) *International review of cell and molecular biology*. Academic Press, pp 119–196
- Peruzzo R, Costa R, Bachmann M, Leanza L, Szabó I (2020) Mitochondrial metabolism, contact sites and cellular calcium signaling: Implications for tumorigenesis. *Cancers* 12:1–19
- Petkovic M, O'Brien CE, Jan YN (2021) Interorganelle communication, aging, and neurodegeneration. *Genes Dev* 35:449–469
- Pfaff J, Meister G (2013) Argonaute and GW182 proteins: an effective alliance in gene silencing. *Biochem Soc Trans* 41:855–860
- Phillips MJ, Voeltz GK (2016) Structure and function of ER membrane contact sites with other organelles. *Nat Rev Mol Cell Biol* 17:69–82
- Prinz WA, Toulmay A, Balla T (2020) The functional universe of membrane contact sites. *Nat Rev Mol Cell Biol* 21:7–24



- Raturi A, Simmen T (2013) Where the endoplasmic reticulum and the mitochondrion tie the knot: The mitochondria-associated membrane (MAM). *Biochim Biophys Acta Mol Cell Res* 1833:213–224
- Rieusset J (2018) The role of endoplasmic reticulum-mitochondria contact sites in the control of glucose homeostasis: an update. *Cell Death Dis* 9:388
- Rowland AA, Voeltz GK (2012) Endoplasmic reticulum-mitochondria contacts: function of the junction. *Nat Rev Mol Cell Biol* 13:607–615
- Sahoo MR, Gaikwad S, Khuperkar D, Ashok M, Helen M, Yadav SK, Singh A, Magre I, Deshmukh P, Dhanvijay S et al (2017) Nup358 binds to AGO proteins through its SUMO-interacting motifs and promotes the association of target mRNA with miRISC. *EMBO Rep* 18:241–263
- Saxton RA, Sabatini DM (2017) mTOR signaling in growth, metabolism, and disease. *Cell* 168:960–976
- Scorrano L, De Matteis MA, Emr S, Giordano F, Hajnóczky G, Kornmann B, Lackner LL, Levine TP, Pellegrini L, Reinisch K et al (2019) Coming together to define membrane contact sites. *Nat Commun* 10:1287
- Shen Q, Wang YE, Truong M, Mahadevan K, Wu JJ, Zhang H, Li J, Smith HW, Smibert CA, Palazzo AF (2021) RanBP2/Nup358 enhances miRNA activity by sumoylating Argonautes. *PLoS Genet* 17:e1009378
- Simoes ICM, Morciano G, Lebedzinska-Arciszewska M, Aguiari G, Pinton P, Potes Y, Wieckowski MR (2020) The mystery of mitochondria-ER contact sites in physiology and pathology: a cancer perspective. *Biochim Biophys Acta Mol Basis Dis* 1866:165834
- Spead O, Zaepfel BL, Rothstein JD (2022) Nuclear pore dysfunction in neurodegeneration. *Neurotherapeutics* 19:1050–1060
- Stoica R, De Vos KJ, Paillusson S, Mueller S, Sancho RM, Lau KF, Vizcay-Barrena G, Lin WL, Xu YF, Lewis J et al (2014) ER-mitochondria associations are regulated by the VAPB-PTPIP51 interaction and are disrupted by ALS/FTD-associated TDP-43. *Nat Commun* 5:3996
- Stoica R, Paillusson S, Gomez-Suaga P, Mitchell JC, Lau DH, Gray EH, Sancho RM, Vizcay-Barrena G, De Vos KJ, Shaw CE et al (2016) ALS/FTD-associated FUS activates GSK-3 $\beta$  to disrupt the VAPB-PTPIP 51 interaction and ER-mitochondria associations. *EMBO Rep* 17:1326–1342
- Szabadkai G, Bianchi K, Várnai P, De Stefani D, Wieckowski MR, Cavagna D, Nagy AI, Balla T, Rizzuto R (2006) Chaperone-mediated coupling of endoplasmic reticulum and mitochondrial Ca<sup>2+</sup> channels. *J Cell Biol* 175:901–911
- Szved A, Kim E, Jacinto E (2021) Regulation and metabolic functions of mTORC1 and mTORC2. *Physiol Rev* 101:1371–1426
- Tubbs E, Rieusset J (2017) Metabolic signaling functions of ER-mitochondria contact sites: Role in metabolic diseases. *J Mol Endocrinol* 58:R87–R106
- Tubbs E, Theurey P, Vial G, Bendridi N, Bravard A, Chauvin MA, Ji-Cao J, Zoulm F, Bartosch B, Ovize M et al (2014) Mitochondria-associated endoplasmic reticulum membrane (MAM) integrity is required for insulin signaling and is implicated in hepatic insulin resistance. *Diabetes* 63:3279–3294
- Vance JE (2020) Inter-organelle membrane contact sites: implications for lipid metabolism. *Biol Direct* 15:24
- Wang C, Cui Y, Xu T, Zhou Y, Yang R, Wang T (2023) New insights into glycogen synthase kinase-3: A common target for neurodegenerative diseases. *Biochem Pharmacol* 218:115923
- Wieckowski MRMR, Giorgi C, Lebedzinska M, Duszyński J, Pinton P (2009) Isolation of mitochondria-associated membranes and mitochondria from animal tissues and cells. *Nat Protoc* 4:1582–1590
- Williamson CD, Wong DS, Bozidis P, Zhang A, Colberg-Poley AM (2015) Isolation of endoplasmic reticulum, mitochondria, and mitochondria-associated membrane and detergent resistant membrane fractions from transfected cells and from human cytomegalovirus-infected primary fibroblasts. *Curr Protoc Cell Biol* 68:3.27.1–3.27.33

Wu H, Carvalho P, Voeltz GK (2018) Here, there, and everywhere: the importance of ER membrane contact sites. *Science* 361:eaan5835

Yang Q, Inoki K, Ikenoue T, Guan KL (2006) Identification of Sin1 as an essential TORC2 component required for complex formation and kinase activity. *Genes Dev* 20:2820–2832

## Acknowledgements

The authors thank C. Miller, T. Hagen and J. Lippincott-Schwartz for sharing reagents; NCCS Bio-Imaging facility staff for help with microscopy; Richa Ricky (IISER, Pune) for critical comments on the manuscript; and members of Joseph and Seshadri Lab for insightful discussions. Stocks obtained from the Bloomington Drosophila Stock Centre (NIH P40OD018537) were used in this study. We thank Girish Ratnaparkhi, IISER, Pune, for sharing UAS-Nup358 RNAi line and Swagatika Panigrahi for the help in generating dNup358 antibody and generating a few constructs. Electron Microscope facility, ACTREC, Tata Memorial Centre, Kharghar, Navi Mumbai is acknowledged for the help with transmission electron microscopy. This work was supported by grants from Department of Biotechnology, Ministry of Science and Technology, India (BT/PR27451/BRB/10/1655/2018), Department of Science and Technology, Ministry of Science and Technology, Government of India (SPR/2021/000352) and Pratiksha Trust Extra-Mural Support for Transformational Aging Brain Research (EMSTAR) (EMSTAR/20230-03) and intramural funding from National Centre for Cell Science to JJ. Financial support from the Council of Scientific and Industrial Research, Ministry of Science and Technology, Government of India to MK and LO; from Department of Biotechnology, Ministry of Science and Technology, India to RS, YB. and PV and from University Grants Commission (UGC), Government of India to AL through research fellowships, is gratefully acknowledged. The authors dedicate this article to the former Director of NCCS, Late Dr. Mohan Wani, for all the encouragement and his immense support towards the publication of this manuscript.

## Author contributions

**Misha Kalarikkal:** Conceptualization; Resources; Data curation; Formal analysis; Validation; Investigation; Visualization; Methodology; Writing—original draft; Writing—review and editing. **Rimpi Saikia:** Conceptualization; Resources; Data curation; Formal analysis; Validation; Investigation; Visualization; Methodology; Writing—original draft; Writing—review and editing. **Lizanne Oliveira:** Conceptualization; Resources; Data curation; Formal analysis; Validation; Investigation; Visualization; Methodology; Writing—original draft; Writing—review and editing. **Yashashree Bhorkar:** Resources; Data curation; Formal analysis; Validation; Investigation; Visualization; Methodology; Writing—review and editing. **Akshay Lonare:** Resources; Data curation; Formal analysis; Validation; Investigation; Visualization; Methodology; Writing—review and editing. **Pallavi Varshney:** Conceptualization; Data curation; Formal analysis; Validation; Methodology; Writing—review and editing. **Prathamesh Dhamale:** Resources; Data curation; Investigation; Methodology; Writing—review and editing. **Amitabha Majumdar:** Resources; Data curation; Formal analysis; Validation; Investigation; Methodology; Writing—review and editing. **Jomon Joseph:** Conceptualization; Resources; Data curation; Formal analysis; Supervision; Funding acquisition; Validation; Investigation; Visualization; Methodology; Writing—original draft; Project administration; Writing—review and editing.

Source data underlying figure panels in this paper may have individual authorship assigned. Where available, figure panel/source data authorship is listed in the following database record: [biostudies:S-SCDT-10\\_1038-S44319-024-00204-8](https://www.ebi.ac.uk/biostudies/studies/S-SCDT-10_1038-S44319-024-00204-8).

## Disclosure and competing interests statement

The authors declare no competing interests.

**Open Access** This article is licensed under a Creative Commons Attribution 4.0 International License, which permits use, sharing, adaptation, distribution and reproduction in any medium or format, as long as you give appropriate credit to the original author(s) and the source, provide a link to the Creative Commons licence, and indicate if changes were made. The images or other third party material in this article are included in the article's Creative Commons licence, unless indicated otherwise in a credit line to the material. If material is not included in the article's Creative Commons licence and your intended use is not permitted by statutory regulation or exceeds the permitted use, you will need to

obtain permission directly from the copyright holder. To view a copy of this licence, visit <http://creativecommons.org/licenses/by/4.0/>. Creative Commons Public Domain Dedication waiver <http://creativecommons.org/publicdomain/zero/1.0/> applies to the data associated with this article, unless otherwise stated in a credit line to the data, but does not extend to the graphical or creative elements of illustrations, charts, or figures. This waiver removes legal barriers to the re-use and mining of research data. According to standard scholarly practice, it is recommended to provide appropriate citation and attribution whenever technically possible.

© The Author(s) 2024

## Expanded View Figures

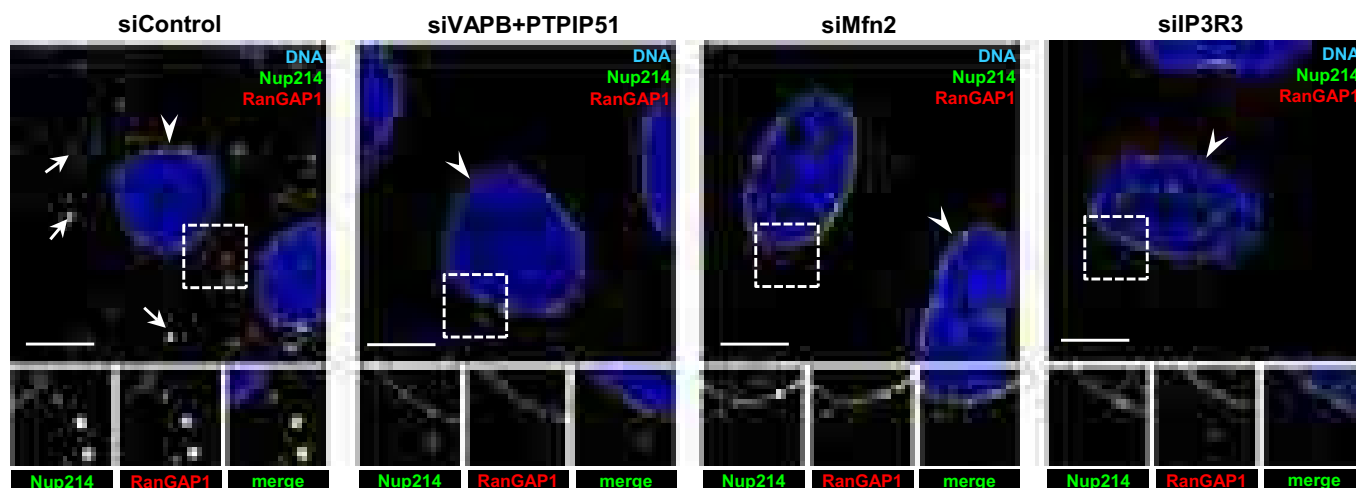


**Figure EV1. ERMCS integrity is important for AL assembly and/or stability.**

Depletion of ERMCS proteins affects AL assembly. HeLa cells were treated with indicated siRNAs and the AL integrity was monitored by presence of cytoplasmic Nup214 (green) and RanGAP1 (red). Here RanGAP1 was used as a surrogate for Nup358, as RanGAP1 is known as a strong binding partner that colocalizes with Nup358 at the nuclear envelope and AL. Number of cytoplasmic puncta, which represent AL (shown in arrows), are significantly reduced when ERMCS proteins are depleted as compared to control cells. Under the same conditions, the NE staining of nucleoporins (arrowheads) was largely unaffected. Scale bar, 10 μm.

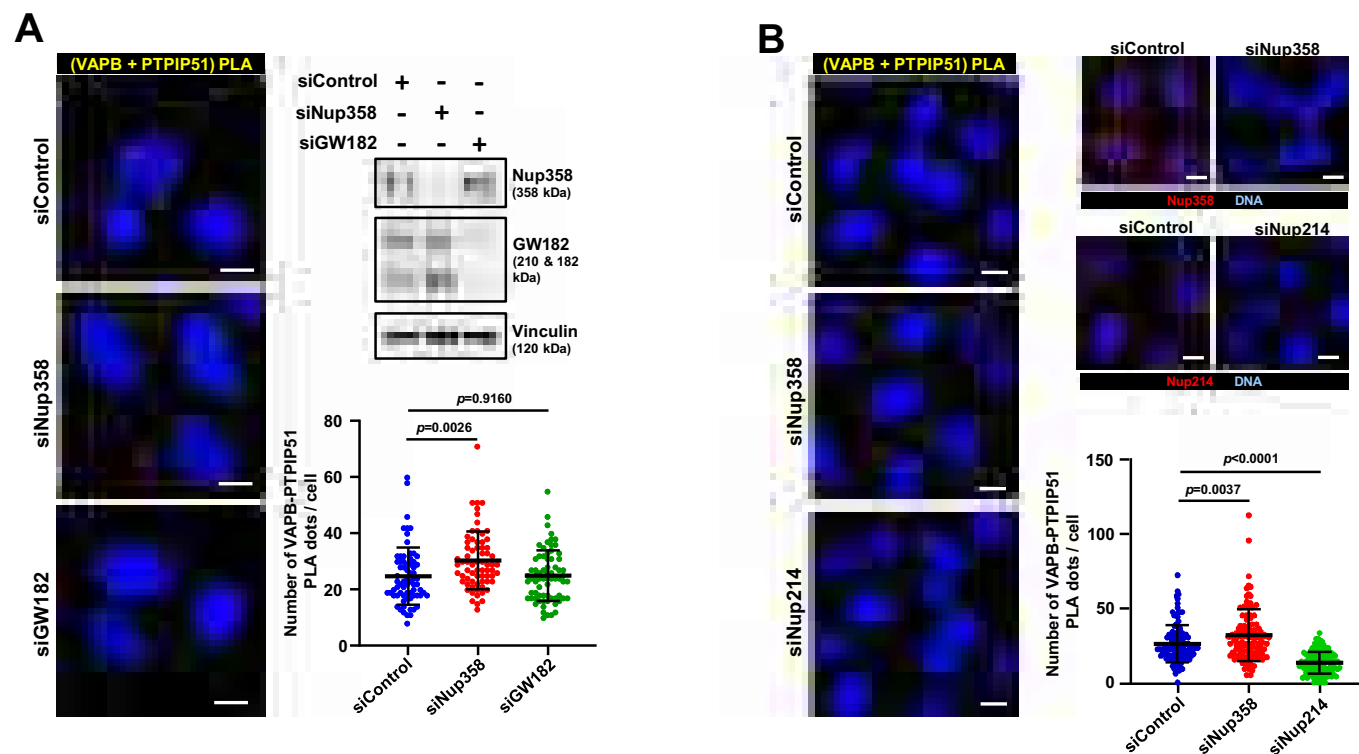


**Figure EV2. Interfering with miRNA pathway does not affect ERMCSs.**

(A) Depletion of GW182 does not affect contacts between ER and mitochondria. HeLa cells were treated with indicated siRNAs and the intactness of ERMCS was monitored in situ by PLA using VAPB and PTPIP51 antibodies. Left: Representative microscopic images showing PLA puncta (yellow) under the indicated conditions. DNA was stained with Hoechst 33342 (blue). Scale bar, 10  $\mu$ m. Right top: Depletion of indicated proteins was confirmed by western blotting. Vinculin was used as loading control. Right bottom: Quantitative data showing number of PLA dots per cell, derived from indicated conditions ( $n = 70$  cells for siControl; 69 cells for siNup358 and 71 cells for siGW182 from 3 independent experiments). Data are mean  $\pm$  SD, unpaired Student's  $t$  test.  $P$  values are indicated. (B) Depletion of Nup214 reduces contacts between ER and mitochondria. HeLa cells were treated with indicated siRNAs and the ERMCS were monitored in situ by PLA using VAPB and PTPIP51 antibodies. Left: Representative microscopic images showing PLA puncta (yellow) under the indicated conditions. DNA was stained with Hoechst 33342 (blue). Scale bar, 10  $\mu$ m. Right top: Depletion of indicated proteins was confirmed by immunostaining with the indicated antibodies (red). Right bottom: Quantitative data showing number of PLA dots per cell, derived from indicated conditions ( $n = 127$  cells for siControl; 106 cells for siNup358 and 116 cells for siNup214 from 3 independent experiments). Data are mean  $\pm$  SD, unpaired Student's  $t$  test.  $P$  values are indicated.

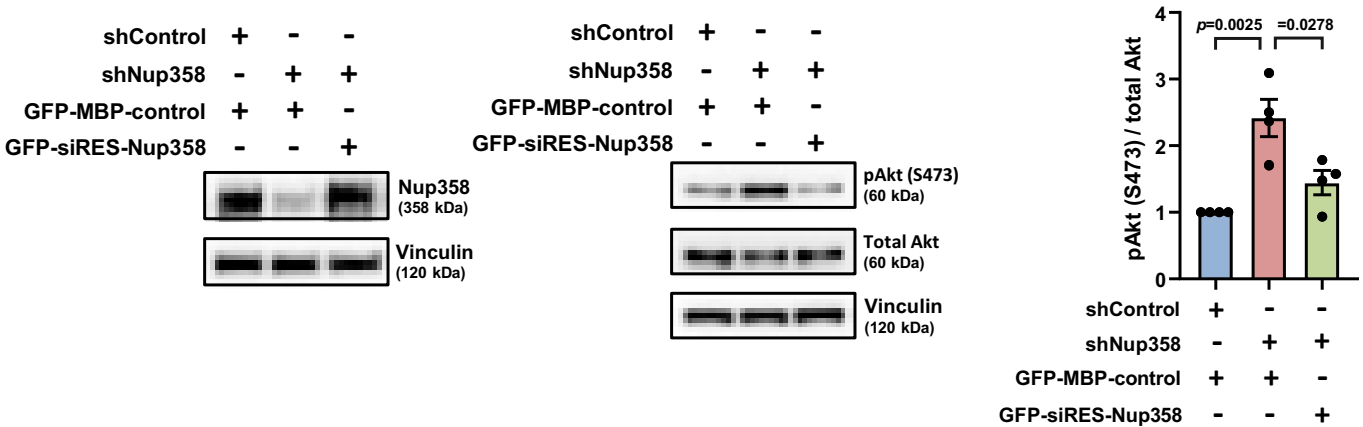


**Figure EV3. Ectopic expression of Nup358 rescues the increased mTORC2/Akt activity in Nup358-deficient cells.**

Stable HEK293T cells with Inducible short hairpin RNA (shRNA) for control (shControl) or Nup358 (shNp358) were initially induced with doxycycline. Later the cells were transfected with GFP-MBP-control or GFP-siRNA-resistant (siRES)-Nup358 construct as indicated. Left: Expression levels of Nup358 in the indicated samples were monitored by western blotting with Nup358 antibodies. Vinculin was used as loading control. Middle: Levels of indicated proteins were assessed by western blotting. Vinculin was loading control. Right: Quantitative representation depicting relative levels of pAkt normalized to total Akt ( $n = 4$  independent experiments) under the indicated conditions. Data are mean  $\pm$  SEM, Student's  $t$  test.  $P$  values are indicated.

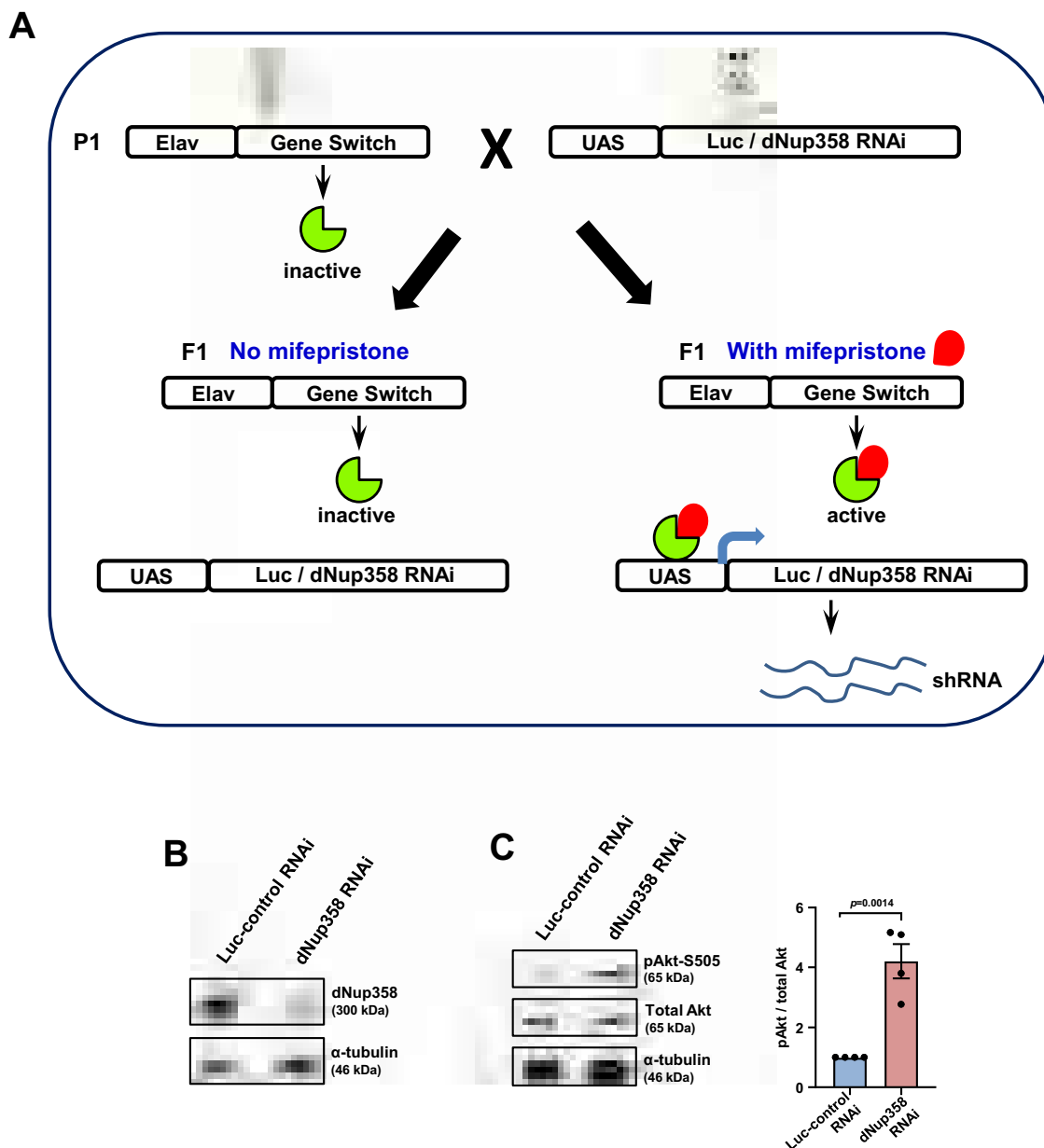


**Figure EV4. Conserved regulatory role of Nup358 in restricting mTORC2/Akt activation in *Drosophila*.**

(A) A schematic showing how F1 progeny was obtained by crossing parental (P) lines as indicated. The adult *Drosophila* flies (F1) were treated with 500  $\mu$ M mifepristone (RU486) for 72 h to induce control shRNA (Luciferase, Luc) or dNup358-specific shRNA. (B) Brains lysates were assessed for dNup358 knockdown by western blotting.  $\alpha$ -tubulin was used as loading control. (C) Left: Lysates were analysed for pAkt (S505) levels by western blotting.  $\alpha$ -tubulin was used as loading control. Right: Quantitative data showing the levels of pAkt (normalized to total Akt) under indicated conditions ( $n = 4$  independent experiments). Data are mean  $\pm$  SEM, unpaired Student's  $t$  test.  $P$  value is indicated.



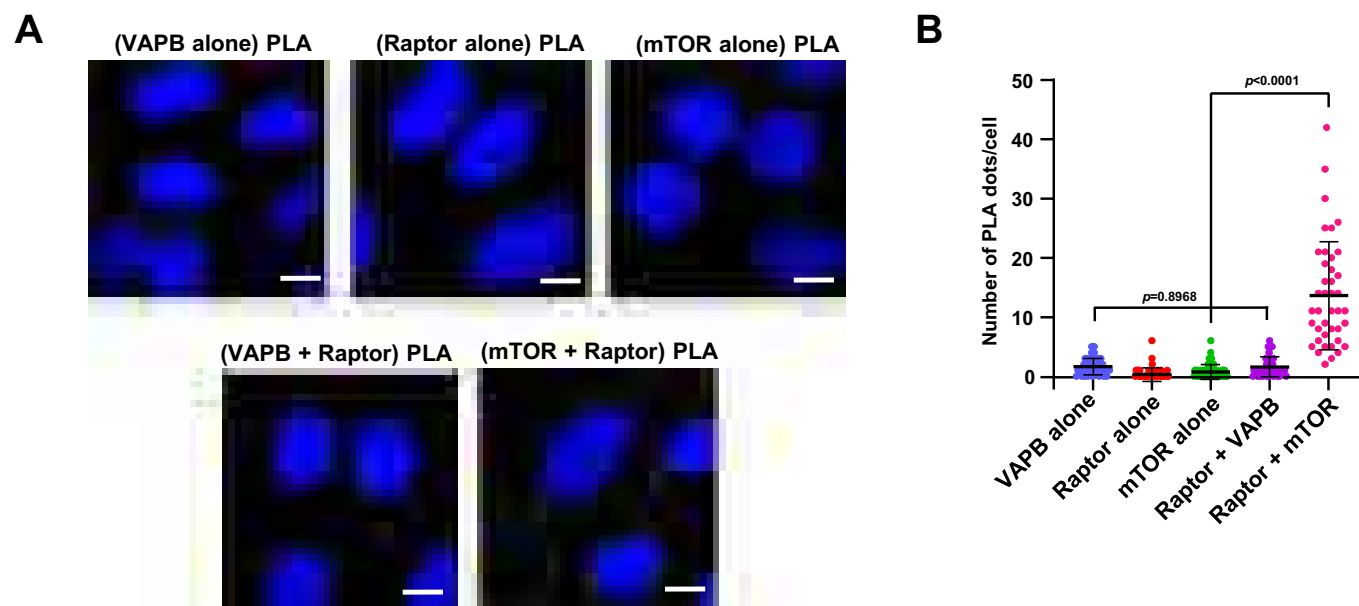



**Figure EV5. VAPB does not interact with the mTORC1-specific subunit Raptor.**

(A) HeLa cells were subjected to PLA (yellow dots) for detecting the VAPB-Raptor interaction and mTOR-Raptor (positive control) interaction, with individual antibody as negative controls. DNA was stained with Hoechst 33342 (blue). Scale bar, 10  $\mu$ m. (B) Quantitation of PLA dots per cell ( $n = 56$  cells for VAPB alone; 41 cells for Raptor alone; 57 cells for mTOR alone; 48 cells for VAPB-Raptor interaction; 41 cells for VAPB-mTOR interaction; from a single experiment). Data are mean  $\pm$  SD, unpaired Student's  $t$  test.  $P$  values are indicated.

# Nup358 binds to AGO proteins through its SUMO-interacting motifs and promotes the association of target mRNA with miRISC

Manas Ranjan Sahoo<sup>1,†</sup>, Swati Gaikwad<sup>1,†</sup>, Deepak Khuperkar<sup>1</sup>, Maitreyi Ashok<sup>1</sup>, Mary Helen<sup>1</sup>, Santosh Kumar Yadav<sup>1</sup>, Aditi Singh<sup>1</sup>, Indrasen Magre<sup>1</sup>, Prachi Deshmukh<sup>1</sup>, Supriya Dhanvijay<sup>1</sup>, Pabitra Kumar Sahoo<sup>1</sup>, Yogendra Ramtirtha<sup>2</sup>, Mallur Srivatsan Madhusudhan<sup>2</sup>, Pananghat Gayathri<sup>2</sup>, Vasudevan Seshadri<sup>1</sup> & Jomon Joseph<sup>1,\*</sup> 

## Abstract

MicroRNA (miRNA)-guided mRNA repression, mediated by the miRNA-induced silencing complex (miRISC), is an important component of post-transcriptional gene silencing. However, how miRISC identifies the target mRNA *in vivo* is not well understood. Here, we show that the nucleoporin Nup358 plays an important role in this process. Nup358 localizes to the nuclear pore complex and to the cytoplasmic annulate lamellae (AL), and these structures dynamically associate with two mRNP granules: processing bodies (P bodies) and stress granules (SGs). Nup358 depletion disrupts P bodies and concomitantly impairs the miRNA pathway. Furthermore, Nup358 interacts with AGO and GW182 proteins and promotes the association of target mRNA with miRISC. A well-characterized SUMO-interacting motif (SIM) in Nup358 is sufficient for Nup358 to directly bind to AGO proteins. Moreover, AGO and PIWI proteins interact with SIMs derived from other SUMO-binding proteins. Our study indicates that Nup358-AGO interaction is important for miRNA-mediated gene silencing and identifies SIM as a new interacting motif for the AGO family of proteins. The findings also support a model wherein the coupling of miRISC with the target mRNA could occur at AL, specialized domains within the ER, and at the nuclear envelope.

**Keywords** annulate lamellae; Argonaute; miRNA; nucleoporin; Nup358

**Subject Category** RNA Biology

**DOI** 10.15252/embr.201642386 | Received 15 March 2016 | Revised 13 November 2016 | Accepted 24 November 2016

## Introduction

Regulation of gene expression at the translational level is shown to be involved in diverse cellular processes and has emerged as an

area of intense investigation. Small non-coding RNAs, particularly microRNAs (miRNAs), appear to significantly contribute to this layer of regulation. miRNAs, which are of ~22 nucleotides length, suppress translation of mRNAs that possess partial or complete sequence complementarity, mostly at the 3'-untranslated region (UTR) [1]. Predictions based on sequence analysis have indicated that miRNAs could target over 50% of human protein-coding genes [2]. The genes encoding miRNAs are generally transcribed by RNA polymerase II to produce primary miRNAs (pri-miRNAs), which are processed into precursor miRNAs (pre-miRNAs) by the microprocessor complex containing Drosha and DGCR8 in the nucleus [3]. The pre-miRNA, in complex with exportin-5 and RanGTP, is exported through the nuclear pore complex (NPC) into the cytoplasm, where it is further processed by Dicer into double-stranded miRNA. One of the strands stably associates with Argonaute (AGO) protein to generate a functional miRISC. Humans have four AGO isoforms: AGO1–AGO4 [4]. A glycine–tryptophan (GW)-rich protein, GW182 (also called TNRC6), interacts directly with AGO proteins and is essential for miRISC-mediated translational repression and/or degradation of target mRNAs through recruitment of deadenylation and decapping complexes. The suppression and/or degradation of target mRNAs is believed to occur in the cytoplasmic foci termed as “processing bodies (P bodies)” [5,6]. As downstream effectors, GW182 family of proteins directly bind to AGO proteins through conserved GW/WG sequence. This motif is also present in other AGO-interacting proteins and is referred to as “AGO hook” [7,8].

Argonaute proteins have a highly conserved role in RNA silencing [4]. AGO family is divided into two clades based on their functions: AGO and PIWI subfamilies. As described earlier, AGO subfamily proteins are present ubiquitously and are involved in small interfering RNA (siRNA)-mediated cleavage of mRNA or miRNA-mediated suppression of mRNA translation [4]. However, the members of PIWI subclade are mostly present in germ cells and

<sup>1</sup> National Centre for Cell Science, S.P. Pune University Campus, Pune, India

<sup>2</sup> Division of Biology, Indian Institute of Science Education and Research, Pune, India

\*Corresponding author. Tel: +91 20 25708084; E-mail: josephj@nccs.res.in

<sup>†</sup>These authors contributed equally to this work

are involved in silencing transposons, maintenance of genome integrity, and gametogenesis [9].

Although the subcellular location where the loading of miRNAs to AGO proteins (miRISC formation) and association of miRISC with the target mRNAs occur is not well understood, recent studies have indicated a role for endoplasmic reticulum (ER) in these processes. It was shown that *Arabidopsis* AGO1 associates peripherally with ER, and miRISC could inhibit the translation of target mRNAs on the ER [10]. Another study indicated that rough ER could be the site for miRNA and siRNA loading to AGO proteins and translational regulation of target mRNAs [11]. A central question that is yet unresolved is how miRISC identifies the target mRNAs *in vivo*. Although a sorting mechanism could be envisaged that couples the RNAs exported from the nucleus with the miRISC, there is no available evidence for the existence of such machinery.

The nuclear envelope (NE) that encircles the nucleus is an extension of ER and is made up of a double-layered membrane. Nuclear pore complexes (NPCs) form the molecular gates on the NE, through which the transport of macromolecules between the nucleus and the cytoplasm occurs [12]. The protein components of NPCs are termed as nucleoporins (Nups), and each mammalian NPC contains around 30 different nucleoporins in multiple copies [13]. The spatial distribution of individual nucleoporins within the NPC structure could vary [14]. Although the nucleoporins are fundamentally expected to be involved in the regulation of nucleo-cytoplasmic transport, several of them are shown to have multiple other functions [15,16].

Apart from the localization to NPCs on the NE, some nucleoporins also accumulate in annulate lamellae (AL), which are stacked ER membrane-containing pore-like structures [17–19]. These AL pore complexes show gross structural similarities to that of NPCs at electron microscopy level [17,19]. Although AL structures have been extensively analyzed in male and female gametes, other proliferating non-germ cells also possess varying quantities of AL [17,19]. The functional role for these structures in any cellular processes is unclear. Previous studies have implicated AL as the storehouse of excess nucleoporins to be supplied as and when the cell requires, for example, to meet the increasing demand for nucleoporins in the assembly of new NPCs during initial zygotic cell divisions. However, there is experimental evidence arguing against such a function [20]. Consistent with being a part of the endoplasmic reticulum, electron microscopic studies also have suggested AL to often have RNA and ribosomes in their close vicinity [17,19]. Previous studies have shown that AL associate with MEX-3-positive RNP granules in the arrested *Caenorhabditis elegans* oocytes and that several nucleoporins play a role in the complete assembly of these RNP granules [21]. However, whether AL associate with other mRNP granules and play a role in their functions is not known.

Nup358 is a nucleoporin that localizes to the cytoplasmic side of the NPC and has been implicated in several functions [22–31]. Depletion of Nup358 does not appear to grossly affect transport of macromolecules across the NE, although some studies suggest a role for this nucleoporin in specific receptor- and cargo-dependent transport [32–36]. Nup358 has been identified as a small ubiquitin-like modifier (SUMO) E3 ligase [28] and is shown to mediate *in vivo* SUMOylation of substrates such as topoisomerase II [37], borealin [38], and Ran [39].

SUMO is a small protein that gets covalently conjugated to target proteins through specific lysine residues and modulates their

function [40,41]. SUMO pathway is shown to be involved in multiple cellular processes [42]. In humans, there are four SUMO isoforms: SUMO1–4. In addition to the covalent interaction, SUMO associates with other proteins through directly binding to specific SUMO-interacting motif (SIM), which is characterized by a conserved set of hydrophobic amino acids [40,41]. Multiple SIMs have been identified in many SUMO-interacting proteins and functionally validated [43]. The presence of a stretch of negatively charged amino acids adjacent to the N- or C-terminus of the hydrophobic sequence (SIM) is shown to contribute to the strength, orientation, and paralog specificity of SUMO binding [42].

SUMO conjugation to the substrate lysine requires concerted action of SUMO-specific E1 (Aos1/Uba2 heterodimer), E2 (Ubc9), and multiple E3 ligases [42]. RanGTPase-activating protein (RanGAP) is the first SUMO substrate identified [44–46]. SUMO gets attached to lysine 524 of human RanGAP, which targets it to the NPC through binding to Nup358. Structural and functional analyses showed that SUMO-RanGAP interacts with Nup358 through a region having internal repeats (IR) harboring two SIMs [47,48]. Nup358-IR also possesses the SUMO E3 ligase activity [28]. Each of the two repeats, IR1 and IR2, has a SIM-binding and a Ubc9-binding domain [49,50]. However, studies have shown that IR1 (SIM1) is involved in SUMO-RanGAP1 interaction, which is stabilized by Ubc9 as it directly binds to IR1, RanGAP1, and SUMO [47,51]. *In vitro* studies have illustrated that SUMO-RanGAP and Ubc9 form a stable complex with IR1, and not with IR2 [51–53]. Although no conclusive evidence exists, it is believed that SUMO-dependent binding of RanGAP1 to Nup358 would enhance RanGAP's ability to activate the hydrolysis of GTP on Ran in the export complex [54,55]. Endogenously, bulk of RanGAP is SUMO-modified and has been shown to associate with Nup358 throughout the cell cycle [25,56].

Here, we show that Nup358-positive AL structures dynamically associate with cytoplasmic mRNPs such as P bodies and stress granules (SGs). Furthermore, our study reveals interaction between Nup358 and components of miRISC, AGO, and GW182. The results suggest an unanticipated function for this nucleoporin in miRNA-mediated gene silencing by aiding in the coupling of miRISC with target mRNAs. The results also indicate a possible role for AL in the miRISC-mRNA coupling process. Interestingly, characterization of Nup358-AGO interaction led to identification of SIM as a new conserved interaction motif for AGO family of proteins. Our data also suggest that Nup358-AGO interaction is essential for miRNA-mediated suppression of mRNA translation.

## Results

### Nup358-positive AL structures and NE associate with SGs and P bodies

Localization of endogenous Nup358 in HeLa cells using a specific antibody showed that, in addition to NE, this nucleoporin is present in cytoplasmic punctate structures along with RanGAP1, a known interacting partner of Nup358 (Fig 1A) [45,46]. To validate whether the cytoplasmic Nup358-positive structures represented AL, we immunostained for other nucleoporins and found these entities to contain Nup214 (Fig 1A) and Nup62 (Fig EV1A), but not Nup153 (Fig EV1A). Moreover, these Nup358-positive structures were

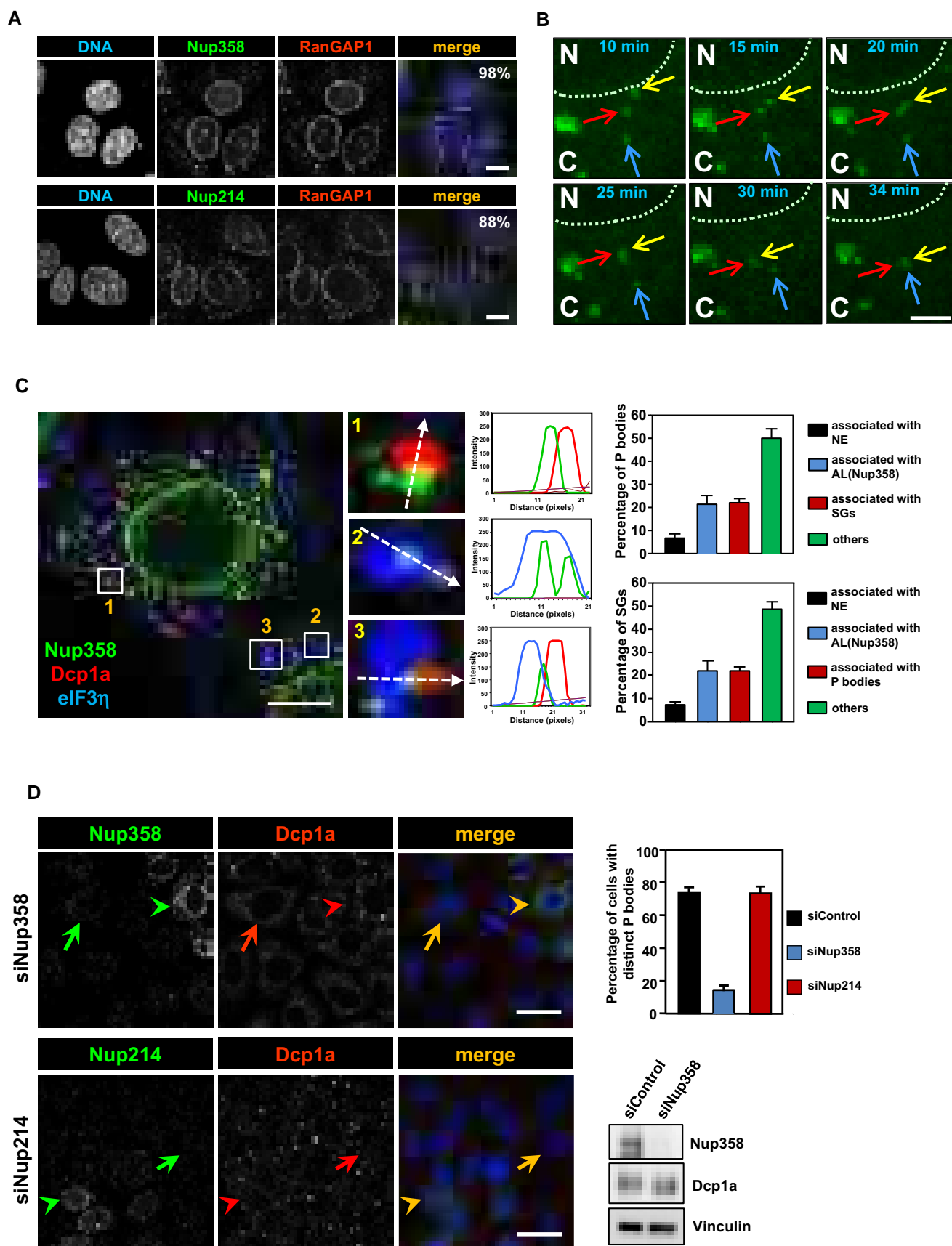


**Figure 1. Nup358-positive AL structures associate with P bodies and SGs, and Nup358 depletion leads to impairment of P body assembly.**

- A Confocal microscopic image showing HeLa cells immunostained for Nup358 (green, upper panel) or Nup214 (green, lower panel) and RanGAP1 (red) using specific antibodies. DNA was stained with Hoechst 33342 (blue). Scale bars, 10  $\mu$ m.
- B COS-7 cells were transfected with GFP-Nup358 and one of the cells was subjected to live imaging using confocal microscopy, and the frames at the indicated time points have been provided. Arrows denoted by different colors indicate individual AL structures. Note that one of the AL structures (marked by yellow arrow) originated from the NE (dotted line) and fused with another AL structure (marked by red arrow), which later fused with a different AL structure (marked by blue arrow). N, nucleus; C, cytoplasm. Scale bar, 5  $\mu$ m.
- C Maximum-intensity projection confocal image of a sodium arsenite-treated HeLa cell immunostained for endogenous Nup358 (green), P bodies (red, Dcp1a as a marker), and SGs (blue, eIF3 $\eta$  as a marker) using specific antibodies. Scale bar, 10  $\mu$ m. The histograms represent fluorescence intensity profile along the dotted arrows. Adjacent graph represents quantitative data showing percentage of P bodies (top) or SGs (bottom) associated with nuclear envelope (NE), Nup358-positive AL, with each other or unassociated with any of the other mentioned structures (others). Data are presented as mean  $\pm$  SD ( $n = 3$ ).
- D HeLa cells were transfected with Nup358 siRNA (siNup358) or Nup214 siRNA (siNup214). Cells were fixed and stained for endogenous Nup358 (green, upper panel) or Nup214 (green, lower panel) and endogenous P body marker (Dcp1a, red). Graph represents the quantitative data as mean  $\pm$  SD. The data were obtained from three independent experiments, and in each experiment, 100 cells were counted from different fields for the presence of intact microscopically distinct P bodies and expressed as percentage. Western blots (WB) indicate the extent of Nup358 depletion and the level of Dcp1a. Arrow indicates Nup358/Nup214 depleted cell and arrow head shows non-depleted cell. Scale bar, 10  $\mu$ m.

associated with ER, particularly marking distinct domains within the ER (Fig EV1B). Co-localization with a set of nucleoporins and association with ER indicated that Nup358-positive cytoplasmic structures represented the previously characterized AL [57,58]. Exogenously expressed GFP-tagged Nup358 (GFP-Nup358) also accumulated in AL, as confirmed by its co-localization with AL-specific nucleoporins such as Nup214 and Nup62 (Fig EV1C).

The nature and origin of AL have been unclear, and to monitor these, we analyzed the dynamics of GFP-Nup358-labeled AL using live cell imaging (Movie EV1). We observed that AL were highly dynamic and often underwent homotypic fusion with neighboring AL structures. Interestingly, we noticed that some AL structures were budding off from the NE and fusing with the pre-existing cytoplasmic AL (Fig 1B and Movie EV2). These results suggested that cytoplasmic AL could originate from NE and are extensively dynamic entities.

Further, we sought to investigate the distribution of AL in relation to other cytoplasmic structures. Interestingly, we found that two cytoplasmic messenger ribonucleoprotein (mRNP) granules, namely SGs and P bodies, were often associated with or present juxtaposed to AL (Fig 1C). We subjected HeLa cells to oxidative stress through sodium arsenite treatment to induce SGs [59] and immunostained for endogenous Nup358, eIF3 $\eta$  (SG marker), and Dcp1a (P body marker). P bodies and SGs were found often juxtaposed to each other in the cytoplasm as previously reported [59]. Interestingly, we observed that many individual Nup358-positive AL structures were present adjacent to SGs or P bodies, and in some cases, all three structures appeared to physically associate with each other (Fig 1C). Quantitative analysis suggested that ~20% of P bodies were associated with either Nup358-positive AL or SGs, whereas ~50% of them were found to be associated with neither AL nor SGs, and ~6% were associated with the NE (Fig 1C). Similarly, ~20% of SGs were associated with either Nup358-positive AL or P bodies, whereas ~50% of them were found to be associated with neither AL nor P bodies, and ~10% were associated with the NE (Fig 1C). In unstressed cells, ~16% of endogenous P bodies associated with Nup358-positive AL structures. The physical association was much more striking when GFP-Nup358 was exogenously expressed along with RFP-Dcp1a (P body marker) or RFP-G3BP1 (SG marker) (Fig EV1D and E). Under this condition, ~47% of P bodies associated with Nup358-positive AL, whereas < 10% associated with the NE (Fig EV1D). Similarly, ~58% of SGs were present

juxtaposed to Nup358-positive AL and ~10% were associated with NE (Fig EV1E). Live cell imaging, interestingly, indicated a dynamic interplay between the two mRNP granules and Nup358-positive AL/NE (Movies EV3 and EV4).

### Depletion of Nup358 disrupts P body formation

The dynamic association of Nup358-positive AL/NE with SGs and P bodies prompted us to investigate whether any functional link exists between these entities. Toward this, we tested whether siRNA-mediated Nup358 depletion caused any effect on the assembly of mRNP granules. Removal of Nup358 did not have any gross effect on SG assembly (assessed by SG-specific marker, eIF3 $\eta$ ) as compared to control cells (Fig EV1F). Neither did depletion of Nup214, another nucleoporin present on the cytoplasmic face of NPC and AL, show any effect on SG assembly (Fig EV1G). Interestingly, knockdown of Nup358, but not Nup214, led to dramatic impairment of P body assembly as assessed by Dcp1a staining (Fig 1D). However, the levels of Dcp1a were comparable between control and Nup358 knockdown cells (Fig 1D). These results demonstrated a specific requirement for Nup358 in P body formation, and possibly in its function.

### Nup358 is required for miRNA-mediated translation suppression

Previous studies have shown that mRNAs suppressed by miRISC localize to P bodies [5,6], and disturbances in miRNA pathway lead to disruption of microscopically visible distinct P body structures [60]. We sought to find out whether Nup358 depletion affected the miRNA pathway. As let-7a is one of the abundant miRNAs expressed in HeLa cells, a *Renilla* luciferase (RL) reporter construct that expresses RL mRNAs containing three imperfect let-7a binding sites in its 3'-UTR (RL-3xBulge) was used to monitor let-7a-mediated translation suppression in HeLa cells [61]. Compared to control *Renilla* luciferase (RL-control) mRNAs that did not have any let-7a binding site, RL-3xBulge generally showed ~60% suppression (Fig 2B). We measured the RL activity in cells depleted of Dicer, Nup214, or Nup358 (Fig 2A) and found that similar to Dicer knockdown, Nup358 depletion caused significant reversal of miRNA-mediated suppression (Fig 2B). Cells with Nup214 knockdown, however, showed no significant change in the reporter activity as compared to control siRNA-treated cells (Fig 2B). These results indicated a specific role for Nup358 in miRNA function.

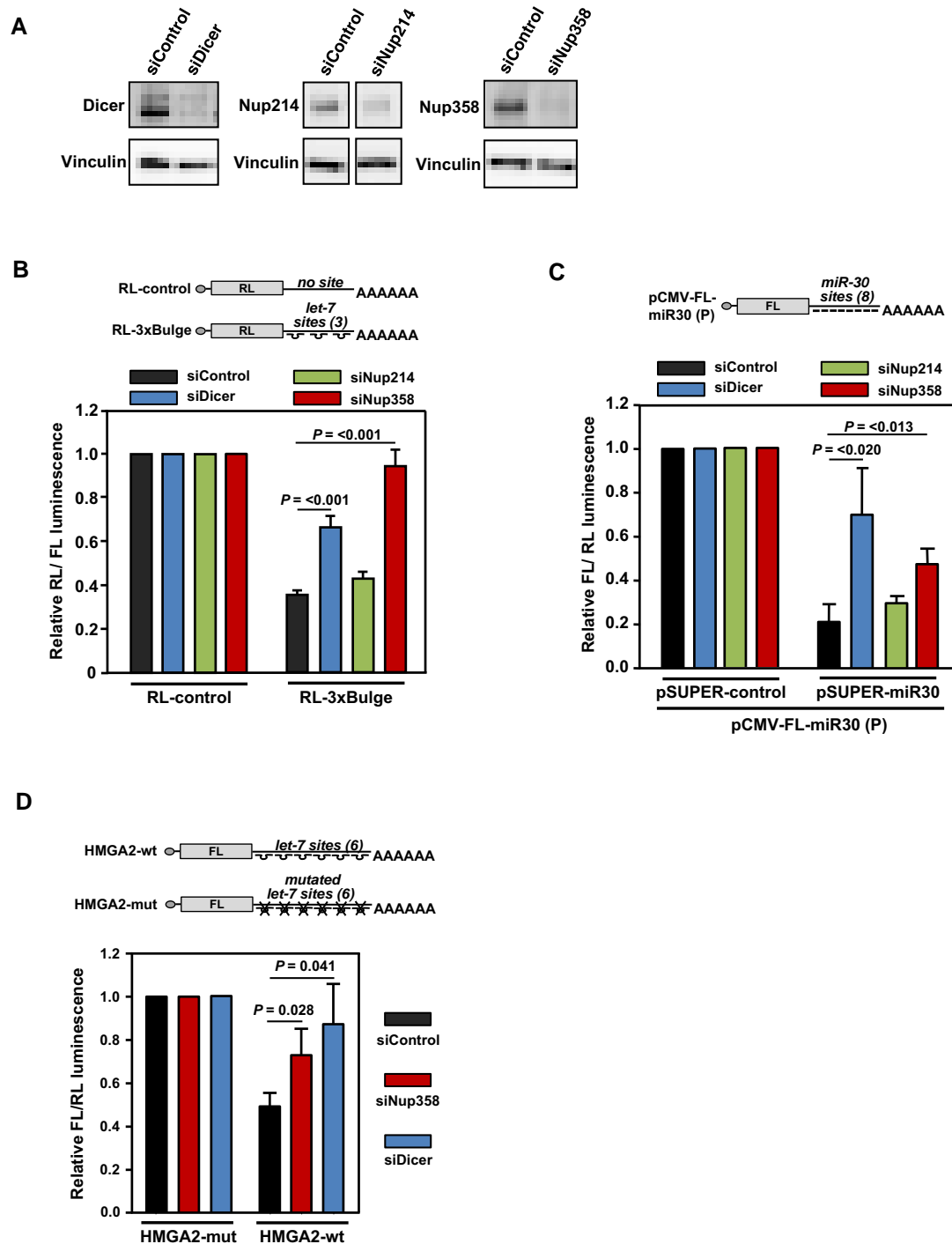


**Figure 2. Nup358 is required for miRNA function.**

- A Western analysis of HeLa cells, treated with control (siControl), Dicer (siDicer), Nup214 (siNup214), or Nup358 (siNup358) siRNA, for assessing the extent of protein depletion using indicated antibodies. Vinculin was used as loading control.
- B HeLa cells were initially transfected with indicated siRNAs, followed by *Renilla* luciferase (RL) reporter constructs: RL-control (no let-7a binding site in the 3'-UTR) or RL-3xBulge (3 imperfect let-7a binding sites in the 3'-UTR). Firefly luciferase (FL) was co-transfected to serve as internal control. RL/FL luminescence ratio was calculated. Data are presented as mean  $\pm$  SD ( $n = 3$ ),  $P$ -values were calculated using Student's  $t$ -test.
- C HEK293T cells were transfected with indicated siRNAs, followed by pCMV-FL-miR30 (P) reporter with either pSUPER-control or pSUPER-miR30 constructs. RL was co-transfected as internal control. FL/RL luminescence ratio was calculated. Data are presented as mean  $\pm$  SD ( $n = 3$ ),  $P$ -values were calculated using Student's  $t$ -test.
- D HeLa cells were initially transfected with control (siControl), Dicer (siDicer), or Nup358 (siNup358)-specific siRNAs, followed by FL constructs containing wild-type (HMGA2-wt) or mutant (HMGA2-mut) HMGA2 3'-UTR, along with RL as internal control. Graph was plotted using data from three independent experiments. FL/RL luminescence ratio was calculated. Data are presented as mean  $\pm$  SD ( $n = 3$ ),  $P$ -values were calculated using Student's  $t$ -test.



To test the generality of Nup358 function in miRNA pathway, we utilized another miRNA reporter system in HEK293T cells, involving firefly luciferase (FL) that contains eight miR-30a perfect binding sites (sequence with complete complementarity to miR-30a) in the 3'-UTR [62]. Nup358 depletion also significantly impaired miR-30a activity (Fig 2C). Additionally, Nup358 was required for let-7-mediated suppression of FL mRNAs engineered to contain the 3'-UTR of *HMGA2* that harbors multiple functional let-7 binding sites (Fig 2D) [63]. Moreover, knockdown of Nup358 using three independent siRNAs targeted to different regions of *Nup358* gene led to significant de-repression of *RL-3xBulge* reporter mRNA (Fig EV2A). When different concentrations of siRNAs were used to deplete Nup358 to varying levels, the de-repression occurred in a dose-dependent manner (Fig EV2B). Ectopic expression of GFP-Nup358 in HeLa cells enhanced miR-30-mediated suppression of FL-reporter mRNA as compared to GFP-control (Fig EV2C). Moreover, exogenous expression of Nup358 also rescued the de-repression caused by Nup358 knockdown (Fig EV2D). Taken together, these results suggested that Nup358 plays an important role in miRNA pathway.

### Nup358 depletion does not affect mature miRNA levels

To test whether Nup358 knockdown affected pre-miRNA export and/or maturation, we measured the levels of mature miRNAs using different methods. Northern blot analysis with specific  $^{32}\text{P}$  radio-labeled miRNA probe indicated that Nup358 depletion did not grossly affect the levels of mature let-7a miRNA in HeLa (Fig 3A, upper panel). As expected, we observed a reduction in the level of mature let-7a in Dicer-depleted cells in comparison with control siRNA-treated cells. These Northern blot results were further confirmed by a TaqMan-based real-time quantitative PCR (qPCR) assay (Fig 3A, lower panel). We also performed deep sequencing of small

RNAs and assessed the relative levels of miRNAs between control and Nup358-depleted HEK293T cells. The results indicated that out of 629 miRNAs commonly detected in control and Nup358 knockdown cells, 494 miRNAs (~78%) showed no significant change in the level of their expression. Among the remaining miRNAs analyzed, ~10% were downregulated and ~12% were upregulated in Nup358-depleted cells as compared to control cells. The relative levels of 50 most abundant miRNAs in HEK293T cells under control and Nup358 knockdown conditions are shown in Fig EV3A. Collectively, these results suggested that Nup358 does not play any significant role in miRNA biogenesis.

As compared to control cells, Nup358-depleted cells did not show any detectable change in the relative distribution of mRNAs between the nucleus and the cytoplasm as assessed by oligo(dT) staining (Fig EV3B). Moreover, the total level and the nucleo-cytoplasmic distribution of specific proteins involved in miRNA pathway were largely unaltered by Nup358 depletion (Fig EV3C). Together, these results indicated that the observed impairment of miRNA function in the absence of Nup358 might not be due to any indirect effect caused by defects in miRNA export and/or processing, mRNA export, or nucleo-cytoplasmic distribution of key proteins involved in miRNA pathway.

### Nup358 is not required for miRISC formation, but is essential for association of target mRNA with miRISC

As the mature miRNA levels were mostly unaffected when Nup358 was depleted, we examined whether this nucleoporin is involved in loading of miRNAs onto AGO proteins. Towards addressing this, AGO2 immunoprecipitation was performed in control or Nup358 siRNA-treated cells, and the immunoprecipitates were analyzed for the presence of specific miRNAs by qPCR. Two abundant miRNAs in HeLa cells (let-7a and miR-17) showed no significant difference in

**Figure 3. Nup358 interacts with AGO and GW182 and is required for coupling miRISC with target mRNAs.**

- A HeLa cells were transfected with control, Dicer, or Nup358-specific siRNAs, as indicated. Upper panel: Total RNA was isolated and analyzed by Northern blotting for let-7a using radiolabeled probe. Ethidium bromide (EtBr)-stained gel indicates equal loading of RNA samples. Bottom panel: Total RNA was isolated from control, Dicer-, or Nup358 siRNA-treated cells and was reverse-transcribed using TaqMan microRNA reverse transcription kit. The levels of let-7a were quantified by qPCR following the manufacturer's instructions. Graph represents the relative levels of miRNAs as compared to U6 RNA control. The values were further normalized to let-7a levels in control siRNA knockdown condition. Data are presented as mean  $\pm$  SD ( $n = 3$ ).
- B HeLa cells were transfected with indicated siRNAs, followed by *RL-3xBulge* construct. Immunoprecipitation (IP) was performed with control mouse IgG (IgG-IP) or anti-AGO2 antibody (AGO2-IP) using lysates prepared from these cells. Total RNA was isolated from control and AGO2 immunoprecipitates and the levels of AGO2-associated let-7a (top left panel) and miR-17 (top right panel) were quantified by qPCR. Graph represents the extent of miRNAs associated with AGO2 as compared to U6 RNA (as a negative control) with AGO2. Bottom left panel: RNA isolated from IgG control or AGO2 immunoprecipitate samples was reverse-transcribed using oligo (dT) primer. *RL-3xBulge* mRNA association with AGO2 was quantified by qPCR and normalized to the level of GAPDH mRNA associated with AGO2. Bottom right panel: AGO2 immunoprecipitates were analyzed by Western blotting using AGO2-specific antibody. Vinculin was used as loading control. Data are presented as mean  $\pm$  SD ( $n = 3$ ).
- C HeLa cells were transfected with control (siControl) or Nup358-specific siRNA (siNup358) for 96 h. Cells were lysed and subjected to immunoprecipitation with control IgG (IgG-IP) or anti-AGO2 (AGO2-IP). Total RNA was extracted from initial lysate and IP samples and analyzed by qPCR for validated miRNA targets, *Serbp1* and *Dnajb11*. GAPDH was considered as negative control. Data expressed as the relative amount of target mRNA associated with AGO2 as compared to GAPDH mRNA. Western blots indicate the extent of Nup358 depletion and AGO2 immunoprecipitation in siControl and siNup358 samples. Vinculin was used as loading control. Data are presented as mean  $\pm$  SD ( $n = 3$ ),  $P$ -values were calculated using Student's  $t$ -test.
- D HeLa cells were treated with indicated siRNAs for 96 h. Cells were lysed and analyzed for extent of Nup358 depletion and for the levels of validated miRNA targets, *Ras* and *c-Myc*, by Western analysis. Vinculin was used as loading control.
- E HeLa cells were lysed and immunoprecipitation was performed with control (IgG-IP) or Nup358 (Nup358-IP, left panel) or AGO2 (AGO2-IP, right panel) using specific antibodies. The immunoprecipitates were washed with a buffer containing (+) or not containing (–) RNase A and probed for the presence of indicated proteins by Western blotting.
- F HeLa cells were transfected with *RL-3xBulge* construct and immunoprecipitation was performed using control (IgG-IP) or Nup358 (Nup358-IP) antibodies. Total RNA was isolated from the immunoprecipitates and analyzed for let-7a miRNA (left panel), *RL-3xBulge* mRNA, and the endogenous miRNA target *Dnajb11* using qPCR (right panel). Fold enrichment in Nup358-IP as compared to IgG control was calculated, and the data are presented as mean  $\pm$  SD ( $n = 3$ ),  $P$ -values were obtained using Student's  $t$ -test.

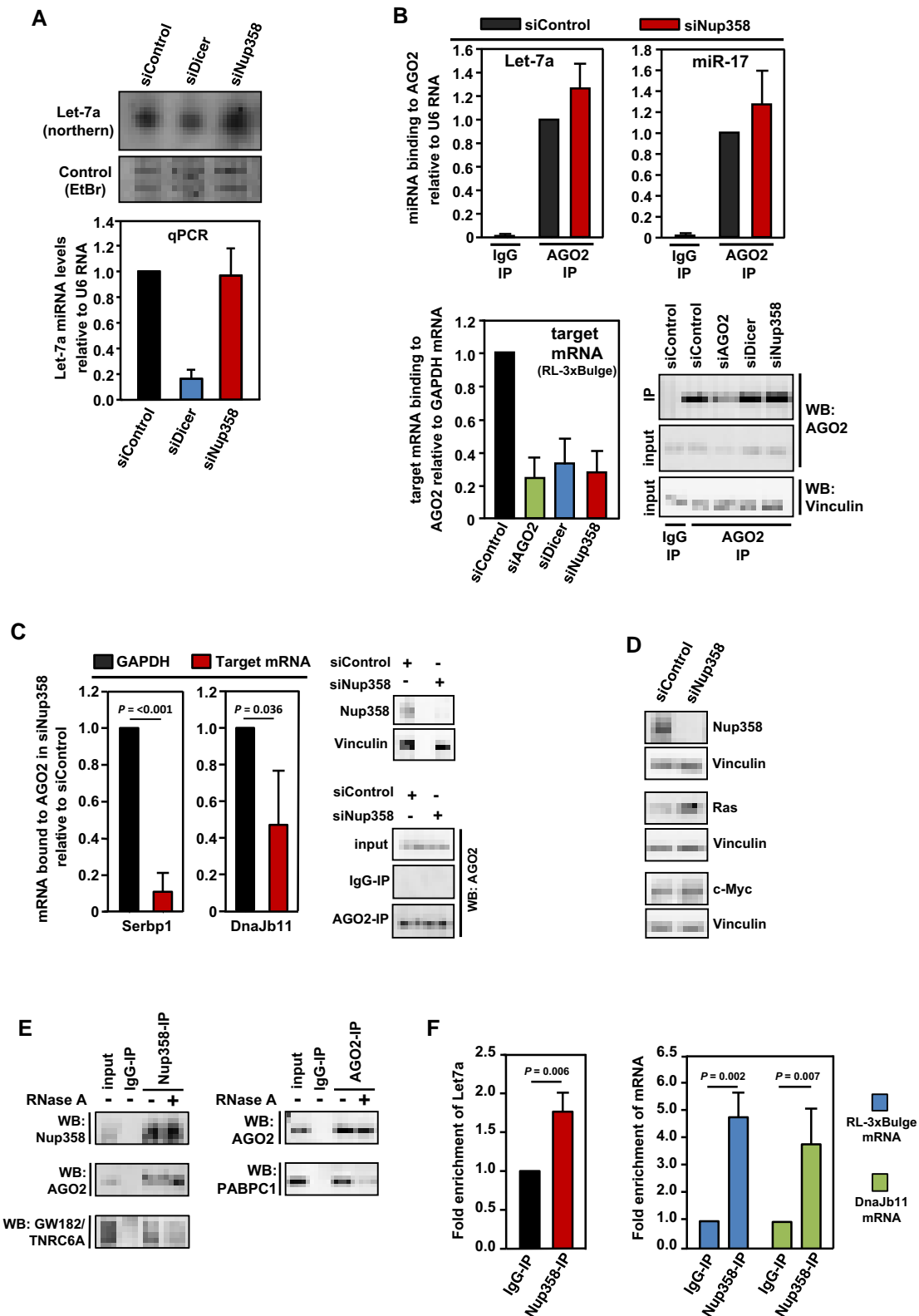


Figure 3.

the extent of their association with AGO2 in the absence or presence of Nup358 (Fig 3B). These results suggested that Nup358 is not involved in loading of miRNA onto AGO2 or miRISC formation.

We next investigated whether Nup358 depletion caused any effect on the interaction of target mRNA with the miRISC. To test this, we immunoprecipitated endogenous AGO2 from HeLa cells

and examined for the presence of *RL-3xBulge* mRNA (a miRNA target that has three imperfect let-7a binding sites) using qPCR. Similar to Dicer- and AGO2-depleted conditions, Nup358 knock-down significantly impaired the ability of miRISC to associate with the *RL-3xBulge* target mRNA (Fig 3B). Furthermore, we analyzed the association of two validated endogenous mRNA targets with AGO2 [63], in the absence and presence of Nup358. In Nup358-depleted cells, binding of AGO2 to Serbp1 and Dnajb11 mRNAs was significantly reduced as compared to that of GAPDH mRNA (Fig 3C). Consistent with a role for Nup358 in miRNA pathway, the protein levels of established miRNA targets such as Ras [64] and c-Myc [65,66] were found to be increased in Nup358-depleted cells (Fig 3D). Collectively, these results indicated that Nup358 is involved in the coupling of target mRNA with miRISC.

To verify this further, we utilized a previously reported artificial AGO2 tethering assay that bypasses the requirement of miRNA for suppression of the target mRNA [67]. The suppression of AGO2-tethered mRNA, however, is dependent on GW182 and downstream effectors [68]. We reasoned that if Nup358 plays a role in the coupling of miRNA with target mRNA, it should be dispensable in a condition where suppression of target mRNA occurs independent of miRNA. Our results showed that Nup358 depletion did not have a specific effect on the ability of tethered AGO2 to suppress the reporter RNA (Fig EV4). This outcome is consistent with the finding that Nup358 is essential for association of target mRNA with miRISC, but is not required once the target mRNA is directly made to interact with the AGO protein. The results also suggested that Nup358 depletion does not cause any general effect on miRNA pathway downstream to miRNA–mRNA association.

#### RNA-binding zinc finger (ZnF) domains of Nup358 are dispensable for miRNA function

Our results suggested that Nup358 could play a role in the coupling of target mRNA with miRISC. Human Nup358 contains eight ZnF domains in the middle region (Fig EV5A), and previous studies have shown these domains to directly bind the signal sequence coding regions present in a subset of mRNAs encoding secretory proteins [69]. Also, RanBP2-type ZnF domains are shown to be present in some RNA binding proteins and contribute to RNA binding [70]. We were interested to examine whether ZnF domains are required for Nup358's function in mRNA–miRISC coupling process. Toward this, let-7a miRNA activity was monitored using reporter assays in Nup358-depleted HeLa cells after expressing a Nup358 deletion mutant that was devoid of ZnF domains. The results showed that the mutant protein was capable of almost completely rescuing the de-repression caused by Nup358 depletion (Fig EV5B), supporting the conclusion that the RNA-binding ZnF domains are dispensable for Nup358's function in miRNA pathway.

#### Nup358 interacts with AGO2 and GW182

Based on the finding that Nup358 functions in coupling the target mRNA to miRISC, we tested whether Nup358 interacts with components of miRISC. We immunoprecipitated endogenous Nup358 from HeLa cells and analyzed the immunoprecipitate for the presence of AGO2 and GW182. The co-immunoprecipitation assay suggested that Nup358 associated with both AGO2 and GW182 *in vivo*

(Fig 3E). This interaction was found to be independent of RNA, as RNase A treatment did not alter the association of Nup358 with AGO2 or GW182 considerably (Fig 3E). Under the same condition, as previously shown, the interaction of AGO2 with PABPC1 was found to be RNA-dependent [63] (Fig 3E).

We further tested whether Nup358 associates with miRISC and target mRNAs *in vivo*. HeLa cells were transfected with *RL-3xBulge* (let-7a target), and RNA–protein cross-linking was performed using formaldehyde. The cell lysates were subjected to immunoprecipitation using IgG control or Nup358-specific antibodies, and the immunoprecipitates were analyzed for the presence of let-7a by qPCR. As compared to IgG control, Nup358 immunoprecipitate had significantly higher levels of let-7a miRNA (Fig 3F). Moreover, the ectopically expressed (*RL-3xBulge*) and endogenous (*Dnajb11*) mRNA targets were also enriched in Nup358 immunoprecipitate (Fig 3F). Collectively, these results suggested that Nup358 associates with the protein and RNA components of the miRNA-induced silencing complex *in vivo*.

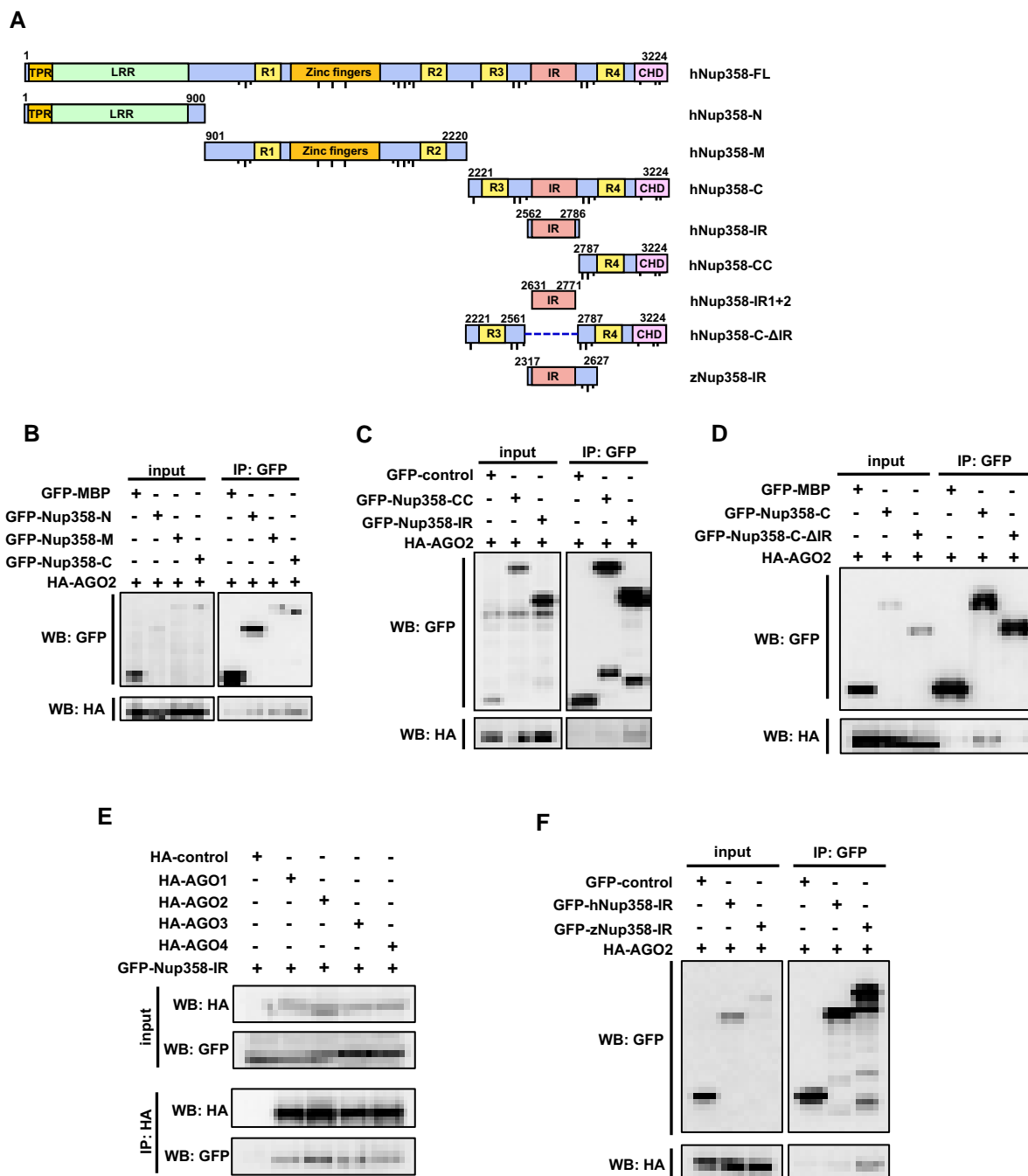
#### Nup358 interacts with AGO proteins through the IR region

Nup358 is a large nucleoporin with multiple domains (Fig 4A). We wished to characterize the interaction between Nup358 and AGO proteins in detail. To delineate the region in Nup358 that is involved in the interaction with AGO, GFP-tagged N-terminal (Nup358-N), middle (Nup358-M), or C-terminal region (Nup358-C) of Nup358 was expressed along with HA-AGO2 in HEK293T cells. Co-immunoprecipitation assays revealed that AGO2 specifically interacted with all three fragments of Nup358, and more prominently with the C-terminal fragment (Fig 4B). Further, we proceeded to identify and characterize the minimum region in Nup358-C required for interaction with AGO2. Experiments with deletion constructs of Nup358-C indicated that the IR region was sufficient to mediate the interaction with AGO2 (Fig 4C). Consistent with this, a deletion mutant of Nup358-C lacking the IR region failed to interact with AGO2 (Fig 4D).

To examine the conservation of interaction between Nup358 and AGO subfamily proteins, GFP-IR was co-expressed with HA-tagged AGO1–4 in HEK293T cells. Co-immunoprecipitation assay confirmed that IR region physically associated with all four AGO proteins (Fig 4E). Moreover, a fragment encompassing the IR region derived from zebrafish Nup358 also showed specific interaction with human AGO2 (Fig 4F). Collectively, these data demonstrated that IR provides a conserved region for interaction with AGO subclade of proteins.

#### SIM is a conserved motif for AGO interaction

As the results suggested that IR region of Nup358 is involved in binding to AGO proteins, we investigated this molecular interaction in detail. Nup358-IR possesses two internal repeats, each of them having a SIM-binding and a Ubc9-binding region (Fig 5A) [50]. Interestingly, we found that both IR1 and IR2 could independently interact with AGO2 in a SIM-dependent manner (Fig 5B). However, as known earlier, IR1, and not IR2, specifically interacted with endogenous SUMOylated RanGAP and Ubc9 [50,51]. Also, deletion of SIM1 from IR1 abrogated the interaction with SUMO–RanGAP, but not with Ubc9 (Fig 5B). To test whether SIM is sufficient for

**Figure 4. AGO proteins interact with IR region of Nup358.**

- A Schematic diagram representing the domains and constructs of human (h) and zebrafish (z) Nup358 used in this study. TPR, tetratricopeptide repeat; LRR, leucine-rich region; R1–R4, RanGTP-binding domain; ZnF, zinc finger domains; IR, internal repeats; CHD, cyclophilin-homology domain. Dotted line indicates the deleted region in the indicated construct. FG and F × FG sequence positions are represented as short and long black lines, respectively. Amino acid positions are indicated in numbers. FL, full-length; N, amino-terminal region; M, middle region; C, carboxy-terminal region.
- B HEK293T cells were co-transfected with GFP-maltose binding protein (MBP) control or GFP-tagged version of indicated Nup358 fragments along with HA-AGO2. Immunoprecipitation (IP) was performed using GFP antibodies and the presence of AGO2 was detected by Western blotting (WB) using HA antibodies.
- C Cells were transfected with indicated constructs and IP and WB were performed as described for (B).
- D HEK293T cells transfected with GFP-MBP (control), GFP-Nup358-C, or GFP-Nup358-C-ΔIR (a mutant devoid of IR region) and HA-AGO2. IP and WB analyses were performed as indicated.
- E Cells were transfected with HA-tagged version of indicated AGO subfamily member and GFP-Nup358-IR. IP and WB analyses were performed using indicated antibodies.
- F Lysates from cells expressing GFP-control, GFP-human (h) Nup358-IR, or GFP-zebrafish (z) Nup358-IR and HA-AGO2 were immunoprecipitated using GFP antibodies, and the immunoprecipitates were analyzed for the presence of HA-AGO2 by Western blotting.

AGO interaction, we co-expressed HA-AGO2 with GFP-SIM1 or GFP-SIM2. Co-immunoprecipitation assay clearly indicated that SIM1 and SIM2 independently were capable of interacting with AGO2, but not with SUMO~RanGAP or Ubc9 (Fig 5C).

It has been shown previously that Ubc9 preferably binds to IR1 and stabilizes the interaction between IR1 and SUMO~RanGAP [50,51]. We wished to test whether Ubc9 is required for the interaction between IR (IR1 + 2) and AGO2. Interestingly, a mutant of IR that is defective in binding to Ubc9 (IR1 + 2<sup>L2651A,L2653A</sup>) [37] still efficiently associated with AGO2, whereas as expected, it failed to interact with SUMO~RanGAP (Fig 5D). Moreover, deletion of SIM1, but not SIM2, from IR disrupted its interaction with AGO2, indicating that in the context of intact IR, AGO2 interaction is mainly dependent on SIM1 (Fig 5E). As expected, SIM1 deletion also impaired the ability of IR to associate with SUMO~RanGAP, and not with Ubc9 (Fig 5E). Taken together, these results suggested that AGO-IR interaction requires neither Ubc9 nor SUMO~RanGAP, and SIM is the minimum region in Nup358 required for the interaction with AGO2.

Earlier studies indicated that within Nup358-SIM1, the hydrophobic amino acids V<sup>2632</sup>, I<sup>2634</sup>, and L<sup>2635</sup> contribute to SUMO binding [48]. We found that substituting these residues with alanine compromised the SIM's ability to bind AGO protein (Fig 6A), indicating that the binding mode of SIM with SUMO and AGO proteins could be similar. The finding that both SIM1 and SIM2 from Nup358-IR independently interacted with AGO2 prompted us to investigate whether SIMs derived from other SUMO-interacting proteins are capable of binding to AGO. Toward this, GFP-fused SIMs from PIAS1 and TTRAP (Fig 6B) were individually co-expressed with HA-AGO2 in HEK293T cells and assessed for their ability to interact with AGO2 by co-immunoprecipitation assays. It has already been shown that PIAS1-SIM interacts with both SUMO1 and SUMO2, whereas TTRAP-SIM shows greater preference for SUMO2 [43]. We found that irrespective of the proteins from which they were derived, both the SIMs interacted with AGO2 (Fig 6B). Moreover, SIM could associate with both AGO1 and AGO2 (Fig 6C). Collectively, these results indicated that SIM provides a binding platform for conserved interaction with AGO subfamily of proteins.

To examine whether SIM directly binds to AGO proteins, we resorted to bacterially expressed recombinant proteins. Mixed bacterial lysates expressing maltose binding protein (MBP, control) or MBP-AGO2 along with GST (control) or GST-SIM1 were used for performing GST pull-down assays. The results suggested that GST-SIM1 specifically interacted with AGO2 *in vitro*, indicating that SIM can directly bind to AGO2 (Fig 6D). Collectively, these experiments suggested that SIM provides a direct binding platform for AGO proteins.

Nup358 contains five potential SIMs as predicted by the GPS-SUMO program at medium SUMO interaction threshold values (<http://sumosp.biocuckoo.org>) [71]. These include one SIM in the N-terminal region (Nup358-N), two within the middle region (Nup358-M), and two in the C-terminal region (Nup358-C) (Appendix Fig S1). The presence of SIMs in all the three regions provides an explanation for the association of all these fragments with AGO2 (Fig 4B).

### SIM can bind to PIWI clade of proteins

As PIWI and AGO subfamilies of proteins share similarity in domain architecture and functions in terms of small RNA-mediated gene

silencing [4], we tested whether SIM could also bind to PIWI proteins. To address this, co-immunoprecipitation assay was performed using HEK293T cells co-expressing GFP-SIM1 and HA-tagged MBP (control), AGO2, MILI, MIWI, or HIWI proteins. The results clearly indicated that PIWI clade proteins, similar to AGO subfamily members, specifically interacted with SIM (Fig 6E). We conclude that SIM provides a general binding platform for interaction with AGO family of proteins.

### Potential SIM-binding sites in AGO2

The finding that AGO proteins bind to SIM raised the possibility that AGO has SUMO-like domains found to be present in a few proteins [72,73]. However, analysis suggested that such domains are absent in AGO proteins. The other possibility included that there could be regions in AGO proteins that are structurally similar to the regions in SUMO that are involved in interaction with SIM [74]. Using a recently developed algorithm, CLICK, probable regions on AGO2 were recognized by structural similarity to the SUMO regions that interact with SIM [75,76]. This structural analysis identified three distinct regions on AGO2 (Fig 6F). The structures of SUMO and AGO2 in the superimposed regions were between 70 and 87% geometrically similar with RMSD values ranging from 1.6 to 1.9 Å. The predicted binding sites comprised amino acids belonging to the N, MID, and PIWI domains of AGO2. These analyses point to the presence of multiple putative SIM-binding sites in AGO proteins.

### Ectopically Nup358-SIM1 functionally interferes with miRNA pathway

As SIM was identified as the minimum region in Nup358 required for binding to AGO proteins, we overexpressed GFP-MBP (control), GFP-Nup358-SIM1, or GFP-Nup358-SIM1-mutant (defective in interaction with AGO) in HeLa cells along with RL-3xBulge reporter to monitor the let-7a miRNA activity [61]. SIM1, but not SIM1 mutant, specifically interfered with the miRNA-mediated suppression of the reporter RNA (Fig 7A), indicating that Nup358-SIM1 has the ability to act in a dominant-negative fashion, possibly by interfering with interaction of endogenous Nup358 with AGO proteins.

Artificial tethering of AGO proteins to the 3'-UTR of reporter mRNA has been shown to suppress the reporter mRNA [67]. We wished to test whether Nup358-IR could be tethered to mRNAs to suppress their expression, presumably by recruiting AGO proteins. As we found that IR1 + 2 mutant (IR1 + 2<sup>L2651A,L2653A</sup>) was incapable of binding to endogenous SUMO~RanGAP or Ubc9, but retained the ability to bind to AGO proteins (Fig 5D), we used this mutant in tethering studies. HEK293T cells were transfected with NΔ-peptide-HA-tagged IR1 + 2<sup>L2651A,L2653A</sup> (N-HA-IR1 + 2<sup>L2651A,L2653A</sup>) along with a reporter construct engineered to express the *Renilla* luciferase mRNA with five BoxB hairpins at its 3'-UTR, which provides binding site for N-HA-tagged proteins [67]. In addition to N-HA-MBP, HA-IR1 + 2<sup>L2651A,L2653A</sup> that is incapable of binding to BoxB hairpin was used as control. The results from tethering assays clearly suggested that N-HA-IR1 + 2<sup>L2651A,L2653A</sup> could significantly suppress the expression of the reporter mRNA (Fig 7B). Collectively, these results support the notion that IR region, and particularly SIM, acts functionally as an AGO-interacting motif.

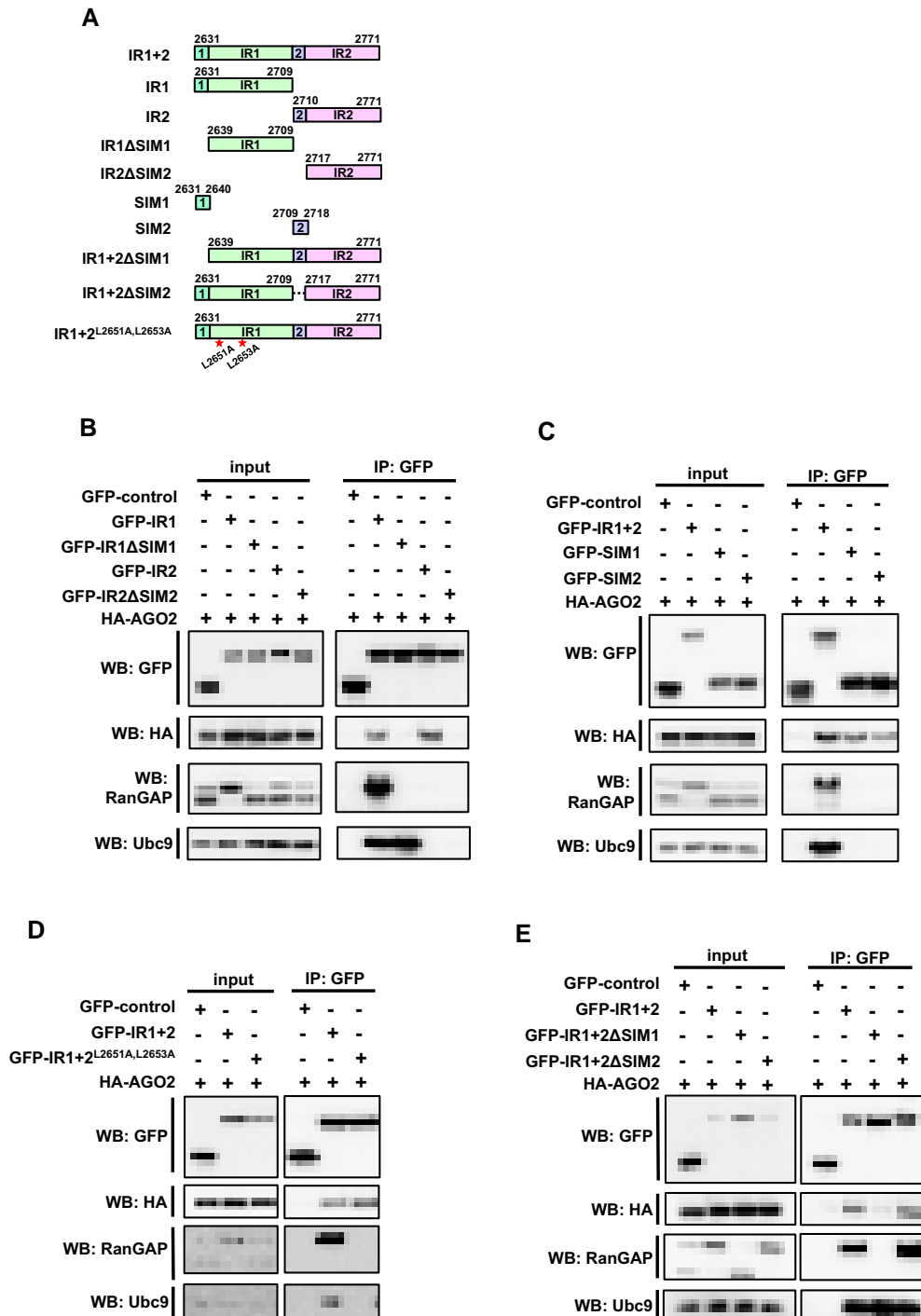


**Figure 5. SIM is the minimum region in Nup358-IR required for binding to AGO2.**

- A Schematic representation of human Nup358-IR region and the constructs used in this study. IR, internal repeats; SIM, SUMO-interacting motif; 1, 2, SIM1 and SIM2. Amino acids substituted in Ubc9 mutant are indicated with red asterisks.
- B HEK293T cells were transfected with indicated constructs, and immunoprecipitation (IP) was performed using GFP-specific antibodies and probed for HA-AGO2 by Western blotting (WB) using HA antibodies. Endogenous RanGAP and Ubc9 were probed with specific antibodies.
- C Lysates prepared from cells expressing the indicated constructs were subjected to IP and WB using indicated antibodies. The presence of endogenous RanGAP and Ubc9 was determined by WB.
- D GFP-control, GFP-IR1 + 2 wild type, or mutants were co-expressed with HA-AGO and IP and WB analyses were performed to detect the interaction using indicated antibodies.
- E Lysates prepared from cells expressing the indicated proteins were immunoprecipitated with GFP-specific antibodies, and the presence of specific proteins in the immunoprecipitates was detected by WB with indicated antibodies.



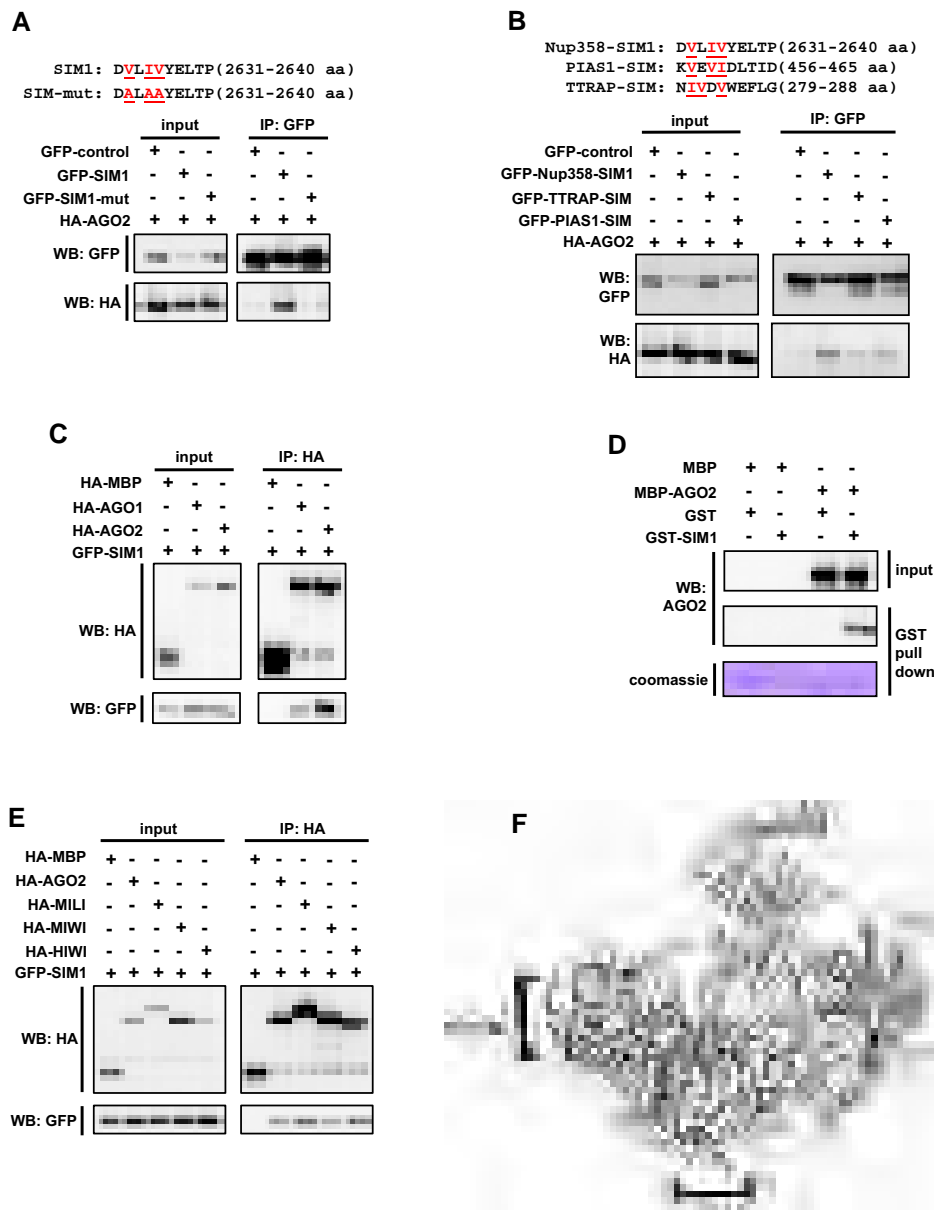


**Figure 6. SIM provides a conserved platform for interaction with AGO family of proteins.**

- A** Top panel: depiction of the amino acid sequence corresponding to the Nup358-SIM1 region and substitutions introduced in the SIM1 mutant. Bottom panel: HEK293T cells were co-transfected with GFP-control, GFP-SIM1, or GFP-SIM1-mut along with HA-AGO2 and immunoprecipitation (IP) was performed with GFP-specific antibodies, and Western analysis (WB) of the input lysate and immunoprecipitates was carried out using indicated antibodies.
- B** Top panel: depiction of the amino acid sequence corresponding to the SIMs in the indicated proteins used in this study. Hydrophobic residues involved in SUMO binding are indicated in red. Bottom panel: Constructs expressing GFP-control or GFP-fused SIMs of indicated proteins were co-transfected with HA-AGO2 in HEK293T cells, and IP and WB were performed to determine the extent of interaction.
- C** HA-MBP-control, HA-AGO1, or HA-AGO2 was co-expressed with GFP-SIM1 and the cell lysates were subjected to IP with HA antibodies and WB analysis with indicated antibodies to detect the presence of proteins in the immunoprecipitates.
- D** SIM1 directly interacts with AGO2. Bacterial lysates expressing MBP control or MBP-AGO2 and GST or GST-SIM1 were mixed and GST pull-down assay was performed. The presence of proteins in the pull-down samples was analyzed by WB using specific antibodies. The extent of GST pull-down was monitored by Coomassie staining of the membrane (Coomassie).
- E** SIM1 interacts with PIWI subfamily of proteins. HEK293T cells were co-transfected with indicated constructs expressing HA-tagged version of PIWI proteins and GFP-SIM1. IP was performed using HA antibodies. The immunoprecipitates were probed for the presence of GFP-SIM1 using GFP-specific antibodies by WB.
- F** Putative SIM-binding regions in AGO2. Three distinct superimpositions of AGO2 (gray) and SUMO (blue), in complex with Nup358-SIM1 (red), are shown in cartoon representation rendered with Chimera [89]. The residue numbers on the AGO2 that could be the putative SIM-binding regions are labeled. To identify possible Nup358 binding sites on AGO2, the 3D structure of AGO2 (PDB ID: 4W50) [88] was compared with that of SUMO (PDB ID: 1Z5S) [47].



### In Nup358-depleted cells, exogenous expression of AGO2 restores P body formation but does not rescue the defect in miRNA pathway

Previous studies have suggested that P bodies are the sites at which miRNA-mediated suppression/degradation of the target mRNA could occur [5,6]. However, other studies indicated that microscopically visible P body formation is a consequence of miRNA-mediated repression [60]. Therefore, it may be possible that Nup358 participates in miRNA pathway by playing a role at the level of formation and/or functioning of P bodies. Interestingly, exogenous expression of HA-AGO2, but not HA-MBP control, restored P body formation in Nup358-depleted cells to a level almost comparable to that in the control siRNA-treated cells (Fig 7C). Next, we tested whether ectopic expression of AGO2 is sufficient to revert back the miRNA-mediated de-repression caused by Nup358 depletion. HeLa cells were treated with control or Nup358-specific siRNA and subsequently assessed for let-7-mediated repression of the *RL-3xBulge* reporter mRNA in the presence of ectopically expressed HA-MBP (control) or HA-AGO2. Interestingly, expression of AGO2 did not rescue the impairment of miRNA pathway caused by Nup358 knockdown (Fig 7C). Collectively, this suggested that restoration of P body assembly in Nup358-depleted cells was not sufficient to rescue the miRNA-mediated suppression defect. Although the mechanism by which AGO2 expression induced P body formation in Nup358 knockdown cells is not clear, the results supported a functional role for Nup358 in miRNA pathway upstream to P body assembly.

### Nup358 depletion does not affect localization of AGO2 to rough ER

Previously, it has been shown that miRNA-loaded AGO2 localizes to the rough ER [11]. To investigate whether Nup358 plays a role in targeting AGO2 to the rER, membrane flotation assay was performed using cells that were treated with control or Nup358 siRNA. The fractionation was verified by using PDI (ER lumen marker), RPL7a (ribosome marker), and LAMP2 (lysosome marker). The results suggested that Nup358 depletion did not affect the overall localization of AGO2 to rER (Fig 7D), indicating that it may not function in targeting AGO proteins to the ER.

Based on the data presented here, we propose the following model (Fig 7E). Exported mRNAs could be sorted at the NE (NPC) and at the ER (AL) for determination of their eventual fate in the cytoplasm. Nup358, as a component of NPC and AL, is involved in the coupling of target mRNA with miRISC to bring about miRNA-mediated suppression. We propose that Nup358 could essentially exert its function both at the NE and ER. The findings thereby also indicate a specific role of ER in coordinating the cytoplasmic events involved in miRNA-mediated gene silencing pathway.

## Discussion

Here, we show that Nup358 plays an important role in miRNA-mediated translational suppression, by aiding in the coupling of target mRNA with miRISC *in vivo*. Consistent with this function, we find that Nup358 physically interacts with the protein and RNA components of the miRNA-induced silencing complex. Further

characterization of Nup358–AGO interaction revealed the previously characterized SIM as a conserved motif for interaction with AGO family of proteins as well. The functional and evolutionary significance of the finding that the same motif performs binding to AGO and SUMO proteins deserves further investigation. Furthermore, our results with tethering and dominant-negative experiments support the idea that SIM-mediated interaction of Nup358 with AGO proteins is important for miRNA function.

Where does the coupling of miRISC with target mRNA occur? Recent studies indicated a role for ER in this process [10,11]. Our live imaging studies clearly show an intimate interaction of mRNP granules such as P bodies and SGs with cytoplasmic AL and NE. We also found that some of the AL could originate from the NE. Although untested, it is possible that AL could carry mRNAs into the cytoplasm, where the fate of these mRNAs could be regulated. The results reported here point to a potential role of AL as platforms for the regulation of exported and/or cytoplasmic mRNAs by coordinating with machineries involved in mRNA remodeling in the cytoplasm. Although a robust, dynamic association of cytoplasmic AL with the mRNP granules was evident from our live imaging studies, we are unsure whether the coupling occurs only at the AL. Further studies are required to delineate the contribution of NPC- and AL-associated Nup358 in this process. Understanding the mechanistic details by which Nup358 gets targeted to these structures would help address this question conclusively.

Interestingly, exogenous expression of AGO2 could almost completely restore P body formation in Nup358-deficient cells, but failed to rescue the impaired miRNA function (Fig 7C), arguing against an indirect role for Nup358 in miRNA pathway through maintenance of P body integrity. These data strengthen the conclusion that Nup358 plays a role in the coupling of mRNA target with miRISC, and P body disruption observed in Nup358-depleted cells could be a consequence of impaired miRNA function. Furthermore, the observation that overexpression of Nup358 enhances miRNA function (Fig EV2C and D) indicates it to be a rate-limiting factor regulating miRNA pathway in mammalian cells.

Whether Nup358–AGO2 interaction increases the quantitative efficiency of AGO2 to associate with the target mRNA through compartmentalization or it affects miRISC–mRNA interaction at the molecular level is unclear. This interaction, however, does not seem to be essential for targeting the miRNA-loaded AGO2 to the rER (Fig 7D). It is possible that Nup358 acts as a scaffold for mediating the coupling of the target RNA with the miRISC in the context of rER. This could involve interaction of Nup358 with target RNA as well as with the miRISC components AGO and GW182. Interestingly, we have observed that depletion of Nup358 affects target RNA suppression mediated by of miRNA (Fig 2B–D) and not when AGO2 is artificially tethered to the target RNA (Fig EV4). How does Nup358 participate in the coupling of mRNA with AGO protein (or miRISC) only in case of miRNA-mediated suppression? One of the possibilities is that Nup358–AGO interaction is required for a conformational change in AGO protein that favors its binding to target RNA and/or facilitates the miRNA–mRNA base pairing within the RNA-binding groove. The extensive interaction between Nup358 and AGO would help achieve this.

A recent study suggested that Nup358 is important for translational activation of a set of mRNAs encoding secretory proteins [69]. The authors have shown that Nup358 interacts with mRNAs

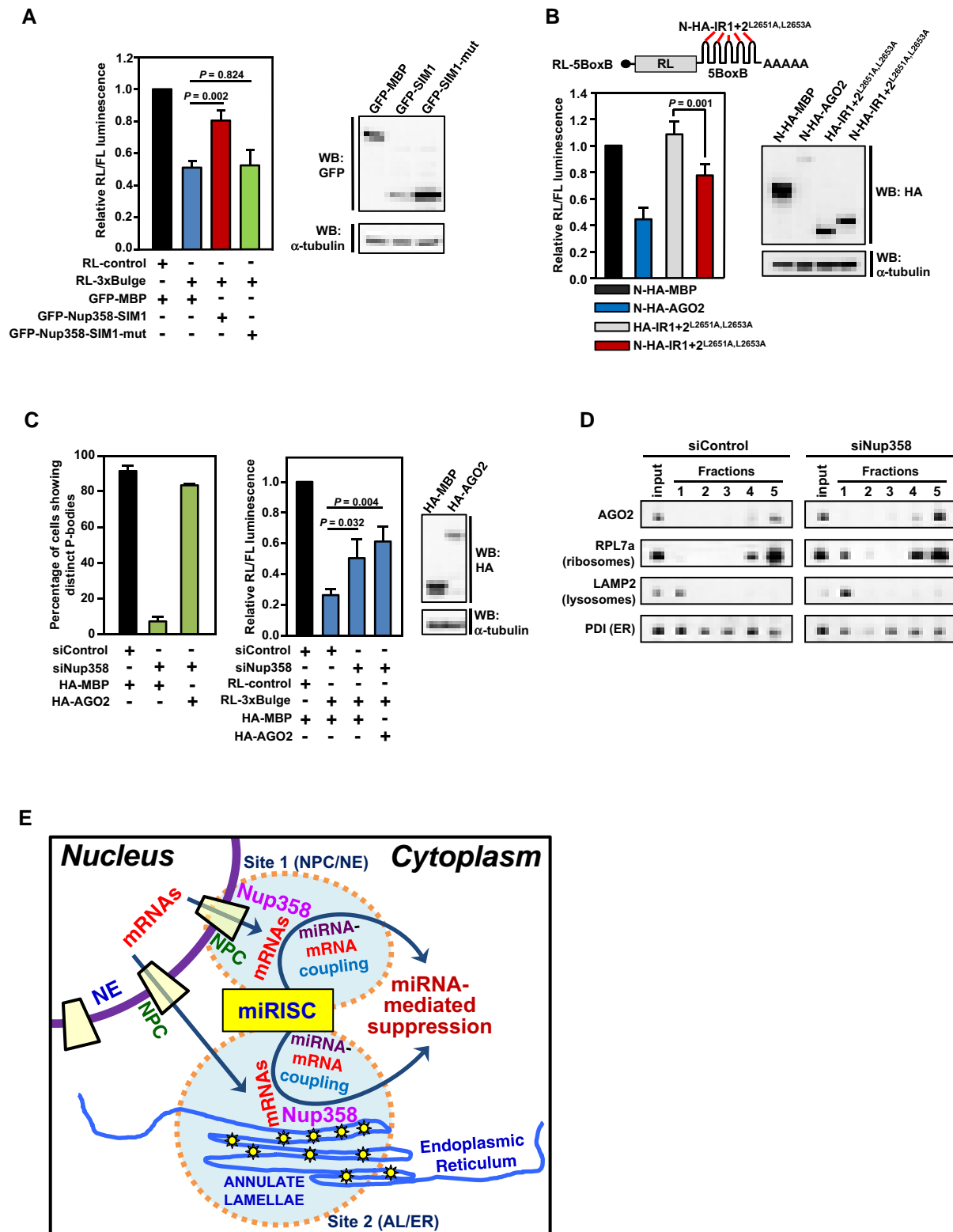


Figure 7.

through the ZnF domains and potentiates their translation. However, the ZnF domains appear to be dispensable for the Nup358's function in miRNA pathway. Combined with the earlier

report, our results suggest that Nup358 might play a general role in determining the cytoplasmic fate of mRNAs (translational activation or suppression), possibly involving different mechanisms.

**Figure 7. Functional relevance of the AGO-interacting motif in miRNA pathway.**

- A Left panel: HeLa cells were co-transfected with GFP-MBP (control), GFP-SIM1, or GFP-SIM1-mut (AGO interaction-defective) along with RL-control or RL-3xBulge. Firefly luciferase was used as transfection control. Dual-luciferase assay was performed. RL/FL luminescence ratio was plotted after normalization with GFP-control. Data are presented as mean  $\pm$  SD ( $n = 3$ ),  $P$ -values were calculated using Student's  $t$ -test. Right panel: Western blots showing the expression of transfected constructs using indicated antibodies.  $\alpha$ -Tubulin was used as loading control.
- B Top panel: Reporter construct used in this study [61]. Bottom left panel: HEK293T cells were co-transfected with indicated expression constructs and the RL reporter. Firefly luciferase (FL) was used as transfection control. Dual-luciferase assay was performed. The ratio of RL/FL luminescence was plotted after normalization with N-HA-MBP control. Data are presented as mean  $\pm$  SD ( $n = 3$ ), and  $P$ -value was calculated using Student's  $t$ -test. Bottom right panel: Western blot for monitoring the expression levels of indicated proteins using antibodies.  $\alpha$ -Tubulin was used as loading control.
- C Ectopic expression of AGO2 restores P body formation, but fails to rescue the impairment in miRNA function in Nup358-depleted cells. HeLa cells were transfected with control (siControl) or Nup358 (siNup358)-specific siRNA, followed by indicated constructs. Left panel: Quantitative representation showing the number of cells showing microscopically distinct P bodies in different indicated conditions. The data were obtained from three independent experiments, and in each experiment, 100 cells were counted from different fields for the presence of intact P bodies and expressed as percentage. Middle panel: HeLa cells were transfected with indicated siRNAs, followed by expression constructs and miRNA RL reporters. FL was used as transfection control. The ratio of RL/FL luminescence was calculated. Data are presented as mean  $\pm$  SD ( $n = 3$ ), and  $P$ -values were obtained using Student's  $t$ -test. Right panel: Western blot analysis for the relative expression of indicated constructs in HEK293T cells.  $\alpha$ -Tubulin was used as loading control.
- D HeLa cells were transfected with siControl or siNup358 and subjected to membrane flotation assay. Fractions were collected and analyzed for the presence of indicated proteins by Western blotting.
- E Model for the role of Nup58 in miRNA-mediated translational suppression. Exported mRNAs could be sorted for miRNA-mediated suppression at two potential sites in the cytoplasm: site 1—the nuclear pore complex (NPC) as a part of nuclear envelope (NE); and/or site 2—annulate lamellae (AL) as a part of endoplasmic reticulum (ER). Nup358, a component of the NPC and AL, plays an important role in the coupling of target mRNA with miRISC.

Our findings show that SUMO–RanGAP interacts with the same region (SIM1) to which AGO also binds. Association of SUMO–RanGAP with the IR region could be competed with increasing levels of AGO2 in cells, indicating that the binding of AGO and SUMO–RanGAP is mutually exclusive (Appendix Fig S2). However, the binding of SUMO–RanGAP and Ubc9 with IR appears to be rather stronger and AGO2 does not completely compete out this interaction. Understanding the functional relevance of mutually exclusive Nup358 complexes, containing either SUMO–RanGAP or AGO proteins, requires further investigation. This could spatially and temporally regulate aspects of Nup358 function within the cell. Intriguingly, the binding of AGO proteins to IR region might influence RanGAP's function and Nup358's SUMO E3 ligase activity.

Previous studies have shown that human AGO2 gets SUMOylated at lysine 402 [77,78]. Consistent with this, we also found that the lysine residue 402, but not 266 or 693, of human AGO2 is modified by SUMO (Appendix Fig S3A). Interestingly, similar to wild type, SUMO-defective mutant (K402R) of AGO2 retained the ability to associate with IR region (Appendix Fig S3B), indicating that the binding of AGO2 to SIM is not dependent on SUMO modification. Moreover, we noticed that unmodified AGO is capable of binding to IR/SIM as revealed by our co-immunoprecipitation assays.

Does AGO bind to IR/SIM as a potential substrate for SUMO modification? We believe it to be unlikely because of the following reasons. Firstly, previous studies have shown that IR acts as an E3 ligase by not directly binding to the substrate, rather binding to SUMO–Ubc9 thioester to enhance the Ubc9 (E2) activity for SUMOylation [47,53]. Secondly, among the four AGO subclade members, only AGO1 and AGO2 have the conserved lysine residue (K402 in AGO2) that undergoes SUMOylation [78]. In spite of this, we found all AGO proteins to have the ability to efficiently bind to IR. Thirdly, binding of SIM to SUMO (as a part of SUMO–Ubc9 thioester) is required for the IR to act as an E3 ligase [50,79], and due to the mutually exclusive nature of interaction between SUMO and AGO with SIM, AGO binding to the SIM would in principle affect IR's E3 ligase activity.

It is worth noting that many RNP structures are found either to be associated with the NE or to be present in close proximity to the

nucleus in different organisms. For example, many germ cell RNP granules are present in the perinuclear region, often adjacent to NE or NPCs, and genome-wide screenings have identified some nucleoporins in having roles in the assembly and function of these structures [80–83]. The physical proximity of these RNP granules to NE or NPCs could also help coupling the exported RNAs to machineries involved in RNA regulation in the cytoplasm.

Is the AL-RNP granule association conserved across evolution? In earlier studies, AL are shown to associate with MEX-3-positive RNP granules in the arrested *C. elegans* oocytes [21]. Interestingly, depletion of npp-9, the Nup358 homolog in *C. elegans*, led to disruption of MEX-3 granules, indicating a role for this nucleoporin in the mRNP assembly [21]. In another study, it was shown that P granules in *C. elegans* are present in the perinuclear region, often adjacent to NPC clusters enriched in npp-9 [84]. This nuclear association was implicated to play a role in collection of mRNAs by P granule components prior to their release into the cytoplasm. The nucleoporin npp-9 also was shown to physically interact with P granules that were released into the cytoplasm [84]. However, the functional role of npp-9 in this context is currently unknown and requires further investigation.

In summary, we have elucidated a novel function for Nup358 in coupling miRISC with the target mRNAs, and a possible role for ER (AL) in this process. Further studies on the interaction between Nup358 and AGO proteins revealed that the previously characterized SUMO interaction motif acts as a binding motif for AGO family of proteins as well. These findings provide a framework not only for exploring the mechanistic details of how Nup358 functions in miRNA pathway, but also to understand the role of ER (AL) in miRNA-mediated suppression.

## Materials and Methods

### Cell culture, treatments, and transfection

HeLa S3, HEK293T, and COS-7 cells were grown in Dulbecco's modified Eagle's medium (Invitrogen) with 10% fetal bovine serum

(v/v) (Invitrogen) and 10 µg/ml ciprofloxacin antibiotics in a humidified incubator at 37°C under 5% CO<sub>2</sub>. For induction of SGs, cells were grown to 60–80% confluency and were subjected to 0.5 mM sodium arsenite treatment for 30 min.

In each well of 24-well plates,  $8 \times 10^4$  cells were seeded on glass coverslip (for immunofluorescence), or  $3 \times 10^5$  cells in each well of 6-well plates or  $1.2 \times 10^6$  cells in each 100-mm dish (for immunoprecipitation). After 12 h, cells were transfected using Lipofectamine 2000 (Invitrogen) for HeLa or polyethyleneimine, linear (PEI, MW-25,000; Polysciences Inc.) for HEK293T and COS-7 cells, following the manufacturer's instructions.

For siRNA transfections, Lipofectamine RNAiMax (Invitrogen) was used according to the manufacturer's instructions. Unless otherwise indicated, all siRNAs were used at a final concentration of 40 nM. The siRNAs were synthesized (Dharmacon) against the following target sequences for different genes: siNup358-A (5' GGTGAAGATGGAT GGAATA 3'), siNup358-B (5' GGTGTGAAATAAAAGTTTA 3'), siNup358-C (5' GGACAGTGGGATTGT AGTG 3'), siControl (5' TTCTC CGAACGTGTCACGT 3'), siNup214 (5' TCAAATA CCTCTAACCTAT 3'), siDicer (5' TTGTTGCGAGGTTGATTCT 3'), and siAGO2 (CAGAGT CCCGTGTGTCCTA 3'). siNup358-A was used as siNup358 in every experiment, unless mentioned otherwise. siNup358-B is directed against 3'-UTR of human Nup358 and was used for rescue experiments.

### Plasmid constructs

GFP-tagged versions of full-length (FL) and fragments of human Nup358 (GFP-Nup358-N, GFP-Nup358-M and GFP-Nup358-C) have been described earlier [31]. GFP-Nup358-CC (2,787–3,224) and GFP-Nup358-IR (2,652–2,786) were generated from GFP-BPC by deleting required 5' and 3' regions using appropriate restriction sites and end-filling. GFP BPCΔIR was generated by replacing the SpeI/KpnI fragment with specific annealed oligos to delete amino acids 2,562–2,786 and to keep the reading frame intact. pEGFP-Nup358ΔM was generated by removing the ApaI fragment corresponding to Nup358-M in pEGFP-Nup358-FL, and replacing it with two annealed oligos (5' CAA GCT TCG CGG CCC GCC CCG GGC C 3' and 5' CGG GGC GGG CCG CGA AGC TTG GGC C 3') to keep N-terminal and C-terminal regions of Nup358 in frame. For generation of deletion mutants of IR, specific primers were used to amplify regions corresponding to 2,631–2,771 (IR1 + 2), 2,631–2,709 (IR1), 2,710–2,771 (IR2), 2,639–2,771 (IR1 + 2ΔSIM1), 2,639–2,709 (IR1ΔSIM1), and 2,717–2,771 (IR2ΔSIM2) using pEGFP-Nup358-IR as the template. The PCR products were cloned at EcoRI/SalI sites of pEGFP-C2 (Clontech). Zebrafish Nup358-IR was amplified using specific primers from a cDNA sample prepared from zebrafish embryos. The region corresponding to 2,317–2,627 amino acids of zebrafish Nup358 was PCR-amplified and cloned into pEGFP-C2 at EcoRI site. To generate 2,631–2,709 + 2,717–2,711 (IR1 + 2ΔSIM2) mutant, appropriate primers were used to PCR-amplify the entire pEGFP-Nup358-IR construct devoid of SIM2 region. The PCR product was self-ligated to obtain the deletion mutant. The resultant construct was verified by sequencing.

The mutant GFP-IR1 + 2<sup>L2651A,L2653A</sup> was generated using a similar strategy as described above, except that the template used for PCR amplification was HA-RanBP2 (2,553–2,838)<sup>L2651A,L2653A</sup> (a kind gift from Jan van Deursen, Mayo Clinic College of Medicine,

USA) [37]. To obtain N-HA-IR1 + 2<sup>L2651A,L2653A</sup>, the PCR product obtained by using appropriate primers and GFP-IR1 + 2<sup>L2651A,L2653A</sup> as the template was cloned at the EcoRI/EcoRV sites of pCI-neo-N-HA vector. To obtain HA-IR1 + 2<sup>L2651A,L2653A</sup>, EcoRI/XhoI fragment from GFP-IR1 + 2<sup>L2651A,L2653A</sup> was subcloned at respective sites in pcDNA-HA vector. For generating Nup358-SIM1 (2,631–2,640), Nup358-SIM2 (2,709–2,718), PIAS1-SIM (456–465), and TTRAP-SIM (279–288), annealed oligos containing these coding sequences with EcoRI/XhoI overhangs were cloned into pEGFP-C2 (Clontech) at EcoRI/SalI sites. HA-AGO2 was generated by subcloning hAGO2 open reading frame (ORF) from pCMV-SPORT-hAGO2 (a gift from Shigeyuki Yokoyama, RIKEN Genomic Sciences Center, Yokohama, Japan) into pcDNA-HA vector using appropriate restriction sites. To generate HA-MBP control, MBP ORF was PCR-amplified from pMAL-p2 (New England Biolabs) as the template, and the product was cloned at EcoRI/SmaI sites of pCI-neo-N-HA. A similar strategy was used to clone MBP into pEGFP-C2 vector to generate GFP-MBP control. For *in vitro* interactions, pMAL-AGO2 was generated by cloning the BamHI fragment having AGO2 ORF from pCMV-SPORT-hAGO2 into pMAL-c2 (New England Biolabs). To generate GST-SIM1, Nup358-SIM1 oligos were annealed and cloned into EcoRI/XhoI sites of pGEX-6P1 vector (GE healthcare). HA-AGO2 mutants—K693R, K402R, and K266R—were generated by PCR-based method using pcDNA-HA-AGO2 as a template and verified by sequencing. pEGFP-SUMO1G and pEGFP-SUMO1GG were generated by PCR-amplifying the SUMO ORF using specific primers and subcloning into pEGFP-C1 (Clontech) at KpnI and SmaI sites.

For generation of shNup358, the oligos (forward: 5' GATCCCCGGTGAAGATGGATGGAATATTCAGAGATATTCATCCA TCTTCACCTTTTGGAAA 3'; reverse: 5' AGCTTTTCCAAAAGG TGAAGATGGATGGAATATCTCTTGAATATTCATCCATCTTCACCG G 3') were annealed and cloned into pSUPER-EGFP (a gift from Ian Macara, Vanderbilt University Medical Center, TN, USA) at BglII-HindIII sites. pSUPER-EGFP vector was used as control.

siRNA-resistant GFP-Nup358ΔM was generated for rescue experiments used in Fig EV5. The siRNA target sequence in Nup358 was changed from 5' GGTGAAGATGGATGGAATA 3' to 5' GGCGAGG ACGGCTGGAACA 3', which results in no change in amino acids. Underlined nucleotides are the ones that were changed. The construct was verified by sequencing.

The constructs, RL-control, RL-3x3Bulge, RL-5BoxB reporters, N-HA-AGO1, N-HA-AGO2, N-HA-AGO3, N-HA-AGO4, N-HA-LacZ, HA-MILI, HA-MIWI, and HA-HIWI were kind gifts from Ramesh Pillai, EMBL Grenoble, France. pCMV-FL-miR30 (P) and pSUPER miR30 constructs were kind gifts from Bryan Cullen (Duke University Medical Center, USA). FL constructs containing wild-type (HMGA2-wt) and mutant (HMGA2-mut) HMGA2 3'-UTR were kind gifts from Gunter Meister (Universität Regensburg, Germany) [63].

### Immunofluorescence microscopy

For immunofluorescence analysis, cells grown on coverslips were fixed using chilled methanol for 5 min. Cells were quickly washed with 0.1% Triton X-100 in Tris-buffered saline (TBS) and then incubated with indicated primary antibodies diluted in TBS containing 2% normal horse serum (Vector Laboratories) for 30 min at room temperature (RT). Cells were washed three times with TBS, followed by addition of fluorescently conjugated secondary



antibodies and incubation for 30 min at RT. Hoechst 33342 dye (Sigma) was used to stain the DNA, which was added to the secondary antibody solution. Cells were again washed three times with TBS, and the coverslips were mounted on glass slides using Vectashield mounting medium (Vector Laboratories). To avoid dehydration, coverslips were sealed using nail polish, and were later observed under microscope. Images were captured with Leica TCS SP5 or Zeiss 510 Meta laser-scanning confocal microscope using a Plan Apochromat 63×/1.4 NA oil immersion objective. Images were processed further in Adobe Photoshop CS2. The microscope has been regularly calibrated for alignment/chromatic aberration between two channels, as evident from the intensity profiles obtained using TetraSpeck beads (Appendix Fig S4).

The following antibodies and dilutions were used for immunofluorescence studies: rabbit anti-Nup358 (1:1,000) generated in the lab [25], mouse anti-Dcp1a (1:1,000; Sigma, WH0055802M6), rabbit anti-Dcp1a (1:2,000; a kind gift from Jens Lykke-Andersen, University of California, San Diego, USA), mouse anti-RanGAP1 (1:500; Santa Cruz, 28322), rabbit anti-Nup214 (1:100; Abcam, ab70497), goat anti-eIF3 $\eta$  (1:500; Santa Cruz, sc-16377), mouse anti-Nup62 (1:100; BD, 610497), mouse anti-protein disulfide isomerase (PDI) (1:1,500; Abcam, ab5484), and mouse anti-Nup153 (a generous gift from Katharine Ullman, University of Utah, USA) antibodies. The following fluorescently labeled secondary antibodies were used: Alexa Fluor 350, 488, 568, or 594 (1:1,000; Invitrogen).

### Live cell imaging

GFP-Nup358 construct has been described earlier [26]. COS7 cells were plated onto 24-mm coverslips (approximately  $2 \times 10^5$  cells). After 12 h, cells were co-transfected with indicated constructs, and after 36 h, coverslips were assembled on Attofluor Cell Chamber (Invitrogen) for live cell imaging in DMEM without phenol red. For analyzing the GFP-Nup358-positive AL dynamics (Fig 1C and Movies EV1 and EV2), the expressing COS-7 cell was imaged for 60 min at 1-min interval, using Zeiss LSM 780 confocal microscope. To analyze P body-Nup358 or SG-Nup358 association (Movies EV3 and EV4), live imaging was performed for 30 min, at 1-min interval, using a laser-scanning confocal microscope (TCS SP5; Leica) with a Plan Apochromat 63× objective (1.4 NA, oil).

For live cell imaging of Nup358 with P bodies or SGs, COS-7 cells were co-transfected with GFP-Nup358 and RFP-Dcp1a (P bodies) (a gift from Ken Fujimura, University of Tokyo, Japan) or RFP-G3BP1 (SGs). The construct RFP-G3BP1 was generated by subcloning human G3BP1-S149A mutant that constitutively induces SGs upon expression [85], from pEGFP-G3BP1-S149A (a generous gift from Jamal Tazi, Institut de Génétique Moléculaire de Montpellier, France) to pDsRed-Express-C1 (Clontech) using appropriate restriction sites.

### Immunoprecipitation and Western blotting

For co-immunoprecipitation of AGO2 and GW182 with Nup358, HeLa cells were washed with ice-cold TBS, scrapped using a cell scraper, and resuspended in chilled lysis buffer (25 mM Tris-HCl, pH 7.4, 150 mM KCl, 0.5% NP-40, 2 mM EDTA) supplemented with 7.5 mM NaF, 0.75 mM sodium orthovanadate, 1 mM PMSF, protease inhibitor cocktail (Roche), leupeptin 50  $\mu$ g/ml, aprotinin 5  $\mu$ g/ml, and pepstatin 2  $\mu$ g/ml. To make a clear lysate, mild

sonication was given (three pulses at 30% amplitude) and repeated 3–4 times depending upon the initial cell volume. Lysate was centrifuged in Eppendorf centrifuge (5417 R) to remove cellular debris at  $\sim 10,600$  g for 10 min at 4°C and was further pre-cleared by incubating with protein A-Sepharose beads (Invitrogen). Starting material was prepared by mixing 1/10<sup>th</sup> volume of the pre-cleared lysate with equal volume 3× SDS-PAGE loading dye and heated at 95°C for 5 min. In the meantime, protein A-Sepharose beads were bound with indicated antibodies by incubating in TBS for 1 h 30 min at 4°C on a rotospin (Bangalore Genei). Antibody-bound beads were then washed with lysis buffer twice, and the pre-cleared lysate was incubated for 2 h at 4°C on rotospin. The immunoprecipitates were then washed with lysis buffer twice, followed by a final wash with TBS before eluting in SDS-PAGE loading dye. The immunoprecipitates were separated on SDS-PAGE and transferred to PVDF membrane (Millipore) using semi-dry transfer apparatus (Bio-Rad or GE). For Western blotting, PVDF membranes were incubated with primary antibody in 1% BSA in TBS with 0.1% Tween-20 (TBST) for 2 h at RT or overnight at 4°C. Membranes were washed thrice with TBST for 3 min each and incubated with HRP-conjugated secondary antibodies in 1% BSA in TBST for 1 h. Membranes were washed thrice with TBST and developed using ECL Plus Western Detection Kit (GE Healthcare or Thermo Scientific) following the manufacturer's instructions. The images were acquired using ImageQuant LAS 4000 (GE Healthcare). EZview™ Red Anti-HA Affinity beads (Sigma) and rabbit GFP antibody [86]-bound protein A beads (Invitrogen) were used for immunoprecipitation of HA- and GFP-tagged proteins, respectively.

For analyzing the RNA dependence of protein interactions, cell lysis and immunoprecipitations were performed using 100 mM Tris-HCl, pH 7.4, 150 mM NaCl, and 0.05% NP-40 supplemented with 7.5 mM NaF, 1 mM PMSF, PIC (Roche), and 80 U/ml of murine RNase inhibitor (New England Biolabs). The immunoprecipitates were washed with lysis buffer once and divided equally into two. One of the samples was incubated with TBS and the other one with TBS containing RNase A (100  $\mu$ g/ml) at 25°C for 10 min. The IP samples were eluted in SDS loading dye and analyzed by Western blotting.

For monitoring the SUMOylation of AGO2, the immunoprecipitation protocol was similar to that used for co-immunoprecipitation as mentioned above, except that 20 mM N-ethylmaleimide (NEM) was used in TBS and lysis buffer (20 mM HEPES, pH 8.0, 10 mM KCl, 1 mM MgCl<sub>2</sub>, 20% glycerol, and 0.01% Triton X-100).

The following antibodies and dilutions were used for Western blotting: mouse anti-Nup358 (1:1,000; Santa Cruz Biotechnology Inc., sc-74518), rabbit anti-Dicer (1:1,500; Santa Cruz Biotechnology Inc., sc-30226), rabbit anti-Nup214 (1:1,000; Bethyl Laboratories, A300-717A), mouse anti-GFP (1:8,000; Santa Cruz Biotechnology Inc., sc-9996), mouse anti-vinculin (1:10,000; Sigma, V9131), mouse anti-tubulin (1:10,000; Sigma, T5168), rabbit anti-TNRC6A/GW182 (1:500; Bethyl Laboratories, A302-329A), mouse anti-HA (1:5,000; Covance Research Products, MMS-101R), rabbit anti-AGO2 (1:1,000; Cell Signaling Technology, #2897), rat anti-AGO2 (1:1,000; Millipore, MABE253), rabbit RPL7a (1:80,000; Abcam, ab70753), rabbit anti-PDI (1:2,000; Santa Cruz Technology, sc-20132), mouse anti-LAMP2 (1:1,000; BD Bioscience, 555803), rabbit anti-exportin-5 (1:3,000; Santa Cruz Biotechnology Inc., sc-66885), mouse anti-PABP (1:5,000; Abcam, ab6125), rabbit anti-TRBP2 (1:3,000; Abcam, ab42018), mouse anti-lamin A/C (1:3,000; Santa Cruz Biotechnology Inc.,

sc-7292), mouse anti-RanGAP1 (1:5,000; Santa Cruz Biotechnology, sc-28322), mouse anti-Ubc9 (1:10,000; BD Biosciences, 610748), mouse anti-AGO2 (1:1,000; Sigma-Aldrich, WH0027161M1), rabbit anti-Ras (1:10,000; Abcam, ab52939), mouse anti-c-Myc (1:1,000; Santa Cruz Biotechnology Inc., sc-40), mouse anti-PABPC1 (1:3,000; Abcam, ab6125), donkey anti-rabbit IgG-HRP (1:10,000; GE Healthcare, NA-934), sheep anti-mouse IgG-HRP (1:10,000; GE Healthcare, NA-931), goat anti-rat IgG-HRP (1:10,000; GE Healthcare, NA935V), and HRP-rec-protein A (1:10,000; Invitrogen, 101123). Rabbit anti-GFP (1:10,000) and rabbit anti-Nup358 (1:3,000) antibodies have been described earlier [25,86].

### Dual-luciferase reporter assay

For dual-luciferase reporter assay,  $4 \times 10^4$  HeLa cells were seeded in each well of a 24-well plate, 12 h prior to siRNA transfection. Control and indicated siRNAs were transfected at a working concentration of 40 nM (unless otherwise mentioned), and cells were incubated for 36 h. Cells were then subjected to a second round of transfection with reporter DNA (20 ng of indicated RL reporter, and 100 ng of pcDNA-FL as internal control) and incubated for 24–36 h. Cells were lysed in passive lysis buffer and the reporter assay was performed using Dual-Luciferase assay system (Promega) in Glomax Multi Detection System (Promega). Relative luciferase activity was calculated; values obtained from control and specific knockdown conditions were individually normalized with respect to RL-control value of each set and plotted with arbitrary units.

For rescue experiments with full-length Nup358 expression (Fig EV2D), HeLa cells were transfected with 20 nM control (siControl) or Nup358-specific siRNA (siNup358-A) for 36 h. Later, reporter constructs (20 ng of RL-control or RL-3xBulge reporter and 100 ng of pcDNA-FL as internal control) along with GFP or GFP-Nup358 construct (500 ng/well in a 24-well plate) were transfected for 36 h, before dual-luciferase assay was performed. For rescue experiments with Nup358 $\Delta$ M (Fig EV5), HeLa cells were transfected with 40 nM of control or Nup358-specific siRNA for 60 h, and later, the reporters (20 ng of RL-3xBulge-mutant-control or RL-3xBulge reporter, and 100 ng of pcDNA-FL as internal control) were co-transfected with indicated plasmid GFP-MBP or GFP-Nup358 $\Delta$ M (100 ng/well in a 24-well plate). GFP-Nup358 $\Delta$ M construct was generated by replacing the middle ApaI fragment with a designed annealed pair of oligos to keep the N-terminal and C-terminal regions in frame. GFP-MBP was generated by PCR-amplifying the ORF for MBP using pMAL-p2 (New England Biolabs) as the template and cloning the product into pEGFP-C2 at appropriate restriction sites. Dual-luciferase assay was performed after 36 h.

For miR30 reporter system,  $8 \times 10^4$  HEK293T cells were seeded 12 h prior to siRNA transfection. Forty-eight hours after siRNA transfection, the following constructs were transfected: pCMV-FL-miR30 (P) reporter (50 ng) with pSUPER-control or pSUPER miR30 constructs (2 ng) and RL as internal control (1 ng). The experiment was terminated 12 h after reporter transfection. Relative luciferase activity (FL/RL) was calculated and normalized with respect to FL-control value of each set and plotted. For HMGA2 3'-UTR-containing FL-reporter (wt and mut) assays, the protocol remained similar to that for RL-3xBulge, except that 10 ng of HMGA2-wt or HMGA2-mut along with 1 ng of RL-control was transfected and the relative FL/RL activity was measured [63].

Dominant-negative effect of Nup358-SIM1 region on miRNA pathway was assessed as described below. For dual-luciferase reporter assay,  $8 \times 10^4$  HeLa cells were seeded in each well of a 24-well plate, 12 h prior to transfection. Cells were transfected with reporter DNA (25 ng of indicated *Renilla* luciferase (RL)-reporter and 100 ng of pcDNA-firefly luciferase (FL) as internal control) and plasmid DNA (500 ng of GFP-MBP or GFP-SIM1 or 130 ng of GFP-SIM1 mutant with 370 ng of fill-in DNA) for 36 h. Transfection was performed using Lipofectamine 2000 (Invitrogen). Dual-luciferase assay was performed as described earlier. Relative luciferase (RL/FL ratio) activity was calculated; values obtained were individually normalized with respect to RL-control value of each set and plotted.

Tethering assay was performed in HEK293T cells.  $4 \times 10^4$  cells were seeded in each well of a 24-well plate. Control or Nup358 siRNA was transfected for 48 h. Then, 25 ng of RL-5BoxB reporter and 50 ng of pcDNA-FL were transfected as internal control. The reporters (500 ng) were co-transfected with HA-AGO2, N-HA-AGO2, or N-HA-LacZ. Assay was performed after 24 h of transfection. In some tethering assays, HA-IR1 + 2, N-HA-IR1 + 2, or N-HA-IR1 + 2<sup>L2651A,L2653A</sup> was used.

Tethering assay using Nup358-IR1 + 2 was performed in HEK293T cells as described below.  $1 \times 10^5$  cells were seeded in each well of a 24-well plate. Then, 25 ng of RL-5BoxB reporter and 100 ng of pcDNA-FL were transfected as internal control. The reporters were co-transfected with N-HA-MBP, N-HA-AGO2, HA-IR1 + 2<sup>L2651A,L2653A</sup>, or N-HA-IR1 + 2<sup>L2651A,L2653A</sup> (500 ng each) for 24 h. Polyethyleneimine (Polysciences Inc.) was used as transfecting reagent. Cells were washed with  $1 \times$  TBS once and lysed in passive lysis buffer, and dual-luciferase assay was performed. Relative luciferase activity (RL/FL ratio) was calculated, and values obtained were individually normalized with respect to the RL-control value with N-HA-MBP and plotted.

### RNA isolation

RNA was isolated from cell lysates using TRIzol (Invitrogen). Three volumes of TRIzol was added to one volume of the lysate and incubated for 15 min at RT. To this,  $1/5^{\text{th}}$  volume of chloroform was added and rigorously agitated for homogenous mixing. The mixture was then incubated on ice for 5 min and centrifuged at  $\sim 15,200$  g for 12 min using Eppendorf centrifuge (5417 R). Upper aqueous layer was aspirated into another tube without disturbing the interface. An equal volume of isopropanol was added and incubated for 1 h at  $-20^\circ\text{C}$ . The tube was then centrifuged at  $\sim 15,200$  g for 12 min. The RNA pellet obtained was washed with 70% ethanol twice, followed by a brief centrifugation. The remaining ethanol was removed and the pellet was left at RT for air-drying. The pellet was then dissolved in autoclaved glass distilled water, heated at  $65^\circ\text{C}$  for 5 min, and stored at  $-80^\circ\text{C}$ . In case of RNA isolation for miRNA qPCR, heating step was not included.

### RNA immunoprecipitation

To analyze the relative association of mRNA with AGO2, HeLa cells were grown in 100-mm culture dishes and were transfected with control, AGO2, Dicer, and Nup358 siRNA and incubated for 36 h. Further, cells were transfected with RL-3xBulge construct and incubated for 24 h. For RNA immunoprecipitation analysis, cells were



washed with ice-cold 1× PBS, removed using a cell scraper, and resuspended in chilled NET2 buffer (100 mM Tris-HCl, pH 7.4, 150 mM NaCl, 0.05% NP-40) supplemented with 7.5 mM NaF, 1 mM PMSF, PIC (Roche), and 100 U/ml of murine RNase inhibitor. To make a clear lysate, mild sonication was given, three pulses at 30% amplitude, and repeated thrice. Lysate was centrifuged to clear cellular debris at ~15,200 g for 10 min at 4°C. Lysate was further pre-cleared by incubating the supernatant with protein G-Sepharose beads (Invitrogen) for 1 h at 4°C. A part of the pre-cleared lysate was taken out as starting material for RNA isolation and Western analysis. For AGO2 immunoprecipitation, mouse anti-AGO2 (Sigma, WH0027161M1) or rat anti-AGO2 (Sigma, SAB4200085) antibodies were used. Mouse IgG (Vector Laboratories) and rat IgG (BD Pharmingen) were used as respective control IgGs. In the meantime, tRNA-saturated beads were prepared by incubating protein A-Sepharose beads with yeast tRNA (Invitrogen), herring sperm DNA (Sigma), and glycogen (Sigma) in NET2 buffer for 90 min at 4°C. Finally, tRNA-saturated beads were incubated with the lysate containing antibodies and incubated for 1 h at 4°C. Beads were then washed 5–7 times with NET2 buffer and the RNA was isolated from beads using TRIzol as mentioned earlier, except that the RNA precipitation was performed for 4 h at –20°C. RNA samples were further used for cDNA synthesis, followed by real-time PCR analysis as described below.

For assessing the extent of AGO2 association with endogenous target mRNAs (Serbp1 or DnaJB1), the same procedure was followed, except that the cells were not transfected with RL-3xBulge construct. The mRNAs in the AGO2-IP were quantified using specific primers described earlier [63].

For analyzing the association of miRNA and mRNA with Nup358, HeLa cells were transfected with the miRNA reporter construct RL-3xBulge. Twenty hours post-transfection, cells were washed thrice with PBS and then cross-linked with 1% formaldehyde for 10 min. Glycine was added to a final concentration of 0.25 M for neutralization for 5 min. The cells were washed with PBS three times and lysed in RIPA buffer (50 mM Tris, pH 8.0, 150 mM NaCl, 1% NP-40, 0.1% SDS, 0.5% sodium deoxycholate) containing PIC (Roche) and 100 U/ml of murine RNase inhibitor. Following a mild sonication, the lysate was centrifuged at 12,000 g for 10 min. The supernatant was then incubated with rabbit IgG (control) or Nup358-specific antibodies for 45 min at 4°C. In the meanwhile, protein A-Sepharose beads were coated with herring serum DNA, tRNA, and glycogen for 30 min. The lysate was then incubated with coated beads for 45 min at 4°C. The immunoprecipitate was given five washes with RIPA buffer containing 1 M NaCl. Delinking was done with 1% SDS, 10 mM DTT, 5 mM EDTA, and 50 mM Tris, pH 7.4, for 1 h at 70°C, followed by proteinase K treatment (10 µg/ml) for 45 min at 55°C. RNA was isolated using TRIzol method as mentioned above, and RNA precipitation was done overnight in the presence of glycogen. cDNA synthesis for miRNA and mRNA and the respective qPCRs were done using the protocols mentioned below.

#### cDNA synthesis and semi-quantitative PCR

Total RNA isolated was subjected to DNase I treatment before cDNA synthesis. One microgram total RNA, 1 µl 10× DNase I reaction buffer, and 1 µl DNase I, Amp grade 1 U/µl (Invitrogen), were

mixed and the volume was made up to 10 µl as per the manufacturer's instructions and incubated for 20–30 min at 37°C. DNase I was inactivated by addition of 1 µl of 25 mM EDTA solution and incubating the mixture for 10 min at 65°C. Reaction was scaled up as per requirement. cDNA synthesis was performed with Oligo (dT)<sub>20</sub> primers or random primers using SuperScript III First-Strand Synthesis kit (Invitrogen) as per the manufacturer's instructions. The synthesized cDNA was further diluted and used as template for PCR amplification.

#### Real-time quantitative PCR

Isolated RNA from input, control, or AGO2 immunoprecipitate was treated with DNase I, and cDNA synthesis was performed as described above. To assess the specific association of miRNA target (RL-3xBulge) with AGO2, quantitative PCR (qPCR) was performed with the following primers on a Rotor-Gene Q (Qiagen) using the SYBR Select Master Mix (Invitrogen). GAPDH was used as negative control. The primers used were *Renilla* luciferase (forward: 5' CGAGACCAAGACAAGATCA 3'; reverse: 5' GTAGGCAGCGAACT CCTCAG 3') and GAPDH (forward: 5' GATTCCACCCATGGCAA TTC 3'; reverse: 5' AGCATCGCCCCACTTGATT 3').

For relative association of let-7a and miR-17 with AGO2, total RNA isolated from input, control, or AGO2 immunoprecipitate was used. Association of U6 RNA with AGO2 was monitored to assess the extent of non-specificity. Using TaqMan MicroRNA Reverse Transcription Kits (Invitrogen, 4427975; ID: 000377, 002308, 001973), the RNA was converted to cDNA with specific microRNA primers supplied with specific kits. qPCR mix was prepared according to the TaqMan Small RNA Assay (Invitrogen) protocol, and the PCR was performed on a Rotor-Gene Q (Qiagen). A similar protocol was followed for isolation and quantitation of let-7a in control and Nup358-depleted HeLa cells.

#### Oligo(dT) staining

HeLa cells seeded on coverslips were fixed with 4% paraformaldehyde in 1× TBS for 15 min at RT. Chilled methanol was added to the cells and incubated for 5 min. This was followed by incubation of the coverslips with 2× SSC at RT for 10 min. Further, hybridization chamber was used to carry out the hybridization process. In the process, moistened strips of filter paper were kept on the edges of the stage to avoid the coverslips from drying out. The hybridization mix was made up of the following components: 40% formamide, 10% dextran sulfate, 0.1 mg herring sperm DNA, and 5 ng/µl of FAM oligo(dT) in a 2× SSC solution. One hundred microliters of the hybridization mix was added per coverslip. Hybridization was carried out at 37°C for 3 h. Further, the coverslips were washed twice with 2× SSC followed by one wash with 0.2× SSC. Followed by three washes with 1× TBS, the cells were incubated with Hoechst 33342 diluted in 1× TBS. Cells were then washed with 1× TBS and coverslips were mounted using Vectashield mounting medium (Vector Laboratories) and observed under microscope.

#### Nucleo-cytoplasmic fractionation

Control and Nup358 siRNA-transfected HeLa cells were resuspended in cytoplasmic extraction buffer (20 mM HEPES, pH 8.0,

10 mM KCl, 1 mM MgCl<sub>2</sub>, 20% glycerol, 0.2% Triton X-100). Cells were lysed by gently pipetting for 45 min at an interval of 15 min. Lysate was centrifuged with Eppendorf centrifuge (5417 R) at ~15,200 g for 20 min. Supernatant was collected as cytoplasmic fraction and the pellet was further processed for nuclear fraction after washing three times with 1× TBS. Nuclear lysis buffer (20 mM HEPES, pH 7.4, 150 mM NaCl, 1.5 mM MgCl<sub>2</sub>, 2 mM EGTA, 2 mM DTT, 1% Triton X-100) was added to the pellet and then sonicated for 5 s with a pulse of 1 s on and 2 s off at 30% amplitude using Vibra-Cell sonicator (Sonics & Materials Inc.). Lysis was carried out for 45 min by sonicating the samples at an interval of 15 min. Lysate was then centrifuged at ~15,200 g at 4°C for 20 min. The supernatant was collected as nuclear fraction. The proteins were separated by SDS-PAGE and analyzed by Western blotting. Vinculin and lamin A/C were used as markers for cytoplasmic and nuclear fractions, respectively. Cytoplasmic and nuclear lysates were mixed in equal proportion to make total protein fraction. For total fraction, double the volume of lysate was loaded for analysis.

### Membrane flotation assay

Membrane flotation assay was carried out as described earlier [11,87]. Briefly,  $6 \times 10^6$  HeLa cells were seeded in each 60-mm dish. Twelve hours later, cells were transfected with 40 nM of control or Nup358 siRNA for 72 h. Cells in each dish were washed twice with ice-cold 1× PBS and lysed in 1 ml of hypotonic buffer [10 mM Tris, pH 8, 10 mM KCl, 1.5 mM MgCl<sub>2</sub>, 10 mM DTT, and EDTA-free protease inhibitor cocktail (Roche)] by passing through a 23-gauge needle 15 times. Lysates were centrifuged at 1,000 g for 5 min at 4°C. The resultant post-nuclear supernatant (446 µl) was mixed with 72% (w/v) sucrose made in hypotonic buffer (1.78 ml) and overlaid with 55% (w/v) sucrose (2.23 ml), followed by 0.54 ml of 10% (w/v) sucrose (0.54 ml). Ultracentrifugation was performed at 140,000 g (4°C) using MLS-50 rotor for 12 h. After centrifugation, 1-ml fractions were collected from top of the gradient. To each fraction, 5 ml of hypotonic buffer was initially added and mixed, followed by 1.5 ml of 100% TCA. Proteins were precipitated by centrifugation at 1,400 g (4°C) for 5 min. The protein pellets were washed four times with ice-cold acetone and air-dried before resuspending in 25 µl of NP-40 lysis buffer. After addition of 25 µl of 3× SDS loading dye, the samples were heated at 95°C for 5 min and subjected to SDS-PAGE for Western analysis.

### Northern blotting

For Northern blotting, 10 µg of total RNA was resolved on a 12% urea-PAGE and electro-transferred to Hybond N<sup>+</sup> nylon membrane (GE Healthcare). The membrane was UV-cross-linked and washed for 1 h at 65°C in prewash buffer (0.1× SSC, 0.1% SDS). Prehybridization was performed at 42°C in hybridization solution (10× Denhardt's solution, 6× SSC, 0.1% SDS) for 6 h. Body-labeled oligonucleotides complementary to miRNAs were used as probes for Northern blotting. Radiolabeled probes were heat-denatured at 65°C for 5 min and added to the hybridization solution and kept for overnight incubation at 42°C. The membrane was washed twice for 10 min at 25°C in wash solution (6× SSC, 0.1% SDS) and was exposed to X-ray film and analyzed by autoradiography.

### miRNA deep sequencing

HEK293T cells were transfected with control or Nup358 shRNA. Total RNA was isolated and miRNA deep sequencing was performed at Genotypic Technology, Bengaluru, India. Small RNA libraries for sequencing were constructed according to the Illumina TruSeq Small RNA preparation Guide. One microgram of total RNA was used as the starting material. Briefly, 3' adaptors were ligated to the specific 3'OH group of small RNAs followed by 5' adaptor ligation. The ligated products were reverse-transcribed with SuperScript II reverse transcriptase. The cDNA was enriched by PCR and cleaned using polyacrylamide gel electrophoresis. The library was size selected in the range of 140–180 bp followed by overnight gel elution and precipitation using glycogen, 3 M sodium acetate, and absolute ethanol. The precipitate was resuspended in resuspension buffer. The prepared library was quantified using Nanodrop and Qubit Fluorometer and validated for quality by running an aliquot on High Sensitivity Bioanalyzer Chip (Agilent). The libraries were sequenced for 54SE small RNA sequencing in GAIIX (Illumina). The relative expression of miRNAs was analyzed by GeneSpring NGS software. The values were log-transformed and the heatmap was generated using Matplotlib. The corresponding fold change has been represented by bar graphs.

### Bacterial expression of proteins and pull-down assays

GST-control (pGEX-6P1), GST-Nup358-SIM1, MBP (pMAL-c2), or pMAL-hAGO2 was transformed in *Escherichia coli* BL21 pLysS strain and induced with 0.5 mM IPTG at 18°C for 6 h. Cells were lysed in lysis buffer (50 mM Tris-HCl pH 7.5, 150 mM NaCl, 0.05% NP-40) supplemented with 7.5 mM NaF, 0.75 mM sodium orthovanadate, 1 mM PMSF, protease inhibitor cocktail (PIC, Roche), leupeptin (50 µg/ml), aprotinin (5 µg/ml), and pepstatin (2 µg/ml) and lysozyme (200 µg/ml). The indicated lysates were mixed and GST pull-down assay was performed. The proteins were eluted in 3× SDS-PAGE loading dye and Western blot analysis was performed as described above.

### Structural analysis

To identify possible Nup358 binding sites on AGO2, we compared the 3D structure of AGO2 (PDB ID: 4W5O) [88] with that of SUMO (PDB ID: 1Z5S) [47]. The chosen SUMO structure was in complex with the SIM1 of Nup358. Structural superimpositions were performed using the CLICK program [75,76] that identifies similar sub-structures regardless of topology. All superimpositions were carried out with full-length AGO2 and a truncated SUMO molecule comprising the residues 20–54 and 86–91. These regions on SUMO consisted of regular secondary structures that were most proximal to the bound Nup358. On superimposing the AGO2 with SUMO structures, the position of the Nup358 was transferred onto the former. Of the 93 different superimpositions obtained, 46 cases had collisions between Nup358-SIM1 and the AGO2 molecule. Therefore, these superimpositions were deemed unphysical and omitted from further consideration. The remaining 47 alignments were clustered by spatial proximity to one another, and one structure was chosen to represent each cluster (Fig 6F).

## Statistical analysis

The experiments were independently repeated at least three times ( $n = 3$ ), and the values are expressed as mean  $\pm$  SD. *P*-values were calculated using Student's *t*-test (SigmaStat2.03). *P*-value  $\leq 0.05$  was considered statistically significant. Graphs were plotted using SigmaPlot8.0.

**Expanded View** for this article is available online.

## Acknowledgements

We thank Ramesh Pillai (EMBL Grenoble, France), Gunter Meister (Universität Regensburg, Germany), Bryan Cullen (Duke University Medical Center, USA), Ken Fujimura (University of Tokyo, Japan), Jamal Tazi (Institut de Génétique Moléculaire de Montpellier, France), Shigeyuki Yokoyama (RIKEN Genomic Sciences Center, Yokohama, Japan), Katharine Ullman (University of Utah, USA), Mary Dasso (NICHD, NIH, USA), and Ian Macara (Vanderbilt University Medical Center, TN, USA) for sharing reagents. We are grateful to Joseph and Seshadri lab members for scientific discussions and helpful suggestions. We thank Shekhar Mande (NCCS, Pune) and Radha Chauhan (NCCS, Pune) for insightful discussions on AGO, SUMO, and SIM structures. Deepa Subramanyam (NCCS, Pune) and Jyotsna Dhawan (CCMB, Hyderabad) are acknowledged for critical reading of the manuscript. Financial support from Council of Scientific and Industrial Research, Government of India, to M.R. Sahoo, D. Khuperkar, S. Gaikwad, S.K. Yadav, A. Singh, I. Magre, and P. Deshmukh, from Department of Biotechnology, Government of India, to M. Ashok, M. Helen, Y. Ramtirtha and S. Dhanvijay, and from INSPIRE (DST) and IYBA (DBT) fellowships to P. Gayathri is gratefully acknowledged. MSM would like to acknowledge the Wellcome trust-DBT India alliance for a senior fellowship. We thank Pankhuri Vyas for generating pSUPER Nup358 shRNA clones, Pravin Sawale for generating GFP-SUMO1G and GFP-SUMO1GG clones, and Ashwini Atre (NCCS, Pune) and Richa Ricky (IISER, Pune) for the help with microscopy. We are grateful to Gaurang Mahajan (NCCS, Pune) for helping with miRNA analysis. The work was partly supported by intramural funding from NCCS and a grant (EMR/2014/001092) from Department of Science and Technology, Government of India.

## Author contributions

MRS conducted most of the experiments regarding Nup358's role in miRNA pathway, SG mostly worked on Nup358-AGO interaction, and DK mainly contributed to the characterization of AL and its association with mRNP granules. MA, MH, SKY, AS, IM, PD, SD, and PKS supported design and execution of some of the experiments. YR, MSM, and PG contributed to identification of putative SIM-binding regions in AGO2. VS contributed to experimental design and provided scientific advice. JJ contributed to overall design and supervision and along with other authors wrote the manuscript.

## Conflict of interest

The authors declare that they have no conflict of interest.

## References

- Bartel DP (2009) MicroRNAs: target recognition and regulatory functions. *Cell* 136: 215–233
- Friedman RC, Farh KK, Burge CB, Bartel DP (2009) Most mammalian mRNAs are conserved targets of microRNAs. *Genome Res* 19: 92–105
- Ha M, Kim VN (2014) Regulation of microRNA biogenesis. *Nat Rev Mol Cell Biol* 15: 509–524
- Meister G (2013) Argonaute proteins: functional insights and emerging roles. *Nat Rev Genet* 14: 447–459
- Liu J, Rivas FV, Wohlschlegel J, Yates JR III, Parker R, Hannon CJ (2005) A role for the P-body component GW182 in microRNA function. *Nat Cell Biol* 7: 1261–1266
- Sen GL, Blau HM (2005) Argonaute 2/RISC resides in sites of mammalian mRNA decay known as cytoplasmic bodies. *Nat Cell Biol* 7: 633–636
- El Shami M, Pontier D, Lahmy S, Braun L, Picart C, Vega D, Hakimi MA, Jacobsen SE, Cooke R, Lagrange T (2007) Reiterated WG/GW motifs form functionally and evolutionarily conserved ARGONAUTE-binding platforms in RNAi-related components. *Genes Dev* 21: 2539–2544
- Till S, Lejeune E, Thermann R, Bortfeld M, Hothorn M, Enderle D, Heinrich C, Hentze MW, Ladurner AG (2007) A conserved motif in Argonaute-interacting proteins mediates functional interactions through the Argonaute PIWI domain. *Nat Struct Mol Biol* 14: 897–903
- Siomi MC, Sato K, Pezic D, Aravin AA (2011) PIWI-interacting small RNAs: the vanguard of genome defence. *Nat Rev Mol Cell Biol* 12: 246–258
- Li S, Liu L, Zhuang X, Yu Y, Liu X, Cui X, Ji L, Pan Z, Cao X, Mo B et al (2013) MicroRNAs inhibit the translation of target mRNAs on the endoplasmic reticulum in *Arabidopsis*. *Cell* 153: 562–574
- Stalder L, Heusermann W, Sokol L, Trojer D, Wirz J, Hean J, Fritzsche A, Aeschmann F, Pfanzagl V, Basselet P et al (2013) The rough endoplasmic reticulum is a central nucleation site of siRNA-mediated RNA silencing. *EMBO J* 32: 1115–1127
- Hetzer MW, Wente SR (2009) Border control at the nucleus: biogenesis and organization of the nuclear membrane and pore complexes. *Dev Cell* 17: 606–616
- Cronshaw JM, Krutchinsky AN, Zhang W, Chait BT, Matunis MJ (2002) Proteomic analysis of the mammalian nuclear pore complex. *J Cell Biol* 158: 915–927
- Hoelz A, Debler EW, Blobel G (2011) The structure of the nuclear pore complex. *Annu Rev Biochem* 80: 613–643
- Chatel G, Fahrenkrog B (2012) Dynamics and diverse functions of nuclear pore complex proteins. *Nucleus* 3: 162–171
- Chow KH, Factor RE, Ullman KS (2012) The nuclear envelope environment and its cancer connections. *Nat Rev Cancer* 12: 196–209
- Kessel RG (1992) Annulate lamellae: a last frontier in cellular organelles. *Int Rev Cytol* 133: 43–120
- Meier E, Miller BR, Forbes DJ (1995) Nuclear pore complex assembly studied with a biochemical assay for annulate lamellae formation. *J Cell Biol* 129: 1459–1472
- Wischnitzer S (1970) The annulate lamellae. *Int Rev Cytol* 27: 65–100
- Onischenko EA, Gubanov NV, Kieselbach T, Kiseleva EV, Hallberg E (2004) Annulate lamellae play only a minor role in the storage of excess nucleoporins in *Drosophila* embryos. *Traffic* 5: 152–164
- Patterson JR, Wood MP, Schisa JA (2011) Assembly of RNP granules in stressed and aging oocytes requires nucleoporins and is coordinated with nuclear membrane blebbing. *Dev Biol* 353: 173–185
- Asally M, Yasuda Y, Oka M, Otsuka S, Yoshimura SH, Takeyasu K, Yoneda Y (2011) Nup358, a nucleoporin, functions as a key determinant of the nuclear pore complex structure remodeling during skeletal myogenesis. *FEBS J* 278: 610–621
- Cho KI, Yi H, Desai R, Hand AR, Haas AL, Ferreira PA (2009) RANBP2 is an allosteric activator of the conventional kinesin-1 motor protein, KIF5B, in a minimal cell-free system. *EMBO Rep* 10: 480–486
- Joseph J, Tan SH, Karpova TS, McNally JG, Dasso M (2002) SUMO-1 targets RanGAP1 to kinetochores and mitotic spindles. *J Cell Biol* 156: 595–602

25. Joseph J, Liu ST, Jablonski SA, Yen TJ, Dasso M (2004) The RanGAP1-RanBP2 complex is essential for microtubule-kinetochore interactions in vivo. *Curr Biol* 14: 611–617
26. Joseph J, Dasso M (2008) The nucleoporin Nup358 associates with and regulates interphase microtubules. *FEBS Lett* 582: 190–196
27. Murawala P, Tripathi MM, Vyas P, Salunke A, Joseph J (2009) Nup358 interacts with APC and plays a role in cell polarization. *J Cell Sci* 122: 3113–3122
28. Pichler A, Gast A, Seeler JS, Dejean A, Melchior F (2002) The nucleoporin RanBP2 has SUMO1 E3 ligase activity. *Cell* 108: 109–120
29. Prunuske AJ, Liu J, Elgort S, Joseph J, Dasso M, Ullman KS (2006) Nuclear envelope breakdown is coordinated by both Nup358/RanBP2 and Nup153, two nucleoporins with zinc finger modules. *Mol Biol Cell* 17: 760–769
30. Salina D, Enarson P, Rattner JB, Burke B (2003) Nup358 integrates nuclear envelope breakdown with kinetochore assembly. *J Cell Biol* 162: 991–1001
31. Vyas P, Singh A, Murawala P, Joseph J (2013) Nup358 interacts with Dishevelled and aPKC to regulate neuronal polarity. *Biol Open* 2: 1270–1278
32. Frohnert C, Hutten S, Walde S, Nath A, Kehlenbach RH (2014) Importin 7 and Nup358 promote nuclear import of the protein component of human telomerase. *PLoS One* 9: e88887
33. Hamada M, Haeger A, Jeganathan KB, van Ree JH, Malureanu L, Walde S, Joseph J, Kehlenbach RH, van Deursen JM (2011) Ran-dependent docking of importin-beta to RanBP2/Nup358 filaments is essential for protein import and cell viability. *J Cell Biol* 194: 597–612
34. Hutten S, Flotho A, Melchior F, Kehlenbach RH (2008) The Nup358-RanGAP complex is required for efficient importin alpha/beta-dependent nuclear import. *Mol Biol Cell* 19: 2300–2310
35. Hutten S, Walde S, Spillner C, Hauber J, Kehlenbach RH (2009) The nuclear pore component Nup358 promotes transportin-dependent nuclear import. *J Cell Sci* 122: 1100–1110
36. Walde S, Thakar K, Hutten S, Spillner C, Nath A, Rothbauer U, Wiemann S, Kehlenbach RH (2012) The nucleoporin Nup358/RanBP2 promotes nuclear import in a cargo- and transport receptor-specific manner. *Traffic* 13: 218–233
37. Dawlaty MM, Malureanu L, Jeganathan KB, Kao E, Sustmann C, Tahk S, Shuai K, Grosschedl R, van Deursen JM (2008) Resolution of sister centromeres requires RanBP2-mediated SUMOylation of topoisomerase IIalpha. *Cell* 133: 103–115
38. Klein UR, Haindl M, Nigg EA, Muller S (2009) RanBP2 and SENP3 function in a mitotic SUMO2/3 conjugation-deconjugation cycle on Borealin. *Mol Biol Cell* 20: 410–418
39. Sakin V, Richter SM, Hsiao HH, Urlaub H, Melchior F (2015) Sumoylation of the GTPase ran by the RanBP2 SUMO E3 ligase complex. *J Biol Chem* 290: 23589–23602
40. Gareau JR, Lima CD (2010) The SUMO pathway: emerging mechanisms that shape specificity, conjugation and recognition. *Nat Rev Mol Cell Biol* 11: 861–871
41. Wang Y, Dasso M (2009) SUMOylation and deSUMOylation at a glance. *J Cell Sci* 122: 4249–4252
42. Flotho A, Melchior F (2013) Sumoylation: a regulatory protein modification in health and disease. *Annu Rev Biochem* 82: 357–385
43. Hecker CM, Rabiller M, Haglund K, Bayer P, Dikic I (2006) Specification of SUMO1- and SUMO2-interacting motifs. *J Biol Chem* 281: 16117–16127
44. Mahajan R, Delphin C, Guan T, Gerace L, Melchior F (1997) A small ubiquitin-related polypeptide involved in targeting RanGAP1 to nuclear pore complex protein RanBP2. *Cell* 88: 97–107
45. Matunis MJ, Wu J, Blobel G (1998) SUMO-1 modification and its role in targeting the Ran GTPase-activating protein, RanGAP1, to the nuclear pore complex. *J Cell Biol* 140: 499–509
46. Saitoh H, Sparrow DB, Shiomi T, Pu RT, Nishimoto T, Mohun TJ, Dasso M (1998) Ubc9p and the conjugation of SUMO-1 to RanGAP1 and RanBP2. *Curr Biol* 8: 121–124
47. Reverter D, Lima CD (2005) Insights into E3 ligase activity revealed by a SUMO-RanGAP1-Ubc9-Nup358 complex. *Nature* 435: 687–692
48. Song J, Durrin LK, Wilkinson TA, Krontiris TG, Chen Y (2004) Identification of a SUMO-binding motif that recognizes SUMO-modified proteins. *Proc Natl Acad Sci USA* 101: 14373–14378
49. Namanja AT, Li YJ, Su Y, Wong S, Lu J, Colson LT, Wu C, Li SS, Chen Y (2012) Insights into high affinity small ubiquitin-like modifier (SUMO) recognition by SUMO-interacting motifs (SIMs) revealed by a combination of NMR and peptide array analysis. *J Biol Chem* 287: 3231–3240
50. Tatham MH, Kim S, Jaffray E, Song J, Chen Y, Hay RT (2005) Unique binding interactions among Ubc9, SUMO and RanBP2 reveal a mechanism for SUMO paralog selection. *Nat Struct Mol Biol* 12: 67–74
51. Werner A, Flotho A, Melchior F (2012) The RanBP2/RanGAP1\*SUMO1/Ubc9 complex is a multisubunit SUMO E3 ligase. *Mol Cell* 46: 287–298
52. Gareau JR, Reverter D, Lima CD (2012) Determinants of small ubiquitin-like modifier 1 (SUMO1) protein specificity, E3 ligase, and SUMO-RanGAP1 binding activities of nucleoporin RanBP2. *J Biol Chem* 287: 4740–4751
53. Pichler A, Knipscheer P, Saitoh H, Sixma TK, Melchior F (2004) The RanBP2 SUMO E3 ligase is neither HECT- nor RING-type. *Nat Struct Mol Biol* 11: 984–991
54. Pemberton LF, Paschal BM (2005) Mechanisms of receptor-mediated nuclear import and nuclear export. *Traffic* 6: 187–198
55. Stewart M (2007) Molecular mechanism of the nuclear protein import cycle. *Nat Rev Mol Cell Biol* 8: 195–208
56. Swaminathan S, Kiendl F, Korner R, Lupetti R, Hengst L, Melchior F (2004) RanGAP1\*SUMO1 is phosphorylated at the onset of mitosis and remains associated with RanBP2 upon NPC disassembly. *J Cell Biol* 164: 965–971
57. Cordes VC, Reidenbach S, Rackwitz HR, Franke WW (1997) Identification of protein p270/Tpr as a constitutive component of the nuclear pore complex-attached intranuclear filaments. *J Cell Biol* 136: 515–529
58. Wu X, Kasper LH, Mantcheva RT, Mantchev GT, Springett MJ, van Deursen JM (2001) Disruption of the FG nucleoporin NUP98 causes selective changes in nuclear pore complex stoichiometry and function. *Proc Natl Acad Sci USA* 98: 3191–3196
59. Kedersha N, Stoecklin G, Ayodele M, Yacono P, Lykke-Andersen J, Fritzler MJ, Scheuner D, Kaufman RJ, Golan DE, Anderson P (2005) Stress granules and processing bodies are dynamically linked sites of mRNP remodeling. *J Cell Biol* 169: 871–884
60. Eulalio A, Behm-Ansmant I, Schweizer D, Izaurralde E (2007) P-body formation is a consequence, not the cause, of RNA-mediated gene silencing. *Mol Cell Biol* 27: 3970–3981
61. Pillai RS, Bhattacharyya SN, Artus CG, Zoller T, Cougot N, Basyuk E, Bertrand E, Filipowicz W (2005) Inhibition of translational initiation by Let-7 MicroRNA in human cells. *Science* 309: 1573–1576
62. Zeng Y, Yi R, Cullen BR (2003) MicroRNAs and small interfering RNAs can inhibit mRNA expression by similar mechanisms. *Proc Natl Acad Sci USA* 100: 9779–9784
63. Weinmann L, Hock J, Ivacevic T, Ohrt T, Mutze J, Schwillie P, Kremmer E, Benes V, Urlaub H, Meister G (2009) Importin 8 is a gene silencing factor that targets argonaute proteins to distinct mRNAs. *Cell* 136: 496–507



64. Johnson SM, Grosshans H, Shingara J, Byrom M, Jarvis R, Cheng A, Labourier E, Reinert KL, Brown D, Slack FJ (2005) RAS is regulated by the let-7 microRNA family. *Cell* 120: 635–647
65. Sachdeva M, Zhu S, Wu F, Wu H, Walia V, Kumar S, Elble R, Watabe K, Mo YY (2009) p53 represses c-Myc through induction of the tumor suppressor miR-145. *Proc Natl Acad Sci USA* 106: 3207–3212
66. Sampson VB, Rong NH, Han J, Yang Q, Aris V, Soteropoulos P, Petrelli NJ, Dunn SP, Krueger LJ (2007) MicroRNA let-7a down-regulates MYC and reverts MYC-induced growth in Burkitt lymphoma cells. *Cancer Res* 67: 9762–9770
67. Pillai RS, Artus CG, Filipowicz W (2004) Tethering of human Ago proteins to mRNA mimics the miRNA-mediated repression of protein synthesis. *RNA* 10: 1518–1525
68. Braun JE, Huntzinger E, Izaurralde E (2013) The role of GW182 proteins in miRNA-mediated gene silencing. *Adv Exp Med Biol* 768: 147–163
69. Mahadevan K, Zhang H, Akef A, Cui XA, Gueroussov S, Cenik C, Roth FP, Palazzo AF (2013) RanBP2/Nup358 potentiates the translation of a subset of mRNAs encoding secretory proteins. *PLoS Biol* 11: e1001545
70. Nguyen CD, Mansfield RE, Leung W, Vaz PM, Loughlin FE, Grant RP, Mackay JP (2011) Characterization of a family of RanBP2-type zinc fingers that can recognize single-stranded RNA. *J Mol Biol* 407: 273–283
71. Zhao Q, Xie Y, Zheng Y, Jiang S, Liu W, Mu W, Liu Z, Zhao Y, Xue Y, Ren J (2014) GPS-SUMO: a tool for the prediction of sumoylation sites and SUMO-interaction motifs. *Nucleic Acids Res* 42: W325–W330
72. Novatchkova M, Bachmair A, Eisenhaber B, Eisenhaber F (2005) Proteins with two SUMO-like domains in chromatin-associated complexes: the RENi (Rad60-Esc2-NIP45) family. *BMC Bioinformatics* 6: 22
73. Urulangodi M, Sebesta M, Menolfi D, Szakal B, Sollier J, Sisakova A, Krejci L, Branzei D (2015) Local regulation of the Srs2 helicase by the SUMO-like domain protein Esc2 promotes recombination at sites of stalled replication. *Genes Dev* 29: 2067–2080
74. Kerscher O (2007) SUMO junction-what's your function? New insights through SUMO-interacting motifs. *EMBO Rep* 8: 550–555
75. Nguyen MN, Tan KP, Madhusudhan MS (2011) CLICK-topology-independent comparison of biomolecular 3D structures. *Nucleic Acids Res* 39: W24–W28
76. Nguyen MN, Madhusudhan MS (2011) Biological insights from topology independent comparison of protein 3D structures. *Nucleic Acids Res* 39: e94
77. Josa-Prado F, Henley JM, Wilkinson KA (2015) SUMOylation of Argonaute-2 regulates RNA interference activity. *Biochem Biophys Res Commun* 464: 1066–1071
78. Sahin U, Lapaquette P, Andrieux A, Faure G, Dejean A (2014) Sumoylation of human Argonaute 2 at lysine-402 regulates its stability. *PLoS One* 9: e102957
79. Truong K, Su Y, Song J, Chen Y (2011) Entropy-driven mechanism of an E3 ligase. *Biochemistry* 50: 5757–5766
80. Schisa JA (2012) New insights into the regulation of RNP granule assembly in oocytes. *Int Rev Cell Mol Biol* 295: 233–289
81. Updike DL, Strome S (2009) A genomewide RNAi screen for genes that affect the stability, distribution and function of P granules in *Caenorhabditis elegans*. *Genetics* 183: 1397–1419
82. Updike DL, Hachey SJ, Kreher J, Strome S (2011) P granules extend the nuclear pore complex environment in the *C. elegans* germ line. *J Cell Biol* 192: 939–948
83. Voronina E, Seydoux G, Sassone-Corsi P, Nagamori I (2011) RNA granules in germ cells. *Cold Spring Harb Perspect Biol* 3: a002774
84. Sheth U, Pitt J, Dennis S, Priess JR (2010) Perinuclear P granules are the principal sites of mRNA export in adult *C. elegans* germ cells. *Development* 137: 1305–1314
85. Tourriere H, Chebli K, Zekri L, Courselaud B, Blanchard JM, Bertrand E, Tazi J (2003) The RasGAP-associated endoribonuclease G3BP assembles stress granules. *J Cell Biol* 160: 823–831
86. Sahoo PK, Murawala P, Sawale PT, Sahoo MR, Tripathi MM, Gaikwad SR, Seshadri V, Joseph J (2012) Wnt signalling antagonizes stress granule assembly through a Dishevelled-dependent mechanism. *Biol Open* 1: 109–119
87. Tahbaz N, Kolb FA, Zhang H, Jaronczyk K, Filipowicz W, Hobman TC (2004) Characterization of the interactions between mammalian PAZ PIWI domain proteins and Dicer. *EMBO Rep* 5: 189–194
88. Schirle NT, Sheu-Gruttadauria J, MacRae IJ (2014) Structural basis for microRNA targeting. *Science* 346: 608–613
89. Pettersen EF, Goddard TD, Huang CC, Couch GS, Greenblatt DM, Meng EC, Ferrin TE (2004) UCSF Chimera—a visualization system for exploratory research and analysis. *J Comput Chem* 25: 1605–1612